THE UNIVERSITY OF EDINBURGH

DEPARTMENT OF

MECHANICAL ENGINEERING

Optimal control of a Duck

Paul Nebel[1]

Department of Mechanical Engineering

University of Edinburgh

May 26, 1992

[1]Supported by a Studentship from the SERC.

Optimal control of a Duck

Paul Nebel[1]
Department of Mechanical Engineering
University of Edinburgh

May 26, 1992

[1]Supported by a Studentship from the SERC.

Abstract

Experimental values have been obtained for optimal (complex-conjugate) control of an Edinburgh Duck model in the presence of unidirectional monochromatic incident waves, in a one-dimensional test tank of intermediate depth. These results are used to predict values at full-scale in the presence of unidirectional Pierson-Moscowitz wave spectra in deep water. Four full-scale configurations are considered. Control matrices are presented for complex-conjugate control in each case, as are the forces, velocities, accelerations and displacements associated with that control. Two sub-optimal control strategies are presented, as are the coefficients required to achieve them. Estimates of efficiency are made for the implementation of these strategies in each case.

Acknowledgements

I would like to thank Peter Woodhead for his help and guidance in this research, and Stephen Salter for providing the facilities which made it possible. Equipment was provided by the Department of Energy.

Contents

1 Introduction

The paper by Nebel [1] described the process for synthesising optimal (complex-conjugate) control of a wave energy device. The complex-conjugate control matrix was derived empirically for a 0.1m diameter Duck operating in monochromatic, unidirectional incident waves. The device was constrained to move in three degrees-of-freedom. The values of force, displacement, velocity and acceleration per unit wave-steepness were measured for three degree-of-freedom motion (the standard case). They were also measured for the device moving in two degrees-of-freedom only, with heave fixed (the fixed-heave case). All figures are given for water of intermediate depth.

If the optimum full-scale diameter of the Duck is to be determined it is necessary to find some measure of the full-scale force, velocity etc. seen by the device in its every-day operation. This paper uses the results given in [1] to approximate full-scale values for real spectra in deep water. Results are also quoted for two further types of constraint; the fixed-aft and translated-axis cases (see section 4.1).

2 Main conclusions

2.1 Sub-optimal control strategies

- Complex-conjugate control produces theoretical mean efficiencies of 100% and measured mean efficiencies of 90% in unidirectional monochromatic incident waves [1]. Efficiency, as it is defined here, cannot exceed 100%.
- Standard three degree-of-freedom individual and annual weighting controllers (based on spring, damping and inertia terms only) both produce mean annual efficiencies of around 70% in unidirectional wave spectra, with no accounting for losses.
- Accounting for power losses at model scale increases mean annual efficiency by some 25%.
- Reducing to a two degree-of-freedom device reduces mean annual efficiency (relative to Standard control) by 10% as the redundancy of the third degree-of-freedom allows a better fit for the constant spring, damping and inertia terms.
- A limit of 100KWm^{-1} on total absorbed power reduces mean annual efficiency by 4-5% relative to a device with unlimited capability.
- In both standard and translated-axis cases the pitch and forward power take-offs together absorb the equivalent of 150% of the incident power, while the aft power take-off puts the equivalent of 80% of the incident power into the water.
- In fixed-heave, most of the power is absorbed in pitch with forward/aft take-offs putting 7% of the incident power into the water (most of which is re-absorbed by pitch).
- In fixed-aft, power is absorbed fairly equally between pitch and forward (i.e. no power is being put back into the water).

- Individual-weight control (in which control parameters are changed for each sea state) gives a 2-3% increase in mean annual efficiency over annual-weighting control (in which control parameters remain fixed).
- Either of the two sub-optimal strategies would provide a good platform from which to develop a more sophisticated pseudo-optimal controller.
- Translated-axis, fixed-heave and fixed-aft control all produce lower torques than standard control, thus reducing the cost of power absorbed in pitch for each case relative to standard control.
- Forward/aft dynamic forces are the same for standard control as for translated-axis control. They are lower than standard for fixed-aft control and are greater than standard for fixed-heave control.
- A combination of fixed-aft and translated-axis control is likely to result in a significant reduction in all forces, a small increase in pitch velocity and a negligable increase in forward/aft velocities relative to standard control. Power will be more evenly distributed between the two working axes, and neither axis will put power into the water.

2.2 Validity of the figures

The forces, velocities, accelerations, displacements and efficiencies quoted in this report are transformations of predicted values (calculated from empirical knowledge of the impedance $\underline{\underline{Z}}$ and the wave-force coefficient $\underline{W}$). This enables the conversion from model-scale to full-scale to be undertaken for any shape with knowledge of $\underline{\underline{Z}}$ and $\underline{W}$ only, and without the necessity for further experiment. It was shown in [1] that the results of prediction and experiment are sufficiently close to justify this decision.

Forces, velocities etc. are quoted for standard wave-steepness (which is defined here as the ratio of wave amplitude to wavelength). Mean annual wave-steepness for the South Uist 399 wave set (see appendix A for more details) is approximately half standard steepness. Therefore, mean annual forces, velocities etc. are approximately half those shown. Forces etc. in individual seas may, however, be equal to or greater than those shown here.

The forces given are dynamic forces only. Static buoyancy forces are not accounted for.

The model-scale values include losses (the causes of which are as yet undetermined) which may not be present at full-scale. The effects of losses on the magnitudes of force and velocity are small. However, the reduction in efficiency due to loss is significant and is presented.

The conversion from intermediate depth water to deep water is achieved using steepness factors defined in this report. It is well established [2] that the properties of waves can be transformed in this manner. There is some question, however, as to whether forces, velocities etc. can be similarly transformed.

The bandwidth of the experimental data is finite, and may not contain frequencies which are significant in certain spectra. For this reason rms values may be underestimated. The

angular spreadings of spectra have been ignored since the experiments were undertaken for unidirectional incident waves. All spectra are assumed to be unidirectional, and to approach the Duck head-on. Unidirectional spectra are likely to produce higher efficiencies than multi-directional spectra. However, isolated plant in a wide tank may be able to exploit point absorber effects which will increase efficiency.

Efficiency is defined here as the ratio of power absorbed by the device to the power available in the sea over a frontage equal to the scaled width of the test tank and cannot, therefore, exceed 100%. The tank is 10% wider than the model. The sea power is evaluated over the experimental frequency range, and not over all frequencies. This may also result in a slight over-estimate of efficiency.

All figures assume linearity, and for the reasons outlined above it is important to view the full-scale values as *approximations* and not as exact quantities.

3 A note on graph axes

For many of the figures contained in this report the relation of the generated values to wave period is such that plotting value vs period (or frequency) is not the most useful representation when seeking to optimise that value. Power fraction can be a more relevant variable than wave period for determining the performance of a device in a mixed sea.

Power fraction is a function of period (see figure 1). It is the sum with period of the power in each of the South Uist 399 spectra, expressed as a fraction of the total power available in the spectra. It shows, for a given range of wave periods, what percentage of the total power in the South Uist set is available in waves within that range. Both the power fraction and the 399 spectra are explained in more detail in appendix A.

The forces, velocities, accelerations and displacements for the standard case are presented as $\log_{10}$ (quantity) vs power fraction for greater clarity. The data for the other three cases are presented as ratios with respect to the standard case so that differences between cases can be highlighted. The units of the log axes are stated on each graph.

Graphs which show similar quantities have been given the same axes where possible.

4 Scaling and rotation of axes

The duck model used for these measurements has a diameter of 0.1m. The full-scale device is expected to have a diameter in the region of 8-14m. The model is assumed to be $\left(\frac{1}{100}^{th}\right)$ scale for the purposes of this report (i.e. full-scale diameter is 10m). It is easy to change from this ratio to another if required. Scaling of the values is achieved using the multiplication factors given in appendix B.

The experimental values are stated in terms of the coordinate system defined in figure 2. At full scale it is expected that the Duck will be moored to the sea bed by members attached at 45°. It is therefore desirable to rotate the heave and surge coordinates to the full-scale system defined in figure 3. The model-scale system is non-standard and was chosen logically to match the motion of the Duck. The full-scale coordinates are defined to be standard right-handed axes.

4.1 Motion constraints

The experimental system, $\mathcal{S}$, is related to the full-scale system, $\mathcal{S}'$, by two transformation matrices; $\underline{\underline{\mathbf{T}}}_F$ which transforms force and $\underline{\underline{\mathbf{T}}}_v$ which transforms velocity. They are defined such that

$$\underline{\mathbf{F}}' = \underline{\underline{\mathbf{T}}}_F \cdot \underline{\mathbf{F}} \tag{1}$$

where

$$\underline{\underline{\mathbf{T}}}_F = \begin{bmatrix} -1 & \mathrm{r}\cos\alpha & \mathrm{r}\sin\alpha \\ 0 & \cos\gamma & \sin\gamma \\ 0 & -\sin\gamma & \cos\gamma \end{bmatrix}$$

$$\underline{\mathbf{F}} = \begin{bmatrix} \tau \\ \mathrm{F_h} \\ \mathrm{F_s} \end{bmatrix}$$

and

$$\underline{\mathbf{v}}' = \underline{\underline{\mathbf{T}}}_v \cdot \underline{\mathbf{v}} \tag{2}$$

where

$$\underline{\underline{\mathbf{T}}}_v = \begin{bmatrix} -1 & 0 & 0 \\ \mathrm{r}\cos(\gamma-\alpha) & \cos\gamma & \sin\gamma \\ -\mathrm{r}\sin(\gamma-\alpha) & -\sin\gamma & \cos\gamma \end{bmatrix}$$

$$\underline{\mathbf{v}} = \begin{bmatrix} \dot{\theta} \\ \dot{\mathrm{h}} \\ \dot{\mathrm{s}} \end{bmatrix}$$

In both matrices γ is the rotation of the full-scale coordinates relative to the model coordinates, and (r, α) is the polar translation of the full-scale origin relative to the model-scale origin.

The control matrix can be transformed by the application of both $\underline{\underline{\mathbf{T}}}_F$ and $\underline{\underline{\mathbf{T}}}_v$ as follows;

$$\underline{\underline{\mathbf{C}}}' = \underline{\underline{\mathbf{T}}}_F \cdot \underline{\underline{\mathbf{C}}} \cdot \underline{\underline{\mathbf{T}}}_v^{-1} \tag{3}$$

Displacement and acceleration can be found from velocity using the equivalence $\frac{d}{dt} \equiv i\omega$.

The derivations of $\underline{\underline{\mathbf{T}}}_F$ and $\underline{\underline{\mathbf{T}}}_v$ are not included in this report, but similar transformations, and the techniques for finding them, can be found in Ránky & Ho [4] and Snyder [5].

Four cases are considered in this report (see figure 5);

4.1.1 Standard case

The standard case is the most general form of constraint that can be applied in the test tank. The Duck is free to move in all three of its available degrees-of-freedom. The full-scale axes are rotated through an angle, γ, of $-45°$. The origin is not translated, so that r and α are both zero.

4.1.2 Translated-axis constraint

In the Standard case the axis about which the Duck pitches is some distance from the point through which all the external dynamic forces pass, resulting in a couple. The torque applied to the Duck must provide a reaction to this couple as well as doing work. Translating the axis of rotation can alter the size of this couple, and hence the total torque on the Duck, without affecting the forward and aft forces (it may, however, alter the forward and aft velocities). Since the cost of the pitch power take-off is largely a function of torque any reduction of torque will result in a reduction the cost of pitch power.

It should be noted that to an outside observer the only difference between the standard case and the translated axis-case is that the mooring lines are attached to the Duck body in a different position. The observed motion will be the same in both cases. Hence the overall efficiency is the same for both cases (see figures 35 and 36), but the efficiencies in the individual degrees-of-freedom differ between (see figures 42 and 43).

Sharing the power more effectively between the degrees-of-freedom can mean that the power rating in one or more degrees-of-freedom can be reduced, and thus the cost of output energy may fall. There is a point of rotation such that the power absorbed by the Duck is shared equally between all three of its degrees-of-freedom (rather than one or more degrees-of-freedom putting power in to the water while the others absorb large amounts of power as in the standard case).It was found, however, that for three degree-of-freedom control (over the frequency range of most interest) this point lay outside the body of the Duck from which these figures are obtained.

By moving the centre of rotation slightly closer ($\simeq$ 2.5m) to the beak of the Duck the power absorbed in pitch at the central wave frequency can be more than halved while the power absorbed by the forward leg is increased by just over half. The power absorbed by the aft leg remains constant as the translation is parallel to the aft axis.

Pitch torque is reduced by 30% (see figure 15) reducing the cost of the pitch primary power

take-off proportionally. Translating the axis by a relatively small amount may therefore reduce overall cost without distorting the shape of the device.

The translated-axis case is defined by a rotation of the axes through -45^o and a translation of the origin by $(2.5, -45)$ relative to the model-scale coordinates.

4.1.3 Fixed-heave constraint

The fixed-heave case is included because it requires a lower rating for the power take-off mechanism than the standard case. The power take-off does not need to react against the large buoyancy forces in heave, which are resisted by anchor cables.

The equation of motion of the duck is given [1] [3] by

$$\underline{\mathbf{F}} = \underline{\underline{\mathbf{Z}}} \cdot \underline{\mathbf{v}} + \underline{\mathbf{W}} \cdot \mathbf{a} \tag{4}$$

where

$\underline{\mathbf{F}}$ is the force on the Duck.

$\underline{\underline{\mathbf{Z}}}$ is the impedance matrix.

$\underline{\mathbf{v}}$ is the velocity of the Duck.

$\underline{\mathbf{W}}$ is the force coefficient vector.

$\mathbf{a}$ is the incident wave amplitude.

The control matrix, $\underline{\underline{\mathbf{C}}}$, is defined such that

$$\underline{\mathbf{F}} = -\underline{\underline{\mathbf{C}}} \cdot \underline{\mathbf{v}} \tag{5}$$

The consequence of equations 4 and 5 is that the control matrix is a function of the impedance of the device. If the fixed-heave case is expressed as a function of all three degrees-of-freedom the control matrix will contain elements which approach infinity. This problem could be bypassed by expressing the equations of motion and control in terms of the device compliance (which is the inverse of impedance). However, the method used here is based on the impedance.

These infinite elements are not a problem as far as the practical control of the device is concerned, but its mathematical description is made easier if we ignore the fixed degree-of-freedom as is done in this report. Velocity is found by solving the following equation [1]

$$\underline{\mathbf{v}}_{fh} = -\left(\underline{\underline{\mathbf{C}}}_{fh} + \underline{\underline{\mathbf{Z}}}_{fh}\right) \cdot \underline{\mathbf{W}}_{fh} \cdot \mathbf{a} \tag{6}$$

where

$$\underline{\underline{\mathbf{C}}}_{fh} = \begin{bmatrix} C_{00} & C_{02} \\ C_{20} & C_{22} \end{bmatrix} \quad (7)$$

$$\underline{\underline{\mathbf{Z}}}_{fh} = \begin{bmatrix} Z_{00} & Z_{02} \\ Z_{20} & Z_{22} \end{bmatrix} \quad (8)$$

$$\underline{\mathbf{W}}_{fh} = \begin{bmatrix} W_0 \\ W_2 \end{bmatrix} \quad (9)$$

The terms C_{ij} and Z_{ij} are the elements of the i^{th} row and j^{th} column of the non-rotated standard control and impedance matrices respectively. The term W_i is the element of the i^{th} row of the non-rotated standard force coefficient vector.

This means that the control equation 5 can only give values for the pitch and surge force. Heave force is found by substituting $\underline{\mathbf{v}}_{fh}$ into equation 4.

Note that the fixed-heave case is solved using *non-rotated* standard elements. The control matrices shown in figures 25, 29 and 33 are all defined in the model-scale axes rather than full-scale axes. This is because fixed-heave control has no real compliment in the full-scale axes.

The fixed-heave system can be simplified to the set-up shown inset in figure 5(c). All the heave force is being resisted by the anchor cables. One or other of the 'pull-only' hydraulic power take-off units will therefore be slack for part of the working cycle. This makes the control discontinuous, and can raise unpleasant practical problems.

The values of force, velocity, displacement and acceleration for the fixed-heave case are given in the *full-scale* coordinates ($\gamma = -45^o$, r and $\alpha = 0$) and represent the 'working cycle' values for each power unit. Velocity is transformed using $\underline{\underline{T}}_v$, but forward/aft force is given by (surge force)$\times \cos^{-1}(\gamma)$ and the maximum dynamic force on the anchor cables is given by (heave force)$\times \cos^{-1}(\gamma)$.

The maximum dynamic force on the anchor cables is presented separately in figure 10. This force will be reduced in a non-linear manner by any forward/aft force, but will not exceed that shown in figure 10.

4.1.4 Fixed-aft constraint

Fixed-heave represents two-degree-of-freedom motion in the model-scale coordinate system. Fixed-aft represents two-degree-of-freedom motion in the full-scale coordinate system. It differs fundamentally from the fixed-heave case in that the buoyancy forces pass through the power take-off units and are not carried by anchor cables. It is potentially easier to achieve than fixed-heave, since it removes the need for a power take-off on the aft mooring lines.

The fixed-aft control matrix is given in the full-scale coordinates ($\gamma = -45^o$, r and $\alpha = 0$) but is only presented for two degrees-of-freedom, for the reasons outlined in section 4.1.3.

5 Depth correction

The test tank is of intermediate depth for the range of test frequencies used in these experiments. At low test frequencies (0.5-0.8 Hz) the tank is effectively shallow ($kh \ll 1$, where k=wavenumber and h=tank depth) and requires correction for depth dependant effects. At high test frequencies (1.2-1.5 Hz) the tank is effectively deep ($kh \gg 1$) and no correction is needed.

The optimum size of a Duck at full-scale has not yet been determined. The data in this report (together with engineering and economic data from other sources) are intended to help calculate this figure. Consequently, the data should be presented such that a change in scale can be achieved using simple multiplication factors (see appendix B and table 1), and does not require further correction for scale dependant effects.

Since the depth of the tank cannot be increased, nor the model scale decreased, without great difficulty, it is necessary to introduce correction factors which translate shallow water values into deep water values. Moreover, these deep water values should in some sense represent figures obtained from real seas. The correction factors must therefore convert values obtained for monochromatic waves of intermediate depth to those obtained for wave spectra in deep water.

There are two ways of doing this. The first is to calculate the monochromatic equivalent of a sea spectrum with energy period T_e. The spectrum shape should be chosen to represent the conditions in which the device is likely to operate. For the Duck, the spectrum will be of the Pierson-Moscowitz (P-M) type [12]. The steepness $\mathcal{W}_e$ of this equivalent wave can then be calculated and expressed as a function of frequency f $(= \frac{1}{T_e})$. $\mathcal{W}_e$ is shown in figure 7, and derived in appendix C.1.

Multiplying force per unit shallow water wave-steepness by $\mathcal{W}_e$ at a particular frequency, f, gives an approximation of the rms force on the device operating in a P-M spectrum with energy period $T_e = \frac{1}{f}$. Similarly, we can approximate the rms displacement, velocity and acceleration (see figures 11 - 20).

The second method is to calculate the spectral wave-steepness $\mathcal{W}_s$ for a particular energy period T_e (see appendix C.2 and figure 8). Multiplying force per unit shallow water wave-steepness by $\mathcal{W}_s$ generates a force spectrum for that T_e.

Figure 9 shows the force spectra for the standard case for several values of T_e. It can be seen that the spectra at the limits of the experimental frequency range are clipped, resulting in an underestimation of the rms values at those limits. When integrated, these spectra give values of rms force as a function of the T_e for those spectra. Repeating the process for displacement, velocity and acceleration gives rms displacement etc. as a function of T_e. These rms values are also shown in figures 11 - 20. They are presented as rms quantities for the standard case, and as ratios with respect to the standard case for each of the other three cases. Note that all forces are dynamic. Static buoyancy forces are not included.

The graphs of rms quantities obtained using $\mathcal{W}_s$ are smoother than those generated using $\mathcal{W}_e$.

This is to be expected, as integrating the quantity spectra to obtain rms values is a smoothing process. The values obtained by the two methods agree well, confirming the results. The clipping effect of the limited experimental frequency range applies to the spectral estimates only, and does not seem to distort the results adversely.

Both $\mathcal{W}_e$ and $\mathcal{W}_s$ are calculated for a standard P-M shape. Real seas are described by this standard shape, together with multiplication factors for fitting this shape to recorded data. Consequently, the South Uist 399 sea set (which best decribes the annual conditions in which a Duck will operate) shows a spread of wave steepnesses around this standard value (see figure 21). The 399 set is described in detail in appendix A.

It is very easy to convert the rms quantities for standard wave steepness to rms quantities for a particular sea. The magnitude of the rms quantities at standard steepness can be found from figures 11 - 20, at the power fraction corresponding to the T_e for that sea. Multpilying the standard steepness magnitude by the H_{rms} multiplier for that sea gives the rms magnitude in that sea. The mean annual 399 set steepness is approximately half standard P-M steepness. Mean annual forces, velocities etc. are therefore approximately half those shown in figures 11 - 20. However, individual seas may have steepnesses (and hence forces etc.) which are equal to or greater than those shown.

The rms quantities are expressed as a function of power fraction. This allows for an estimation of the relative effects of constraints on device performance. If, say, pitch torque is limited to a value of 30MNm^{-1} then for the standard case figure 11 shows that the device can absorb approximately 30% of the annual power available. However, if the torque limit is increased to 100MNm^{-1} with the same motion constraint the device can absorb approximately 70% of the annual power.

6 Passive control elements

The tension legs which attach the Duck to the sea bed are likely to incorporate part of the power take-off system. They may well possess some passive spring, determining their stiffness. The Duck body has inherent inertia. It is sensible to design the Duck such that these inherent elements are as beneficial as possible to its performance.

The frequency dependant coefficients in the control matrix can be approximated by simple spring, damping and inertia terms. If the inherent properties of the device can be chosen to be as close as possible to these approximate constants then they can contribute to its control. The active control system will therefore have less to do, and may well end up being cheaper as a result.

The imaginary part of the control matrix contains components due to the added inertia of the water and the hydrostatic spring of the system. The definition of $\underline{\underline{\mathbf{Z}}}$ in equation 4 is such that the imaginary part of the control matrix also includes a contribution from the device inertia. A spring term alone may not, therefore, give a good approximation to the imaginary part. A better fit will be obtained by approximating the imaginary part of the control matrix by the

sum of a spring and an inertia term. The real part of the control matrix is best approximated by a damping term.

These best-fit springs, dampings and inertias will be referred to as passive terms. In this context 'passive' is intended to indicate a term which is fixed and which may be 'built into' the device. This is as opposed to 'active' terms, which will vary with frequency, and must be provided by a control system of some description. Passive terms are defined here such that they must be non-negative, and may only exist on the leading diagonal of the control matrix (i.e. there are no passive cross-coupling terms). Active terms may be positive, negative or zero, and may exist on the off-diagonal.

The control matrix may therefore be described by;

$$\underline{\underline{C}} = \underline{\underline{C}}_P + \underline{\underline{C}}_A \tag{10}$$

where

$\underline{\underline{C}}_P$ is the passive control matrix (leading diagonal only).

$\underline{\underline{C}}_A$ is the active control matrix.

$\underline{\underline{C}}_P$ is found by applying a least-squares-fit routine (see appendix D) to the leading diagonal complex-conjugate equivalent [1] of the rotated control matrix for each case. This is because the leading diagonal equivalent matrix, whilst being potentially unstable, describes the impedance in each degree-of-freedom by a single term (as opposed to three terms per degree-of-freedom for the full control matrix). Optimising the passive values for this single term (per degree-of-freedom) is equivalent to, and easier than, optimising for all three terms in the full control matrix.

A weighting function has been used in the least-squares-fit routine. This function is the sum of the power densities of the 399 spectra (from which the power fraction is obtained) and is shown in figure 22. It represents the distribution of total annual power within the 399 spectra (see appendices A and D).

The transformed complex-conjugate control matrices are shown in figures 23 to 26. The leading diagonal complex-conjugate equivalents of the transformed control matrices are shown in figures 27 - 30. Also shown on these figures are the passive control elements, C_{ij}^P. These passive elements are summarised in tables 2 - 5. Figures 31 - 34 show the active control matrices for each case.

At present it is unlikely that passive elements will be implemented. It is expected that forces will be provided by an active system. Passive coefficients are presented in the event that they become a desirable option.

7 Benchmark efficiency

The efficiencies given in [1] are achieved using complex-conjugate synthesis. Complex-conjugate control produces optimum results but is difficult, if not impossible, to achieve. The aim of this research is to produce a stable controller which simulates complex-conjugate control as closely as possible over as wide a (useful) bandwidth as possible. A controller of this type will be referred to as a pseudo complex-conjugate controller.

The benchmark controllers described in this section are very simplistic, and are unlikely to be used to control a Duck. However, they represent a first attempt to simulate real controllers. They are capable of achieving efficiencies of 60-70% with no accounting for losses, and perhaps 80-90% efficiency when losses are accounted for. These results are promising in themselves, but the real use of a benchmark controller is to provide a datum against which all subsequent, sophisticated controllers can be compared.

One of the simplest forms of control that we can apply is to approximate the real part of the impedance matrix to a constant damping term, and the imaginary part to the sum of a constant spring and a constant inertia term. This is what was done above to obtain the passive and active control matrices, with the restriction that the best-fit terms should be non-negative and diagonal.

We can extend the idea of the simple control described in section 6 to derive two simple pseudo complex-conjugate controllers, based on spring, damping and inertia terms only. We can approximate all nine elements of the control matrix (not just leading diagonals), and allow the best-fit terms to be positive, negative or zero. This has the same effect as optimising for the leading diagonal equivalent terms only, but it means that best-fit terms can be used to describe cross couplings (whereas previous best-fit terms were by definition forbidden from being cross-couplings). Off-diagonal terms are necessary if a controller is to be effective without being unstable [1].

The first pseudo complex-conjugate controller uses twenty-seven terms in total, being a spring, a damping and an inertia in each of the nine elements of the control matrix. These terms are fixed. They are derived from a best-fit using the 399 set annual power density function as a weighting (see figure 22). It will be called the 'annual-weighting' control.

The next pseudo complex-conjugate controller also contains twenty-seven terms as above, but this time the terms are not fixed and may be varied over time. Rather than optimising for the 399 set as a whole, we can optimise for each of the 399 spectra individually. For each spectrum, the control matrix is approximated by constant coefficients using a weighting function which is the power density for that spectrum.

Spectral conditions change slowly and with a good degree of predictability. Consequently, as conditions change from a T_e of, say, 8s to a T_e of 12s it may be possible to alter the control coefficients from their optimal constant value at 8s to their optimal constant value at 12s. Hence the second pseudo controller, called the 'individual-weighting' control, uses coefficients that may remain constant for hours at a time, but which vary over a period of days.

We can now derive the efficiency of the device as a function of power fraction. The force and velocity resulting from a particular controller can be derived from knowledge of that controller, and of $\underline{\underline{\mathbf{Z}}}$, $\underline{\mathbf{W}}$ and $\mathbf{a}$ [1]. Setting $\mathbf{a}$ to 1m gives the force and velocity per unit wave amplitude, which lead to values of power per unit (wave amplitude)^2 at each frequency. When multiplied by (wavelength)^2 this gives power per unit (wave steepness)^2. Multiplying this by $\mathcal{W}_s^2$ for each of the 399 South Uist spectra gives the device power density for each spectrum, which when integrated gives the rms power absorbed by the device in that sea state. Dividing the rms absorbed power by the total power available in that spectrum over a frontage equal to the scaled width of the test tank gives an estimate of the efficiency of the control in a sea of that T_e. The test tank is 10% wider than the Duck model.

The total power available in each sea is found by integrating the sea power density function over the experimental frequency range. This may result in a slight over-estimate of efficiency, but is more valid than integrating over all frequencies to find total power. The controller is only derived and optimised over this limited range and should, therefore, only be evaluated over this range.

The figures derived by Nebel [1] on which this report is based were found to include power losses. These losses do not significantly alter force, velocity etc. but they do significantly reduce device efficiency. Both Nebel [1] and Skyner [3] describe a method for approximating the effect of these losses. The energy put into the water by a device can be equated with the energy present in the far field radiated wave. This equality enables the prediction of the real part of the radiation impedance (which gives the real part of the complex-conjugate control matrix).

Losses cause the measured real part of the impedance to be greater than the predicted real part (which better represents the true device impedance). Replacing the measured real part of the control matrix $\underline{\underline{\mathbf{C}}}$ with the predicted real part gives a control matrix $\underline{\underline{\mathbf{C}}}_r$ which in some manner accounts for the losses in the model and is therefore better able to achieve true complex-conjugate control.

The annual-weighting and the individual-weighting schemes can be applied to each of the four cases considered in this report. The process can be repeated twice for each case and each scheme: once for the figures containing losses based on the measured control matrix $\underline{\underline{\mathbf{C}}}$, and once for the 'predicted' control matrix $\underline{\underline{\mathbf{C}}}_r$ which attempts to account for losses. This gives rise to sixteen graphs.

The power fraction axis is based on the 399 set with no limit placed on the power which can be absorbed by the device. For a device to be economically viable a limit will have to be placed on this power. In the absence of complete data on the full-scale device an arbitrary limit of 100KWm^{-1} is used here.

The limit applies to power *absorbed* by the device and not to the power which is *available* to the device. A sea may have a mean power of, say, 150KWm^{-1} but if the device is 60% efficient in that sea it will only absorb 90KWm^{-1}. Hence, even though the sea has a mean power which is much graeter than the power limit the device may still be operating below its limit (with an efficiency in this case of 60%).

If the device is 80% efficient in a sea with a mean power of 150KWm^{-1} then it will absorb 120KWm^{-1} unlimited. When limited it can only absorb a maximum of 100KWm^{-1} and hence its efficiency drops from an unlimited value of 80% to a limited value of 66.66% (assuming it can absorb all the power up to this limit).

If each of the sixteen graphs described above is drawn as a function of both unlimited and limited power fraction we will end up with a total of thirty-two estimates of maximum device efficiency. The total efficiencies based on the individual-weighting scheme are presented for each of the four cases in figures 35 and 38. The variation in total efficiency with power-limit and with application of the annual-weighting scheme are only presented for the standard case (see figures 39 - 40), and can be estimated for the other three cases by comparison with these results. Note that here the power limit shown in figure 39 is applied to *total* power only and not to the power absorbed individually by each degree-of-freedom.

Pizer [6] has shown that for three degree-of-freedom control the true control matrix (with losses accounted for) is singular. This singularity occurs because of the dependance between heave and surge, or between forward and aft, and gives a real part to the matrix which has no inverse. The values of force and velocity it produces are unrealistic. However, if we choose a case in which either heave/forward or surge/aft are fixed then the singularity ceases to present a problem.

The effect of loss accounting on efficiency are therefore presented for the fixed-aft case in figure 41. At higher wave periods the efficiencies for this case exceed 100%, which should not be possible since efficiency is based on the (scaled) width of the test tank and not on the width of the device. The reason for this is that the losses are estimated, not measured. The experimental system becomes non-linear at high periods (i.e. low frequencies), and hence loss estimates are likely to be least accurate in this region.

The best-fit coefficients for the application of annual-weighting control for the standard case are presented in table 6. The variation of spring, damping and inertia with non-limited power fraction for the application of standard individual-weighting control with no correction for power loss is shown in figures 46 - 48. The efficiency in each degree-of-freedom for the application of individual-weighting control with no correction for power loss and no power limit is shown in figures 42 - 45.

Efficiencies are underestimated because they include model-scale losses which may not be present at full-scale. However, they are over-estimates because they are calculated over a narrow band-width, and because they do not include the effects of spectrum directionality. The net effect is likely to be a slight over-estimate of efficiency.

The stability (and hence practicality) of annual and individual-weighting control is yet to be established. The 10% improvement in mean efficiency offered by individual-weighting control over annual-weighting may well justify the extra complication it requires. Either of these strategies would provide a good platform from which to develop more sophisticated controllers.

These figures assume linearity. Note that since efficiency is based on the scaled width of the test tank, and not on the width of the device, it cannot exceed 100% (This restriction will not apply to future work in a wide tank).

8 Tables and figures

PARAMETER	INDEX OF SCALE
Wave height and length	1
Period	0.5
Frequency	-0.5
Pitch angle	0
Angular Velocity	-0.5
Angular acceleration	-1
Buoyancy	3
Inertial forces	3
Velocity forces	3
Drift forces	3
Torque	4
Power	3.5
Power per unit length	2.5
Force per unit length	2
Torque per unit length	3
Mass	3
Inertia per unit length	4
Buoyancy spring per unit length	3
Damping per unit length	3.5
Heave and surge distances	1
Heave and surge velocities	0.5
Heave and surge accelerations	0

Table 1: Scale factors

DEGREE-OF-FREEDOM	COEFFICIENT		
	Spring	Damping	Inertia
Pitch	0.0 ($MNmrad^{-1}$)	223.16 ($MNmsrad^{-1}$)	0.0 ($MNms^2rad^{-1}$)
Forward	1.2065 (MNm^{-1})	6.0075 ($MNsm^{-1}$)	0.0 (MNs^2m^{-1})
Aft	0.338572 (MNm^{-1})	0.0 ($MNsm^{-1}$)	0.0 (MNs^2m^{-1})

Table 2: Passive control coefficients for standard control

DEGREE-OF-FREEDOM	COEFFICIENT		
	Spring	Damping	Inertia
Pitch	0.0 ($MNmrad^{-1}$)	88.04 ($MNmsrad^{-1}$)	0.0 ($MNms^2rad^{-1}$)
Forward	0.58017 (MNm^{-1})	4.185 ($MNsm^{-1}$)	0.0 (MNs^2m^{-1})
Aft	0.338583 (MNm^{-1})	0.0 ($MNsm^{-1}$)	0.0 (MNs^2m^{-1})

Table 3: Passive control coefficients for translated-axis control

DEGREE-OF-FREEDOM	COEFFICIENT		
	Spring	Damping	Inertia
Pitch	0.0 ($MNmrad^{-1}$)	59.592 ($MNmsrad^{-1}$)	0.0 ($MNms^2rad^{-1}$)
Surge	2.826 (MNm^{-1})	0.0 ($MNsm^{-1}$)	0.0 (MNs^2m^{-1})

Table 4: Passive control coefficients for fixed-heave control

DEGREE-OF-FREEDOM	COEFFICIENT		
	Spring	Damping	Inertia
Pitch	0.0 ($MNmrad^{-1}$)	5.057 ($MNmsrad^{-1}$)	0.0 ($MNms^2rad^{-1}$)
Forward	1.4364 (MNm^{-1})	1.744 ($MNsm^{-1}$)	0.0 (MNs^2m^{-1})

Table 5: Passive control coefficients for fixed-aft control

DEGREE-OF-FREEDOM	COEFFICIENT		
	Spring	Damping	Inertia
P tor./P vel.	-58.942 ($MNmrad^{-1}$)	22.61 ($MNmsrad^{-1}$)	-82.86 ($MNms^2rad^{-1}$)
P tor./F vel.	5.5346 (MN)	-3.5439 (MNs)	13.77 (MNs^2)
P tor./A vel.	6.925 (MN)	-0.01623 (MNs)	-1.79 (MNs^2)
F force/P vel.	6.1624 ($MNrad^{-1}$)	-3.95 ($MNsrad^{-1}$)	14.51 (MNs^2rad^{-1})
F force/F vel.	-0.9023 (MNm^{-1})	1.465 ($MNsm^{-1}$)	-7.668 (MNs^2m^{-1})
F force/A vel.	-1.5612 (MNm^{-1})	-0.4186 ($MNsm^{-1}$)	0.3098 (MNs^2m^{-1})
A force/P vel.	6.987 ($MNrad^{-1}$)	0.338 ($MNsrad^{-1}$)	-1.94 (MNs^2rad^{-1})
A force/F vel.	-1.552 (MNm^{-1})	-0.4472 ($MNsm^{-1}$)	0.37525 (MNs^2m^{-1})
A force/A vel.	-1.223 (MNm^{-1})	0.7045 ($MNsm^{-1}$)	-5.3834 (MNs^2m^{-1})

Table 6: Best-fit coefficients for standard annual-weighting control

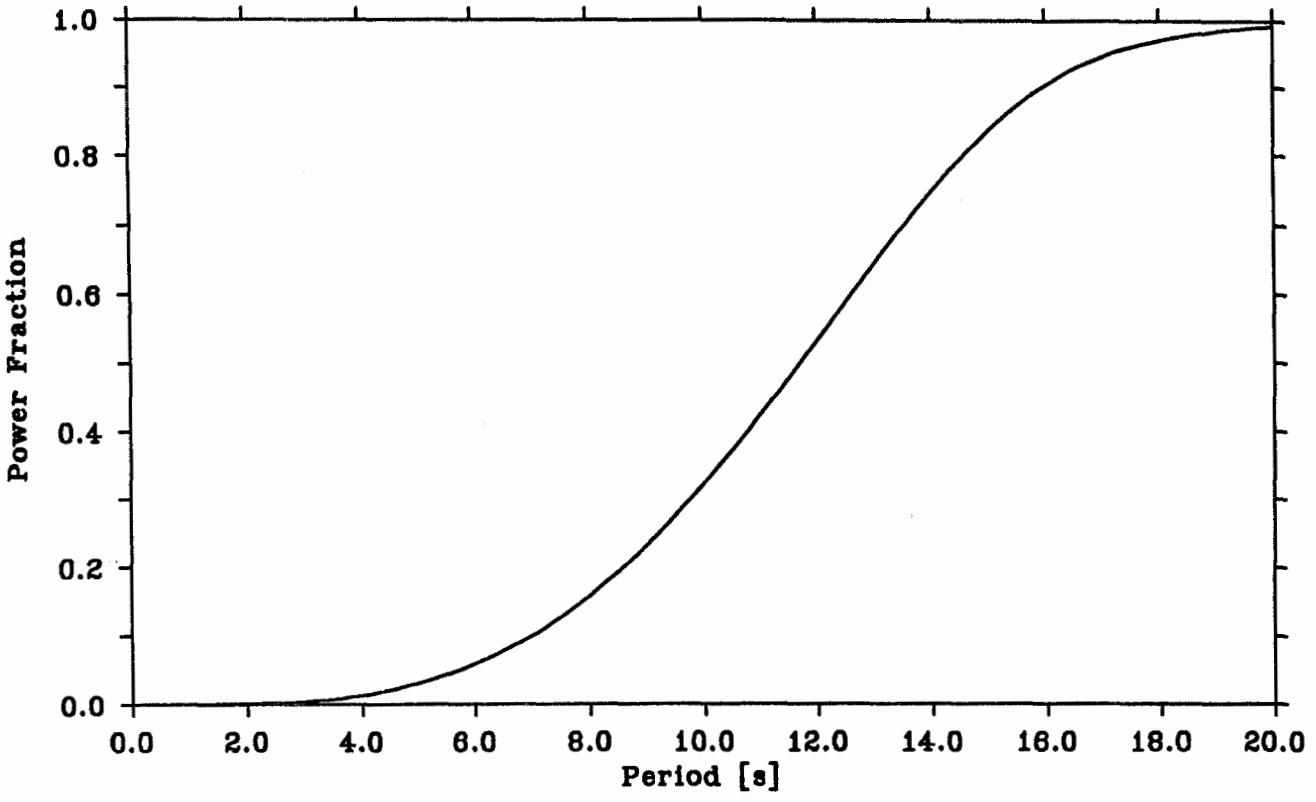

FIGURE 1(a): Power fraction vs wave period

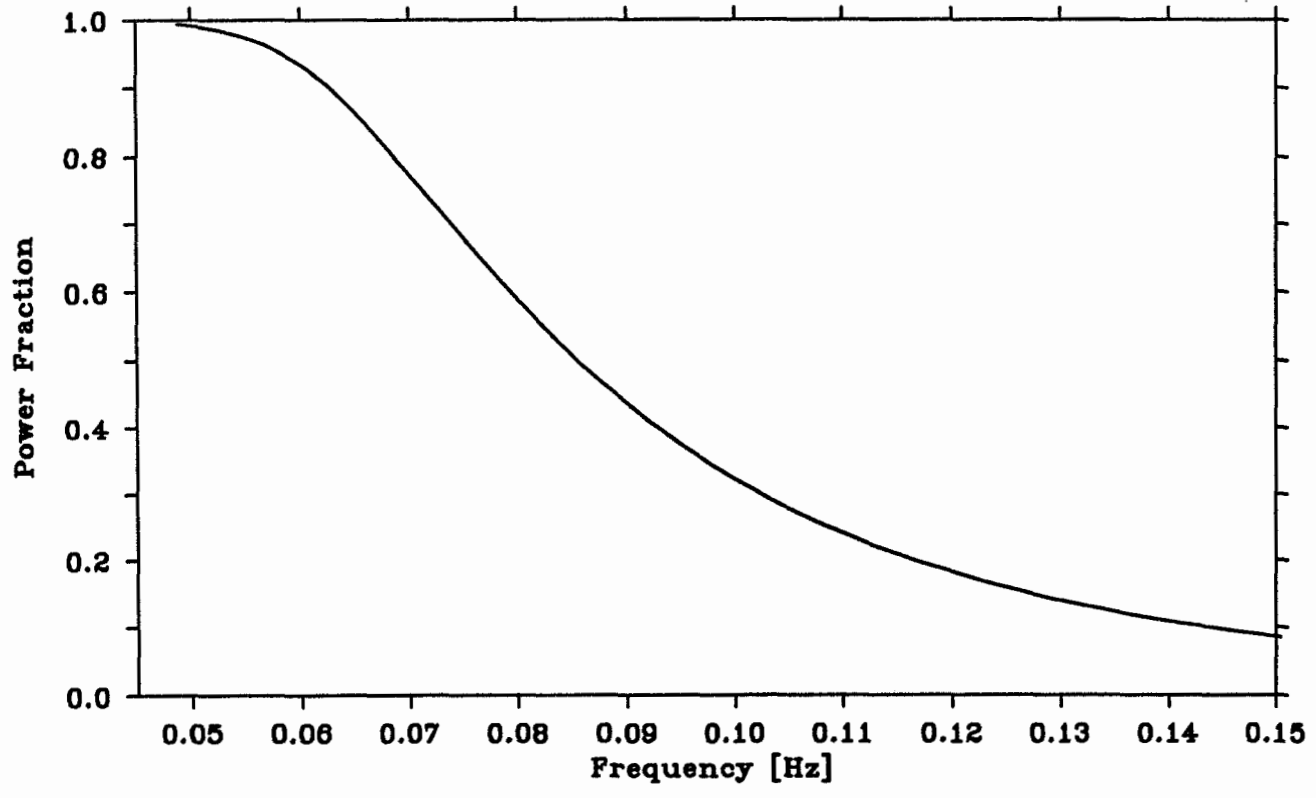

FIGURE 1(b): Power fraction vs wave frequency

Note: All diagrams are schematic

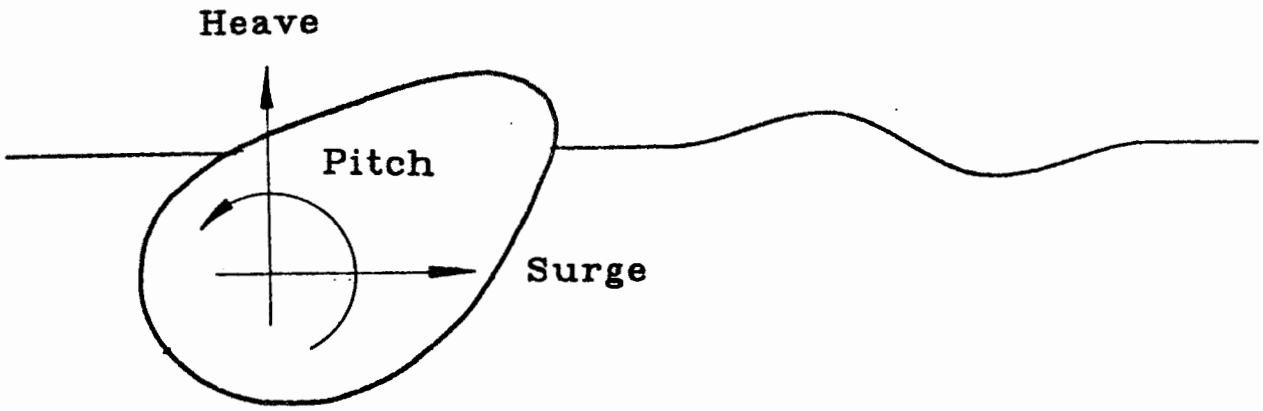

Figure 2: Model-scale co-ordinate system.

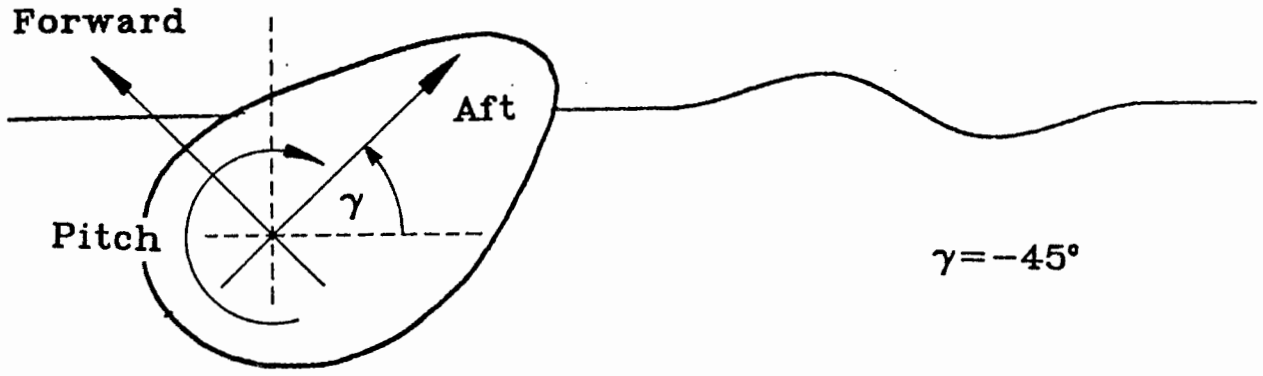

Figure 3: Full-scale co-ordinate system.

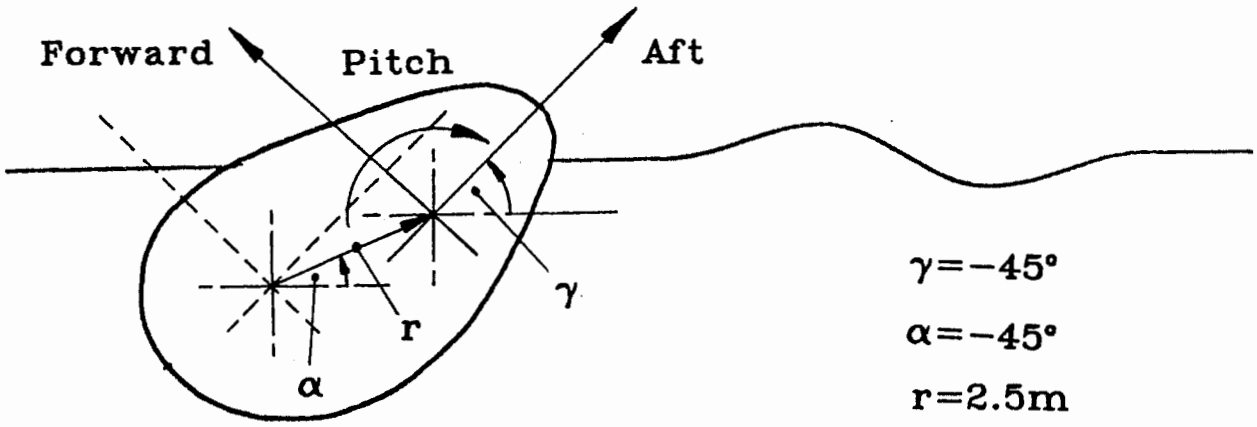

Figure 4: Translated-axis co-ordinate system.

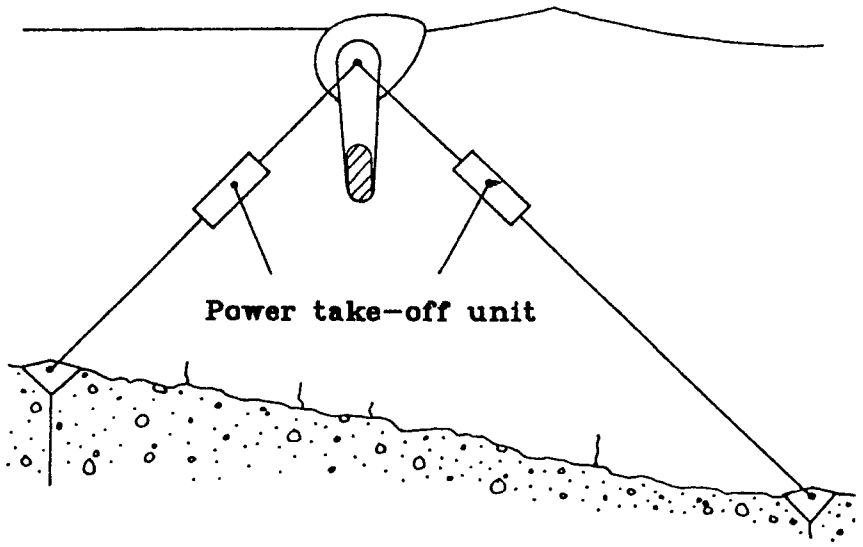

Figure 5(a): Standard case.

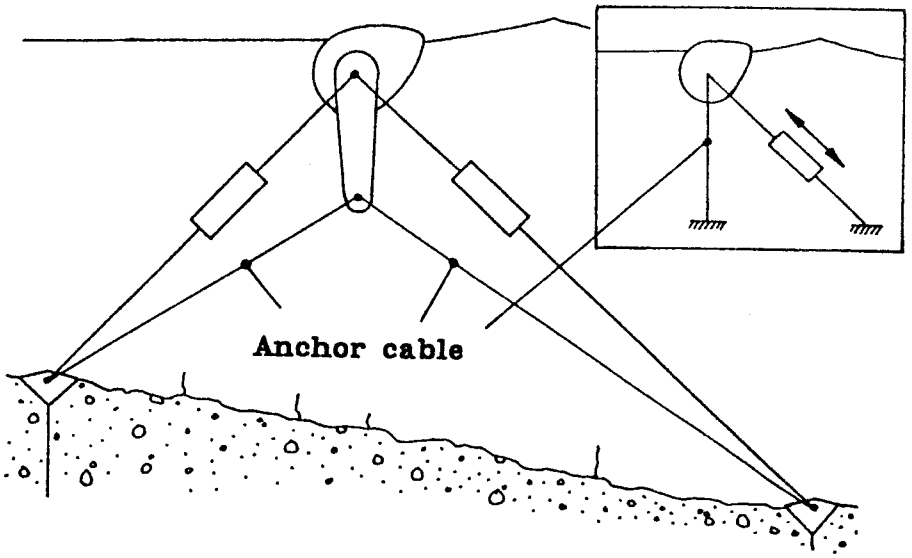

Figure 5(c): Fixed-heave case.

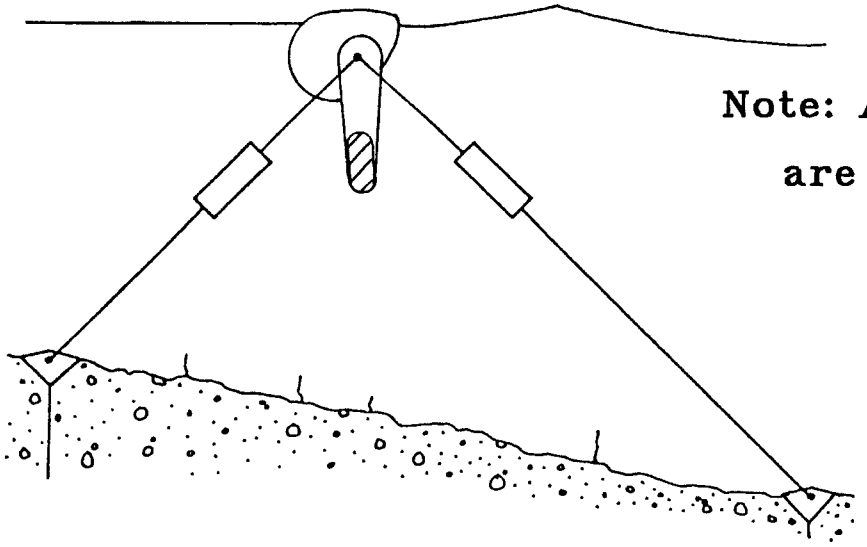

Figure 5(b): Translated-axis case.

Note: All diagrams are schematic

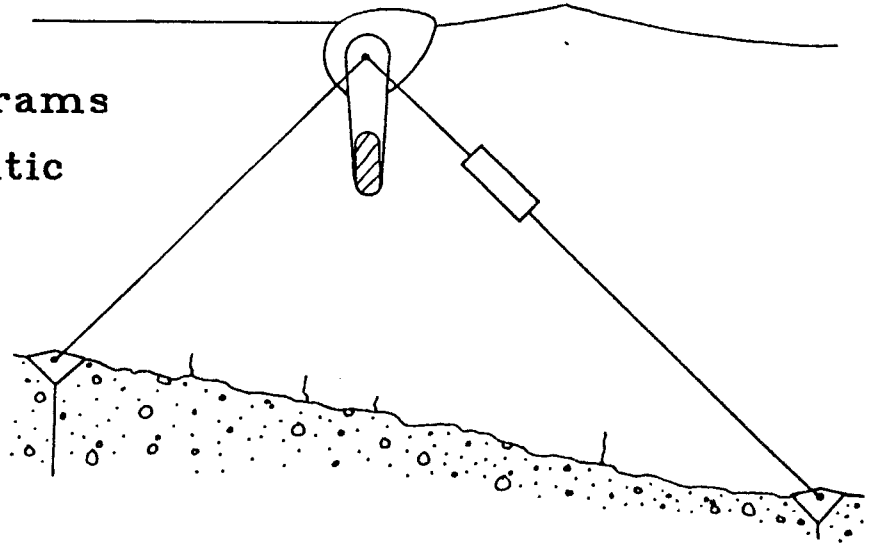

Figure 5(d): Fixed-aft case.

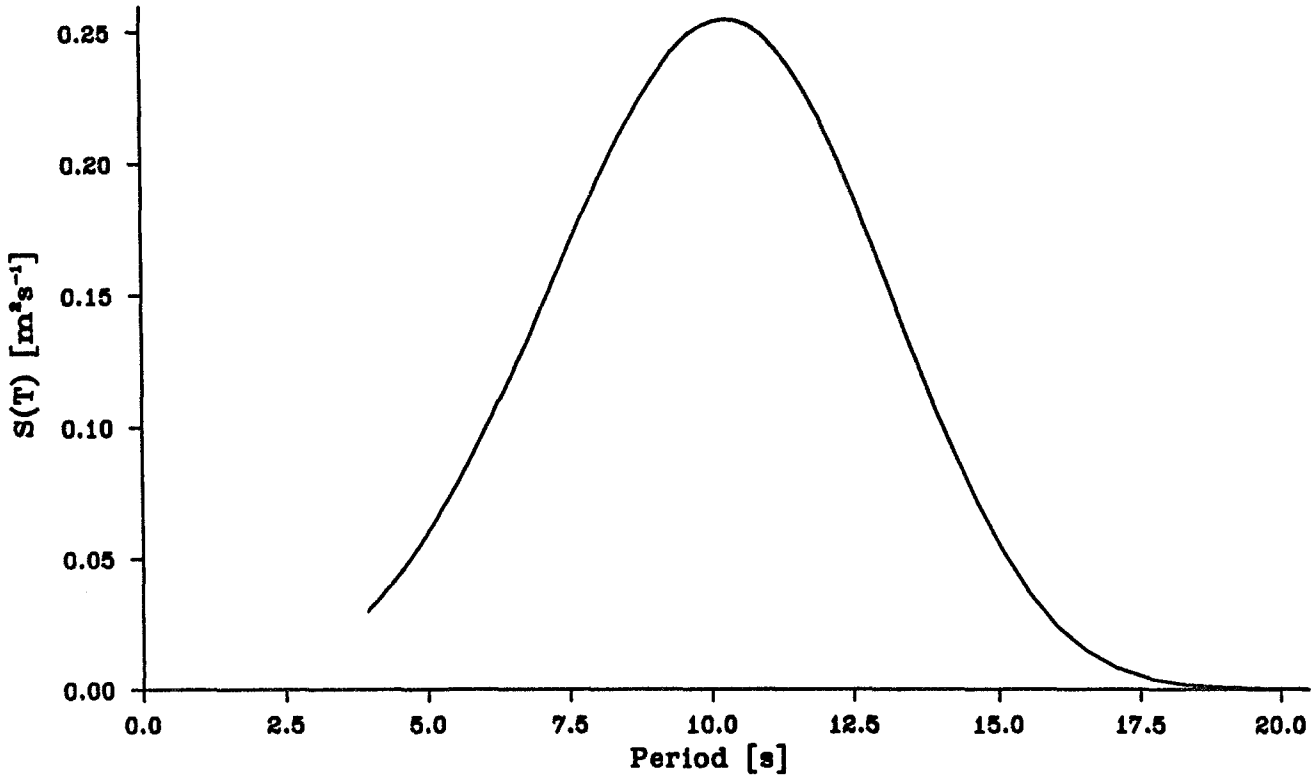

FIGURE 6(a): A typical P–M spectrum (Te=10s) vs period.

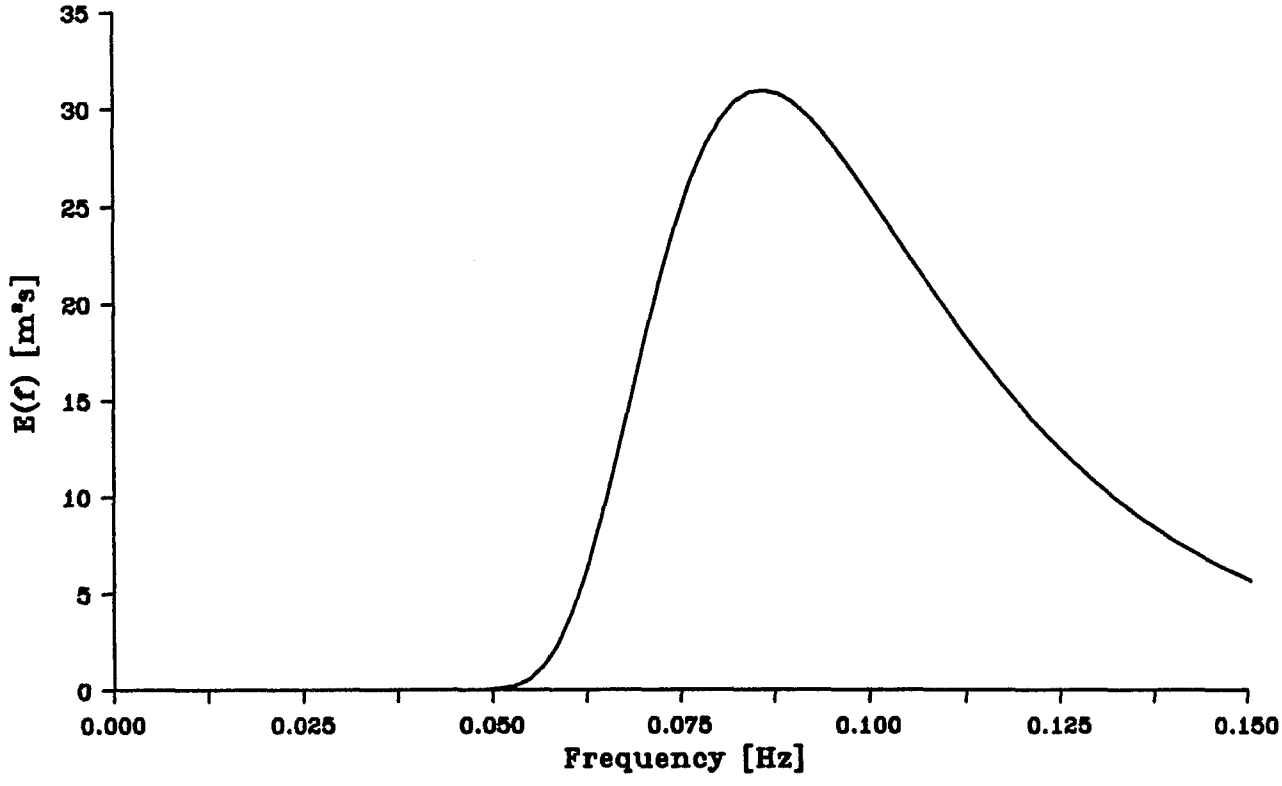

FIGURE 6(b): A typical P–M spectrum (Te=10s) vs frequency.

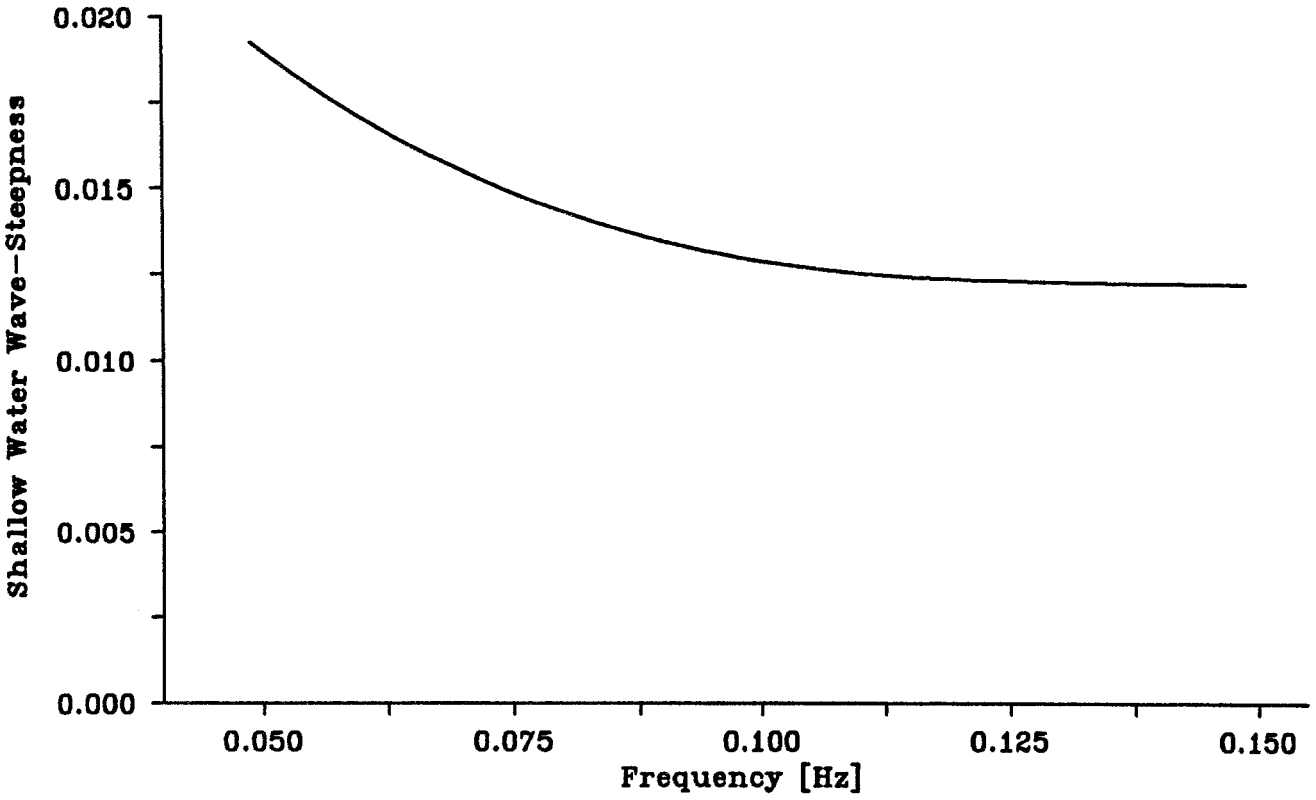

FIGURE 7: Shallow water steepness of monochromatic Pierson-Moscowitz equivalent waves.

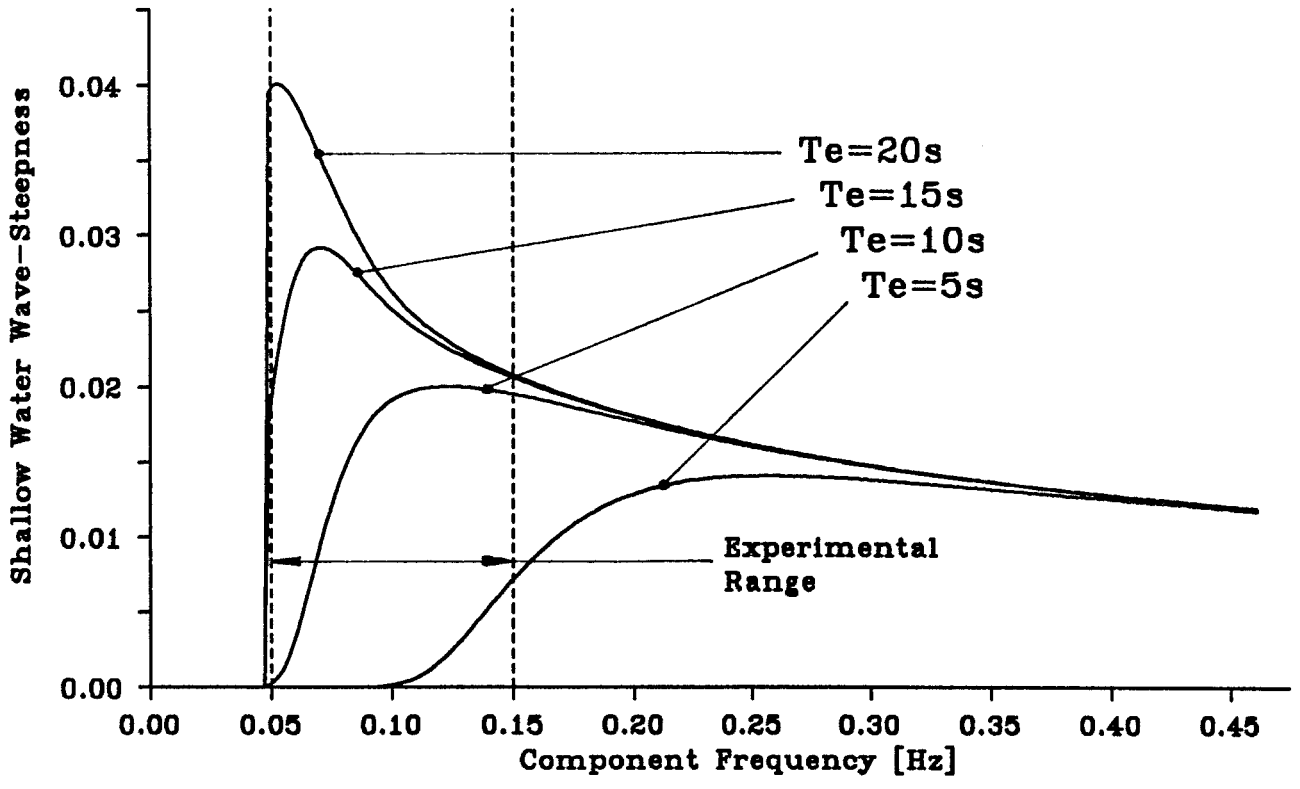

FIGURE 8: Shallow water wave-steepness spectra for Pierson-Moscowitz seas.

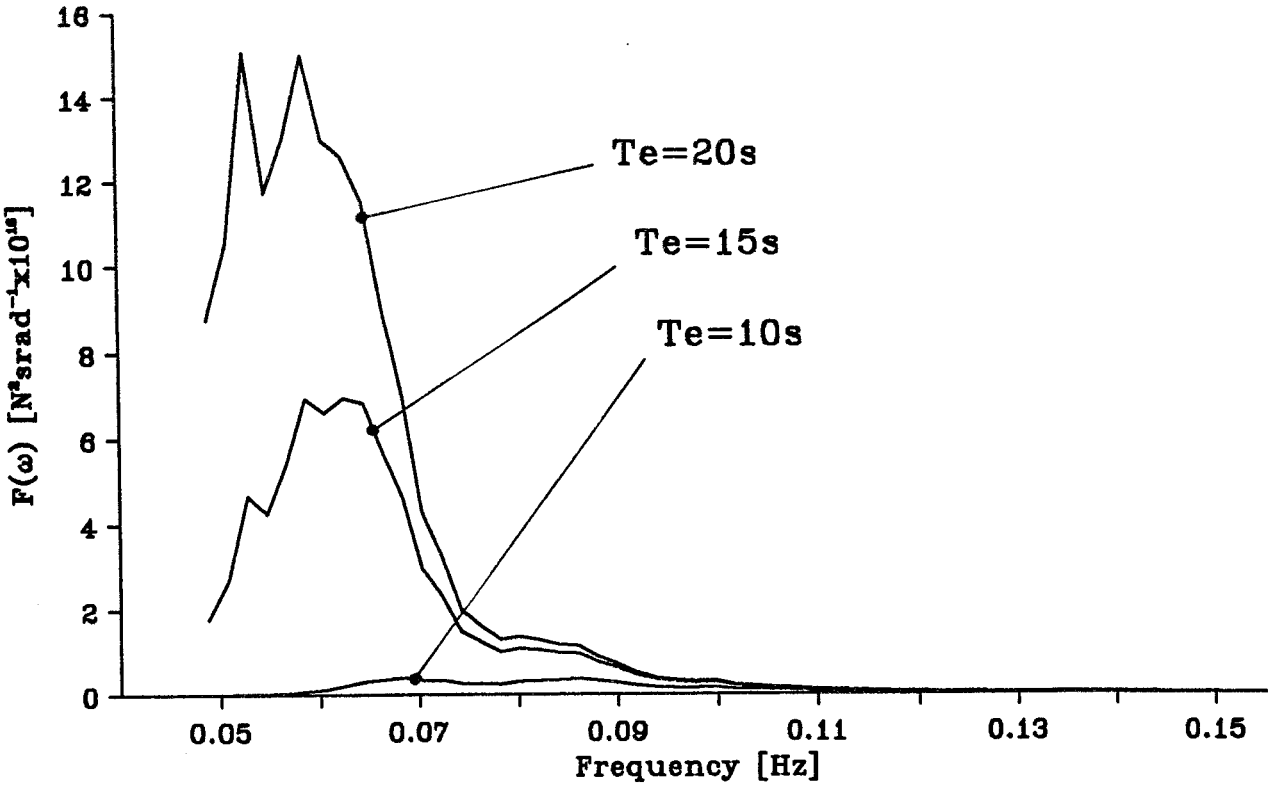

FIGURE 9: Heave force spectra for Standard control in standard P–M seas.

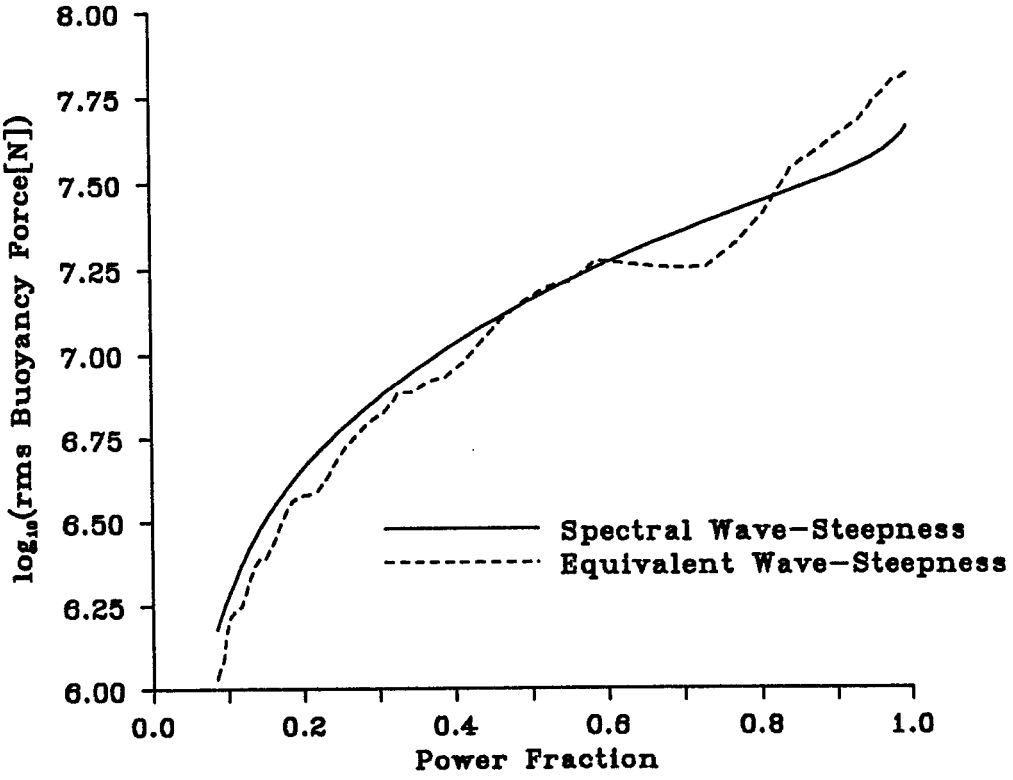

FIGURE 10: rms Buoyancy force for Fixed–Heave control in P–M seas.

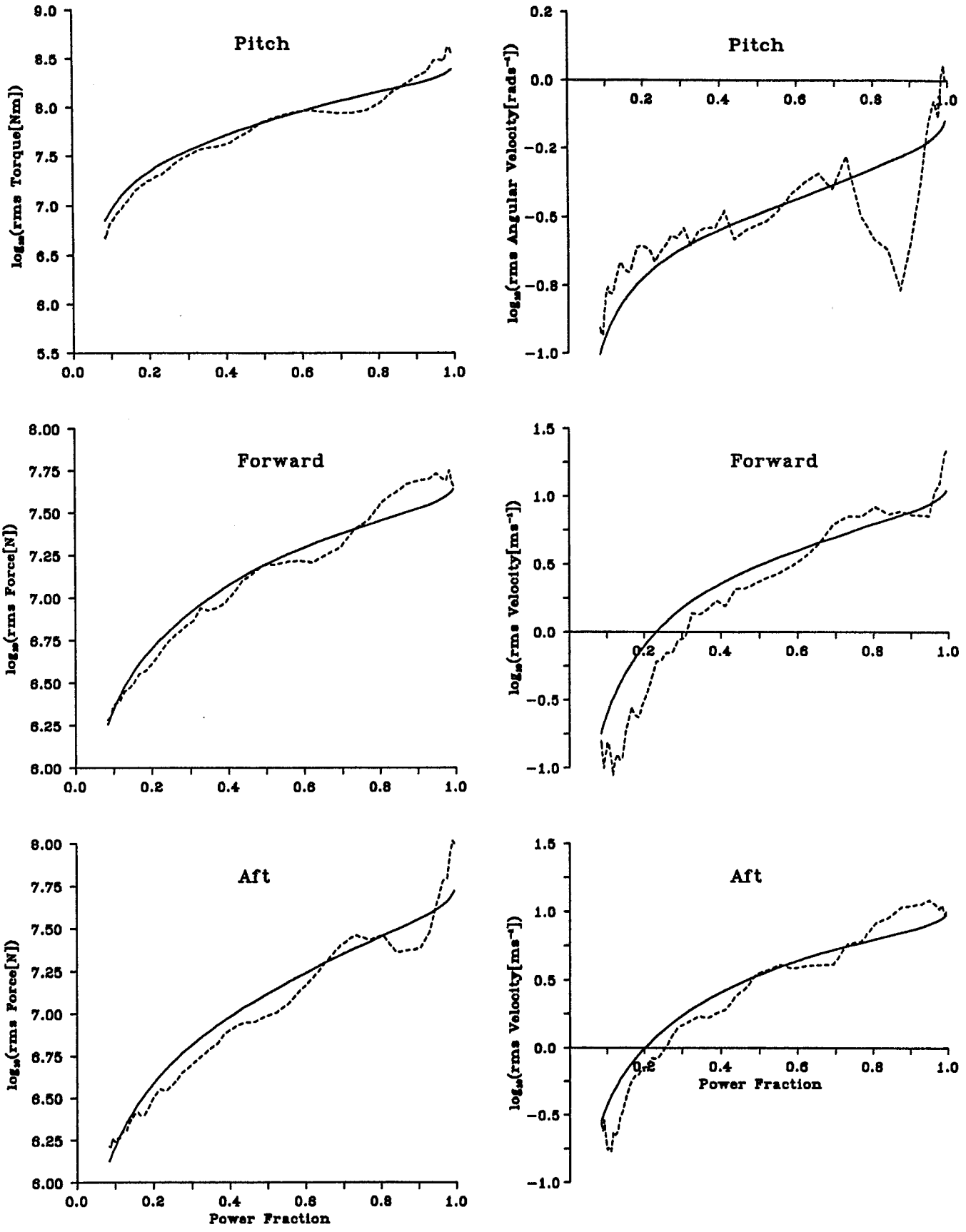

Note: All values are for a 10m dia. device in deep water

FIGURE 11: $\log_{10}$(rms Force) for Standard complex-conjugate control in P-M seas

FIGURE 12: $\log_{10}$(rms Velocity) for Standard complex-conjugate control in P-M seas

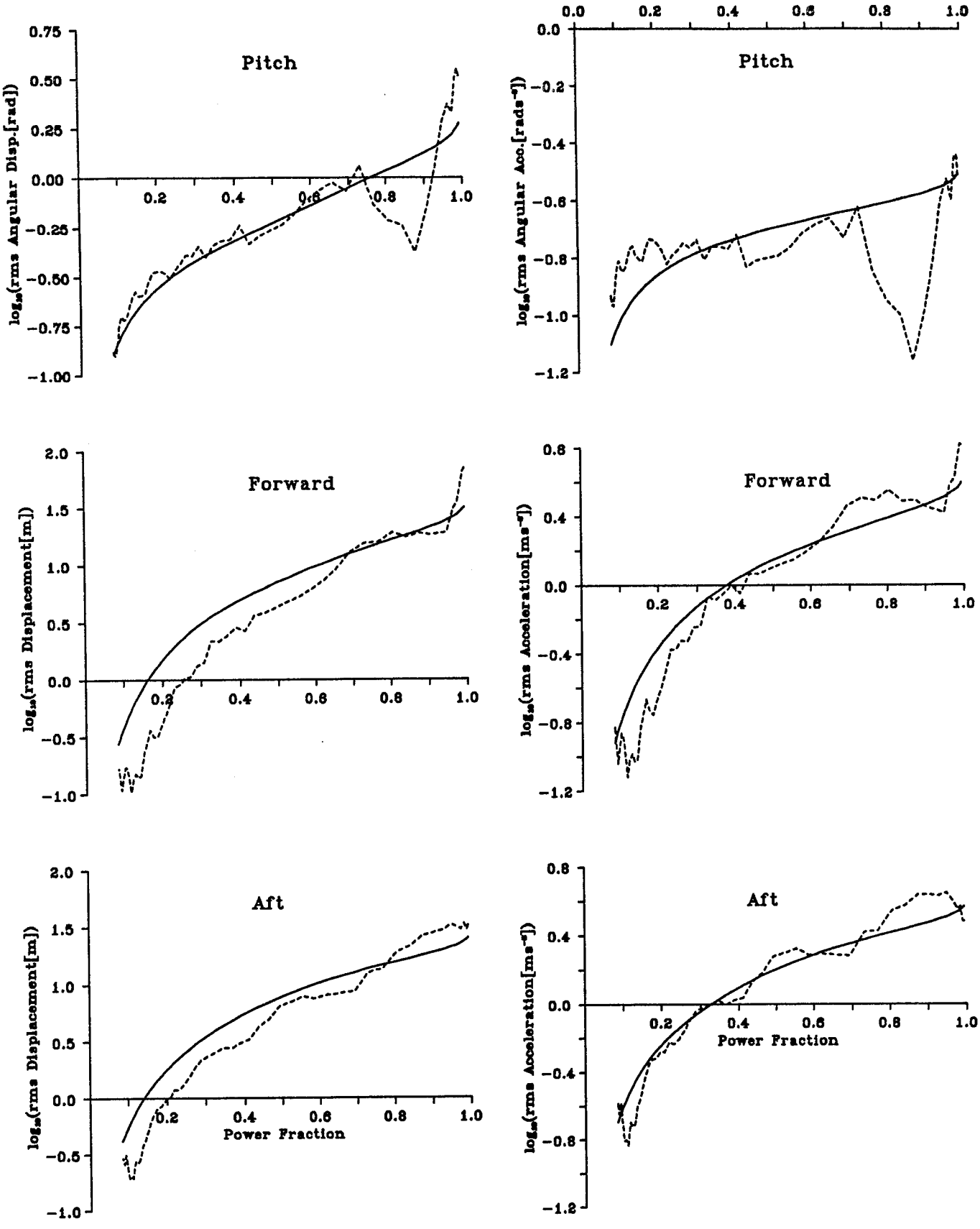

FIGURE 13: $\log_{10}$(rms Displacement) for Standard complex-conjugate control in P-M seas

FIGURE 14: $\log_{10}$(rms Acceleration) for Standard complex-conjugate control in P-M seas

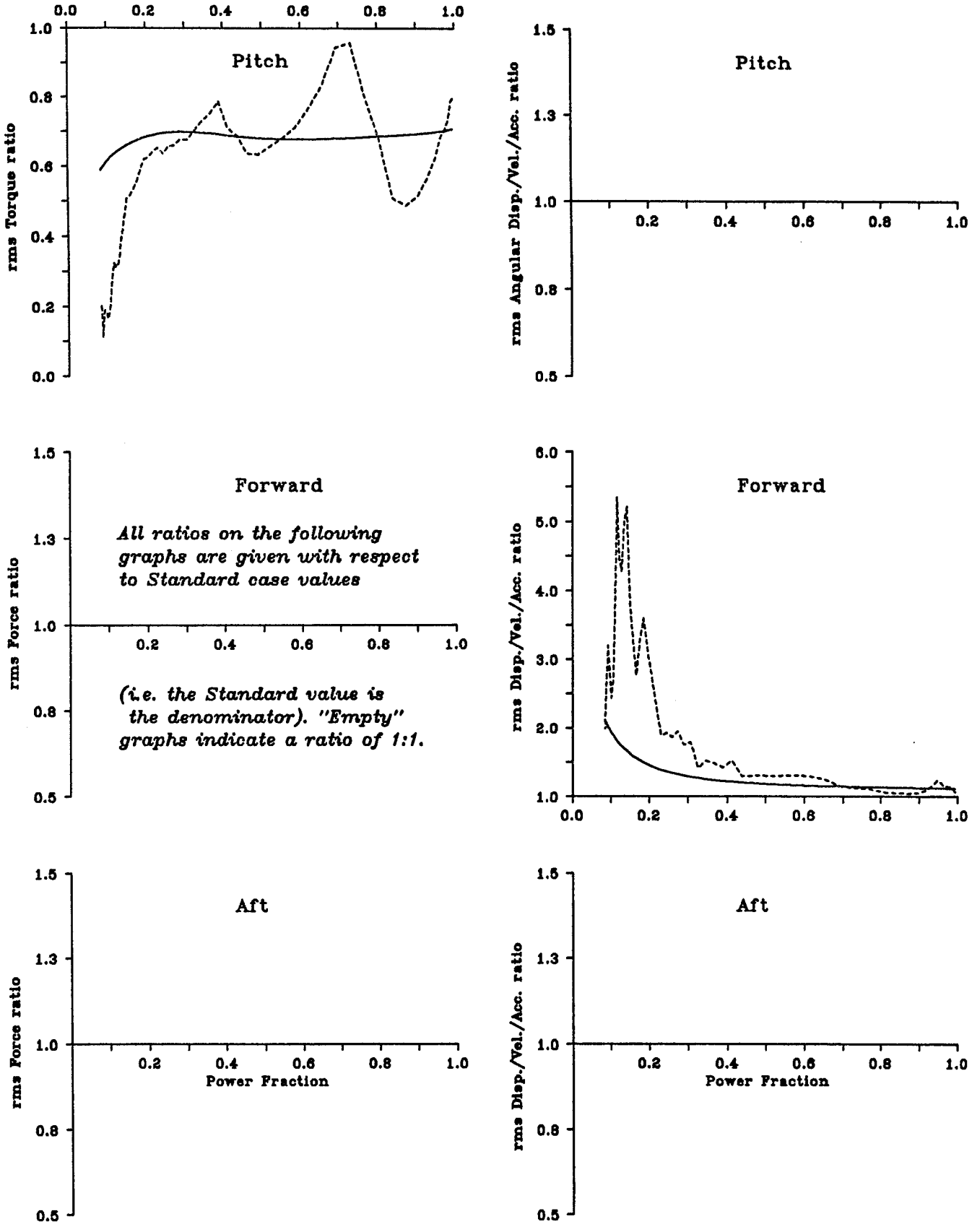

Spectral Wave-Steepness

Equivalent Wave-Steepness

Note: All values are for a 10m dia. device in deep water

FIGURE 15: rms Force ratio for Translated-axis complex-conjugate control in P-M seas

FIGURE 16: rms Displacement, Velocity and Acceleration ratios for Translated-Axis complex-conjugate control in P-M seas

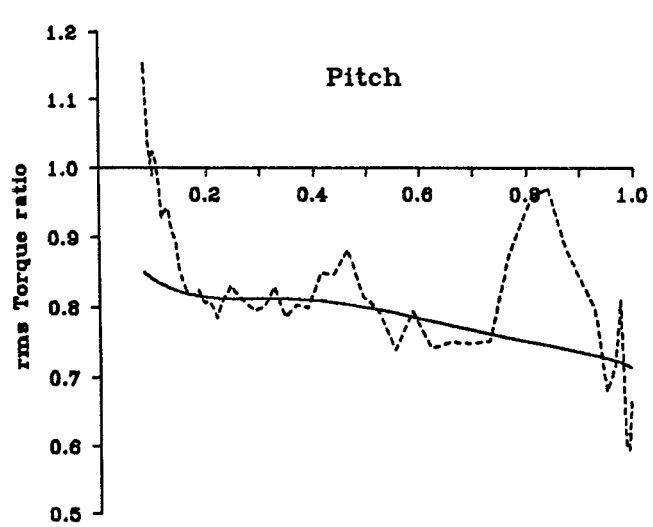

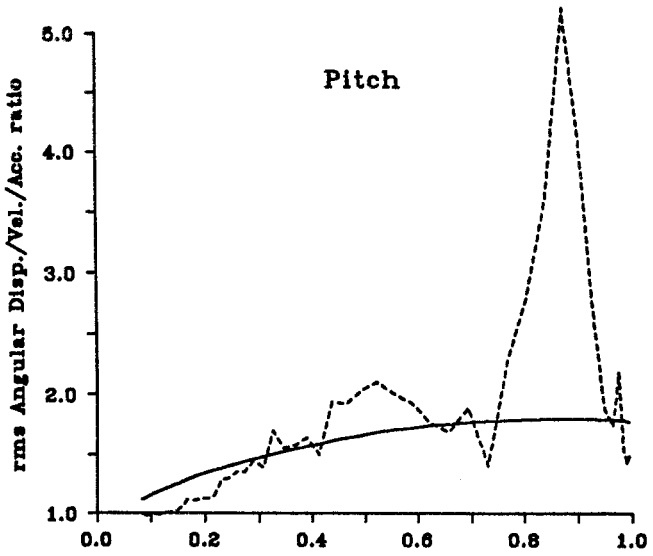

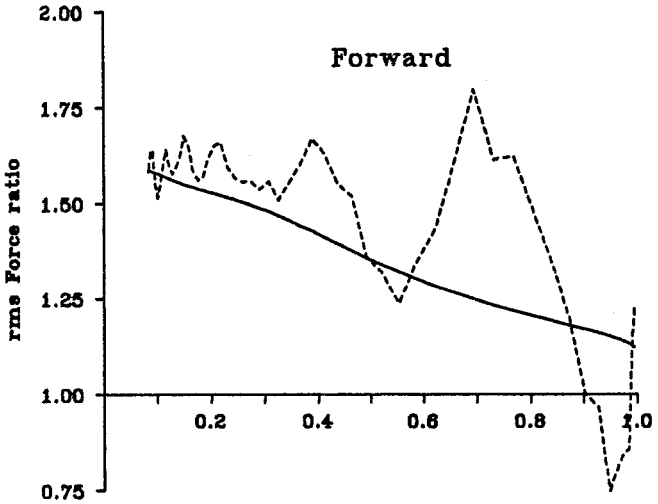

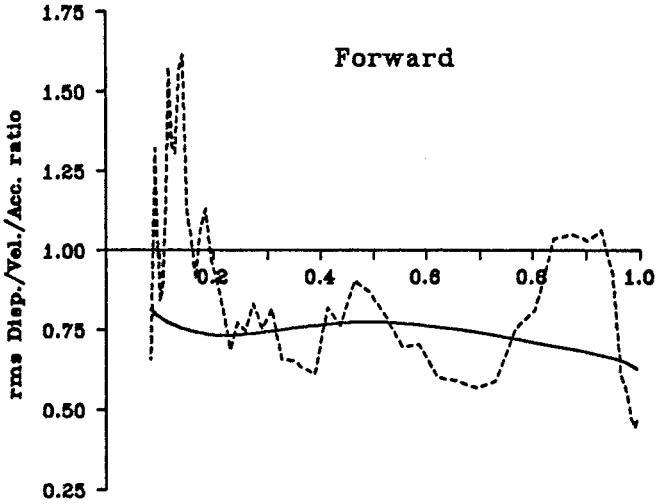

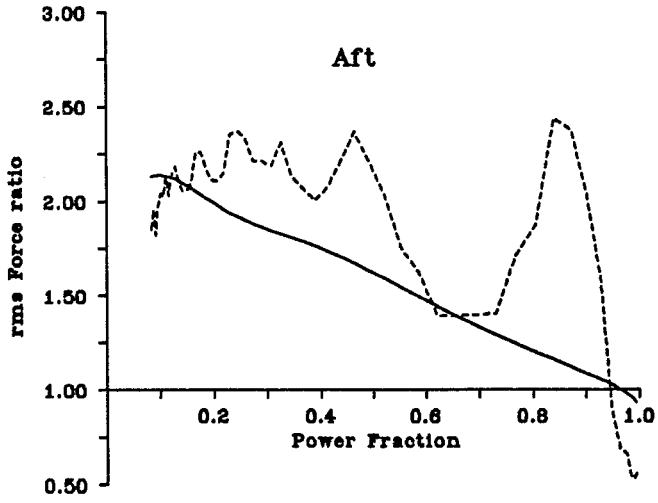

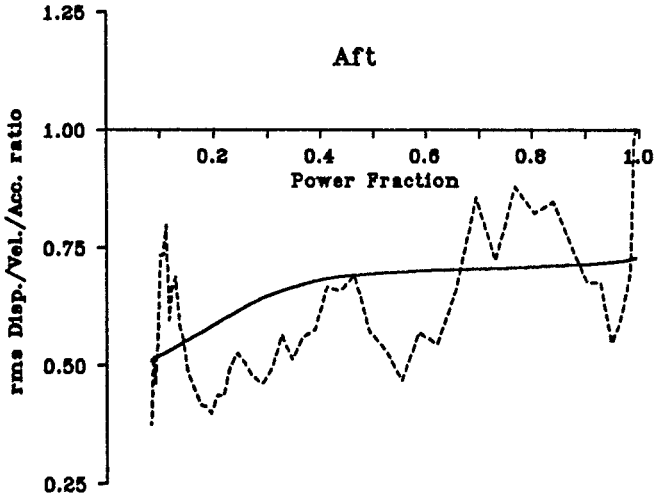

Spectral Wave-Steepness
Equivalent Wave-Steepness

Note: All values are for a 10m dia. device in deep water

FIGURE 17: rms Force ratio for Fixed-Heave complex-conjugate control in P-M seas

FIGURE 18: rms Displacement, Velocity and Acceleration ratios for Fixed-Heave complex-conjugate control in P-M seas

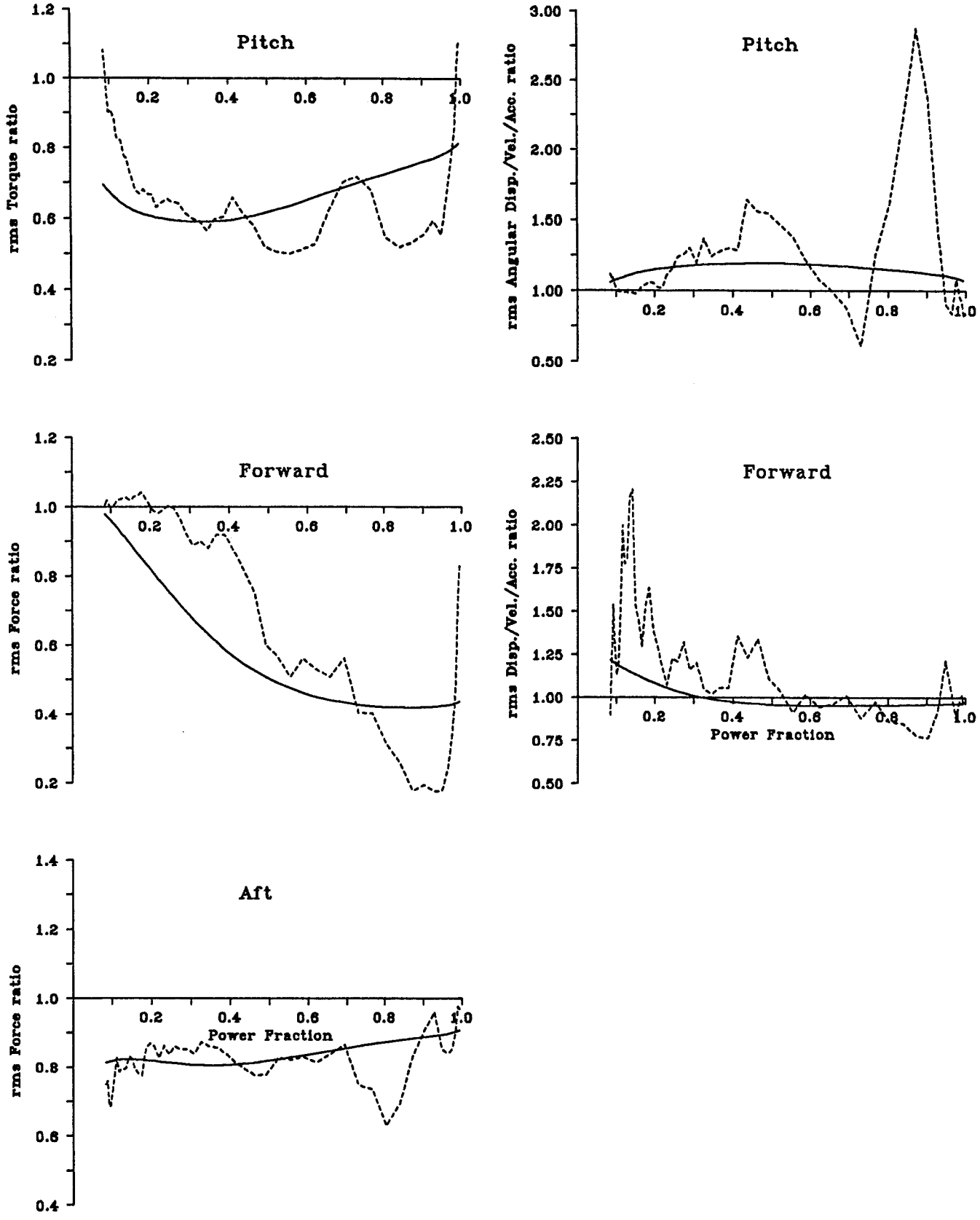

FIGURE 19: rms Force ratio for Fixed-Aft complex-conjugate control in P-M seas

FIGURE 20: rms Displacement, Velocity and Acceleration ratios for Fixed-Aft complex-conjugate control in P-M seas

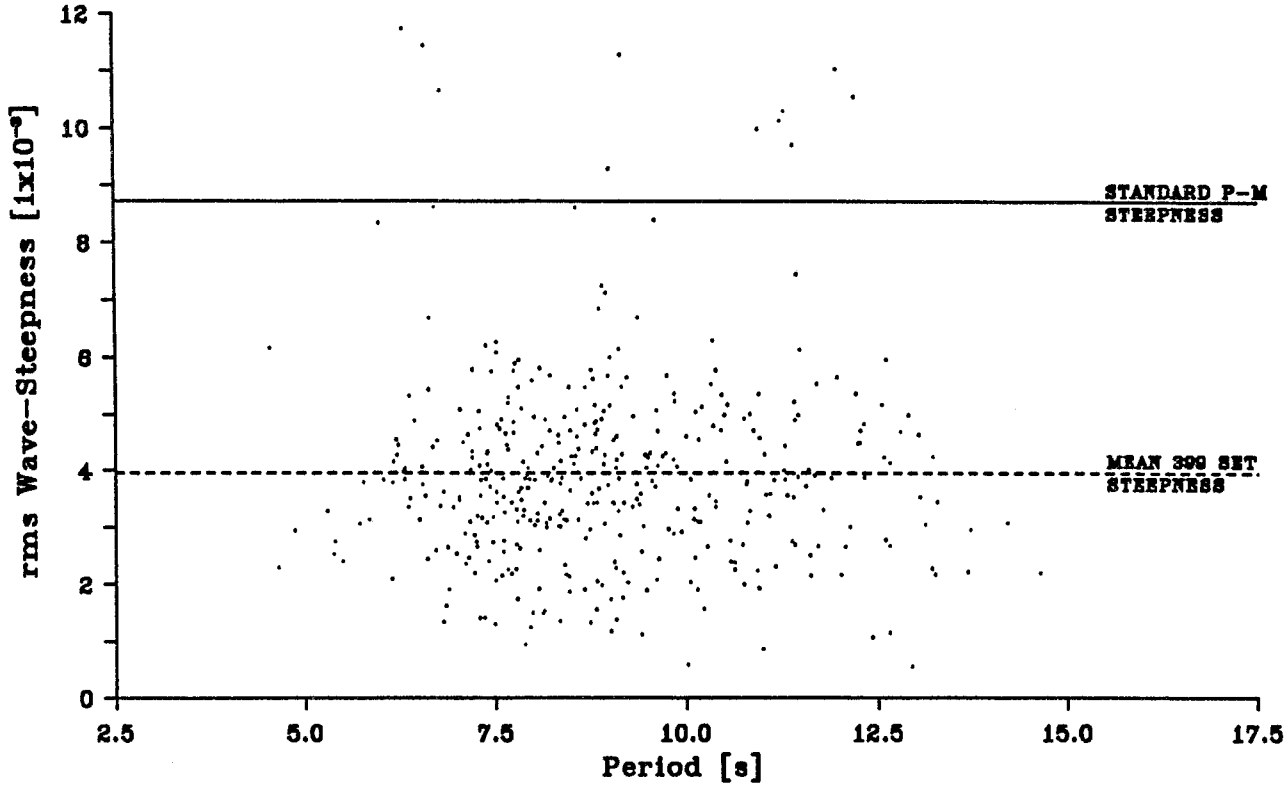

FIGURE 21: Scatter diagram showing the rms wave-steepness of the South Uist 399 set.

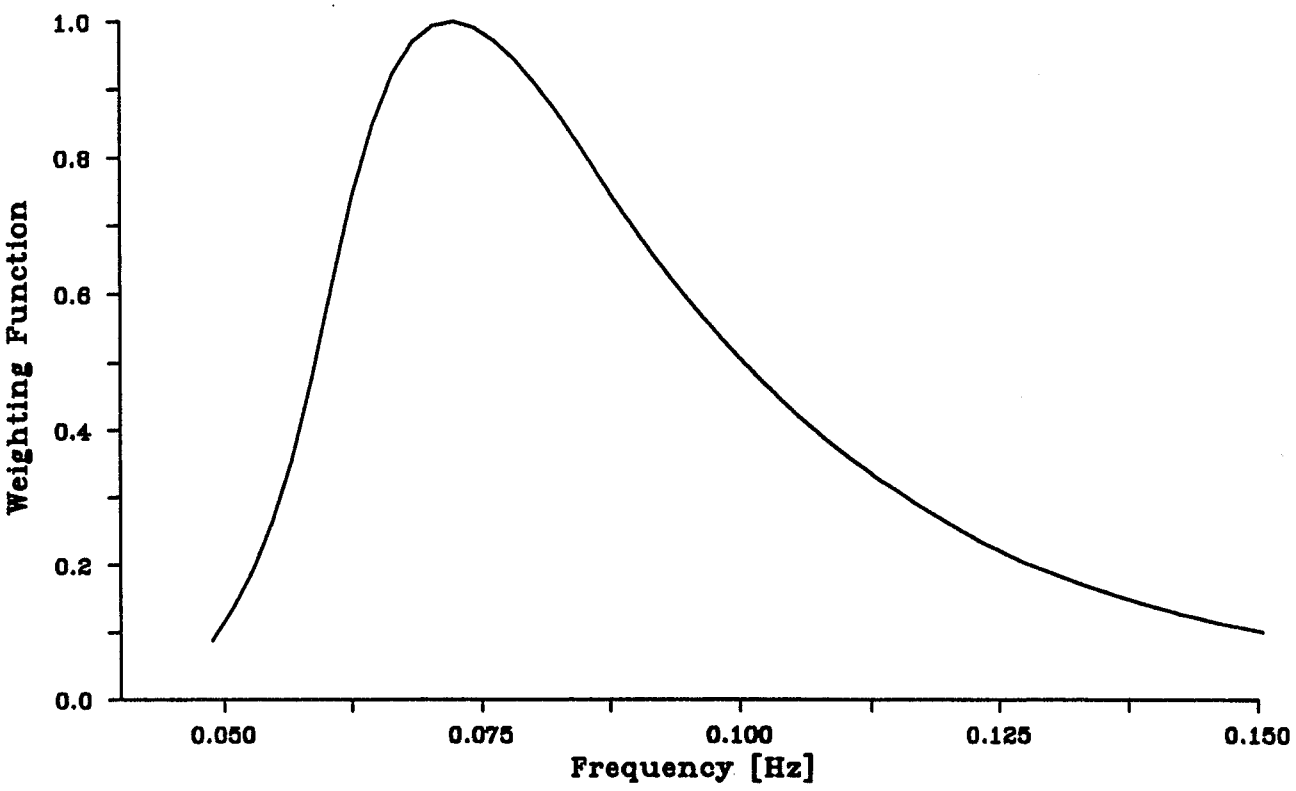

FIGURE 22: Weighting function for 'Annual-Weighting' control.

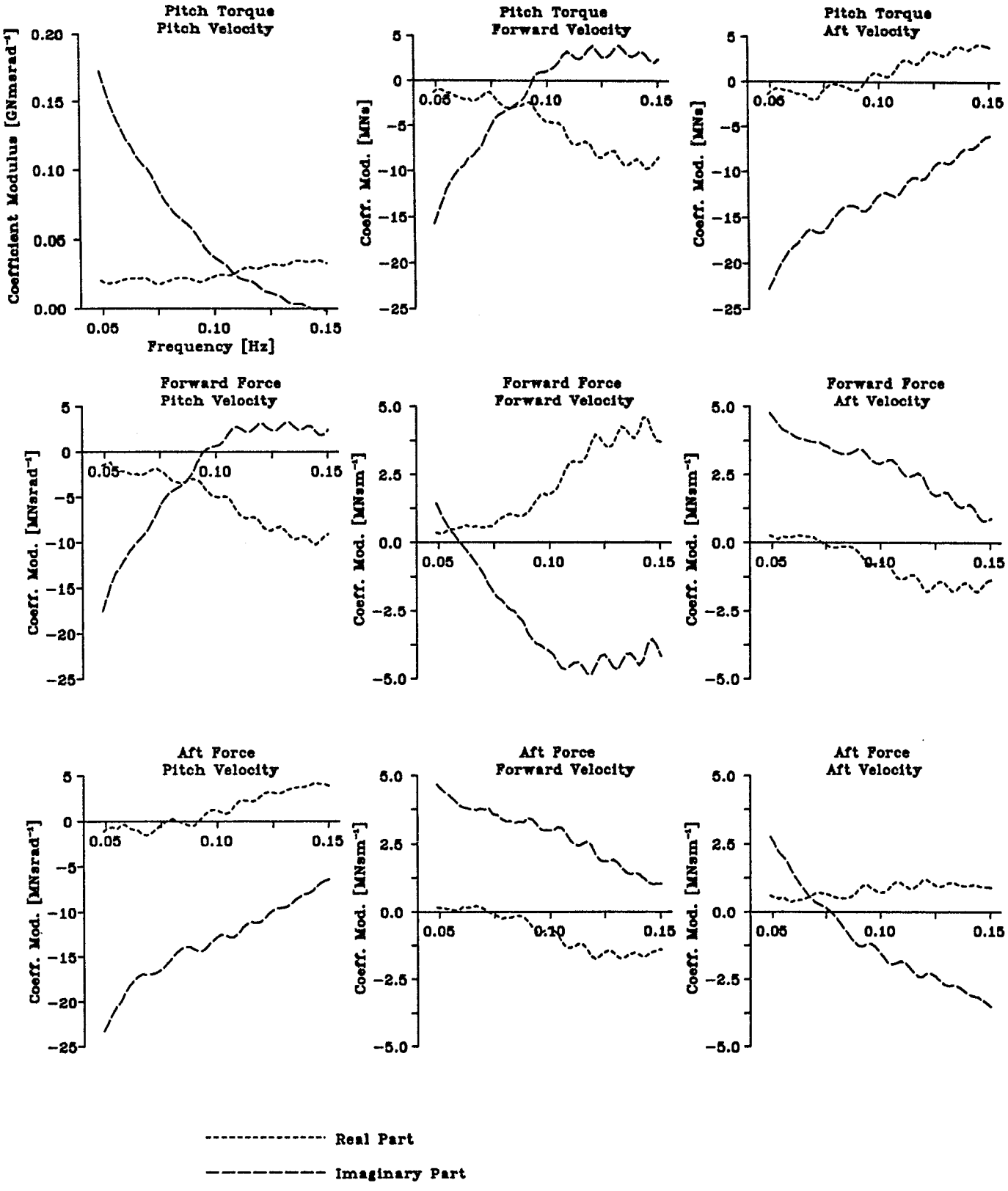

FIGURE 23: Standard complex-conjugate control matrix

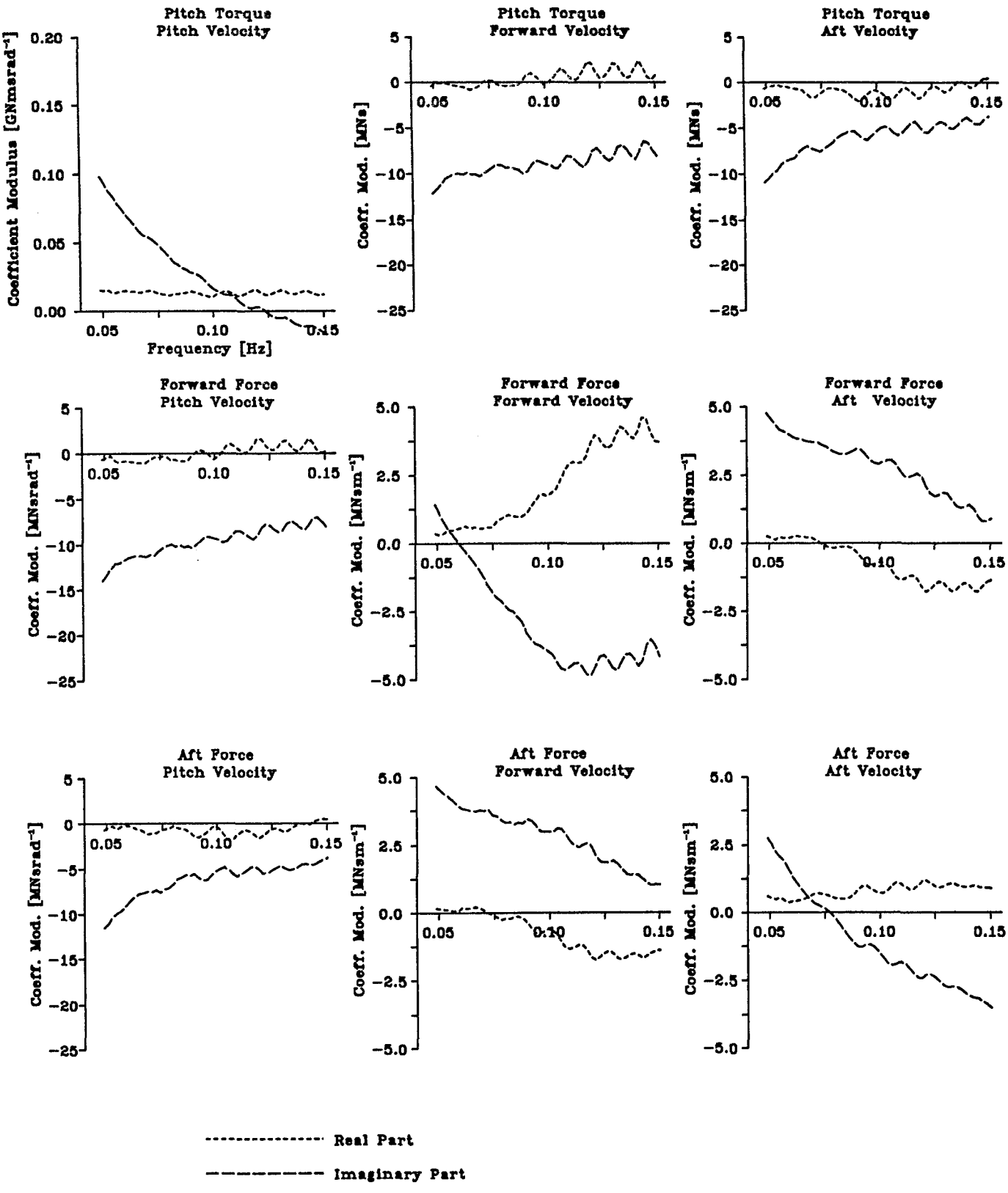

FIGURE 24: Translated–Axis complex–conjugate control matrix

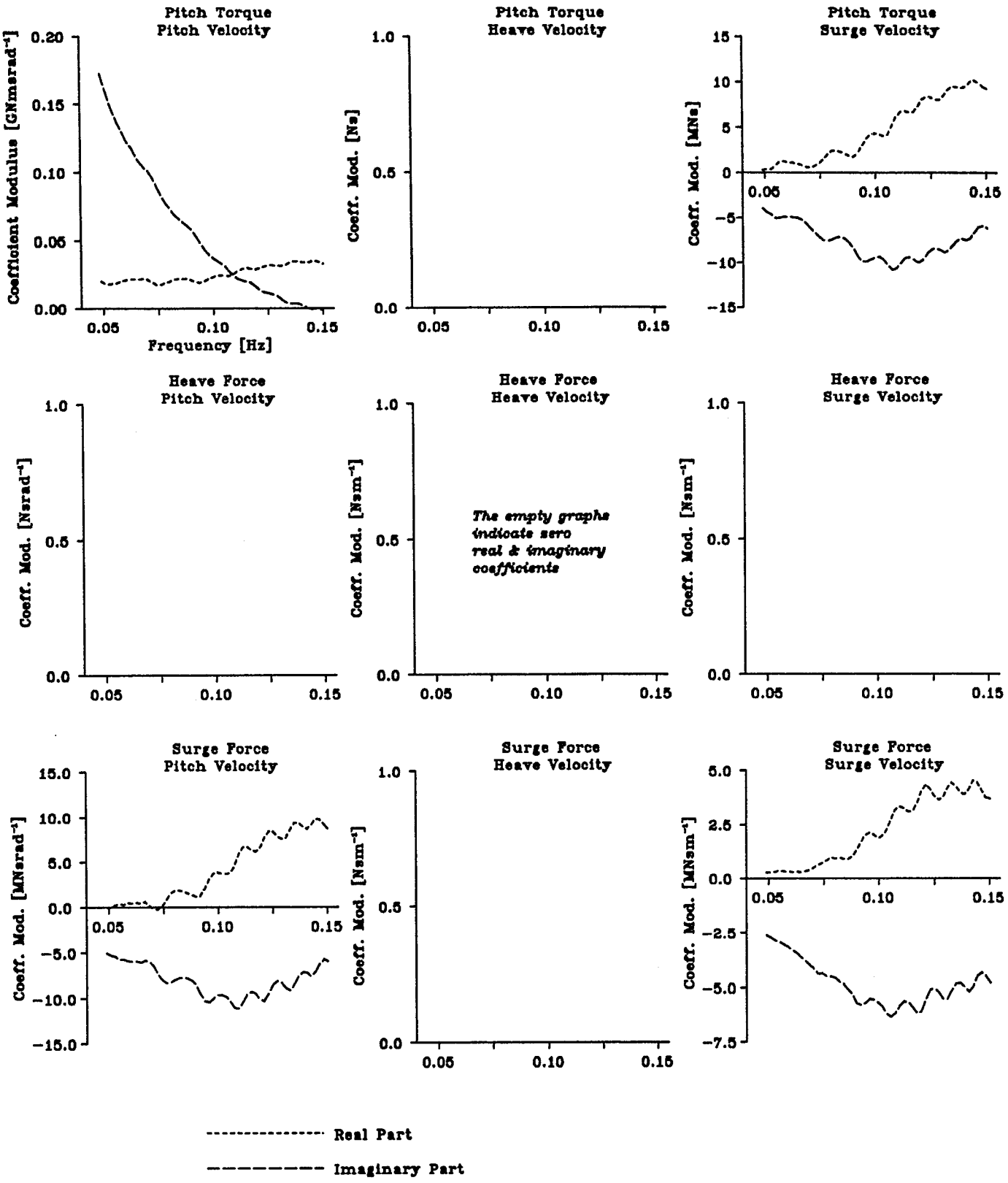

FIGURE 25: Fixed–Heave complex–conjugate control matrix

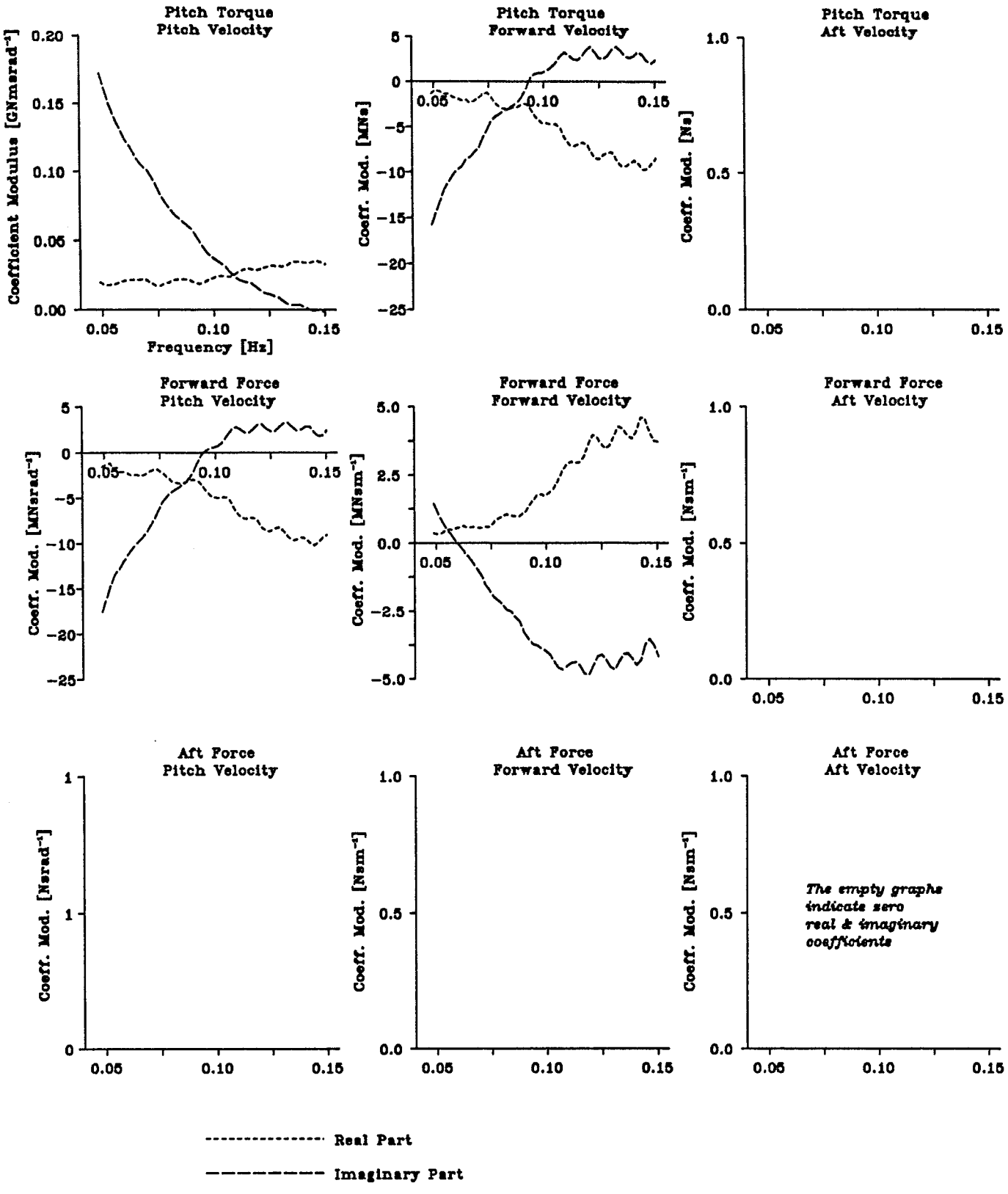

FIGURE 26: Fixed–Aft complex–conjugate control matrix

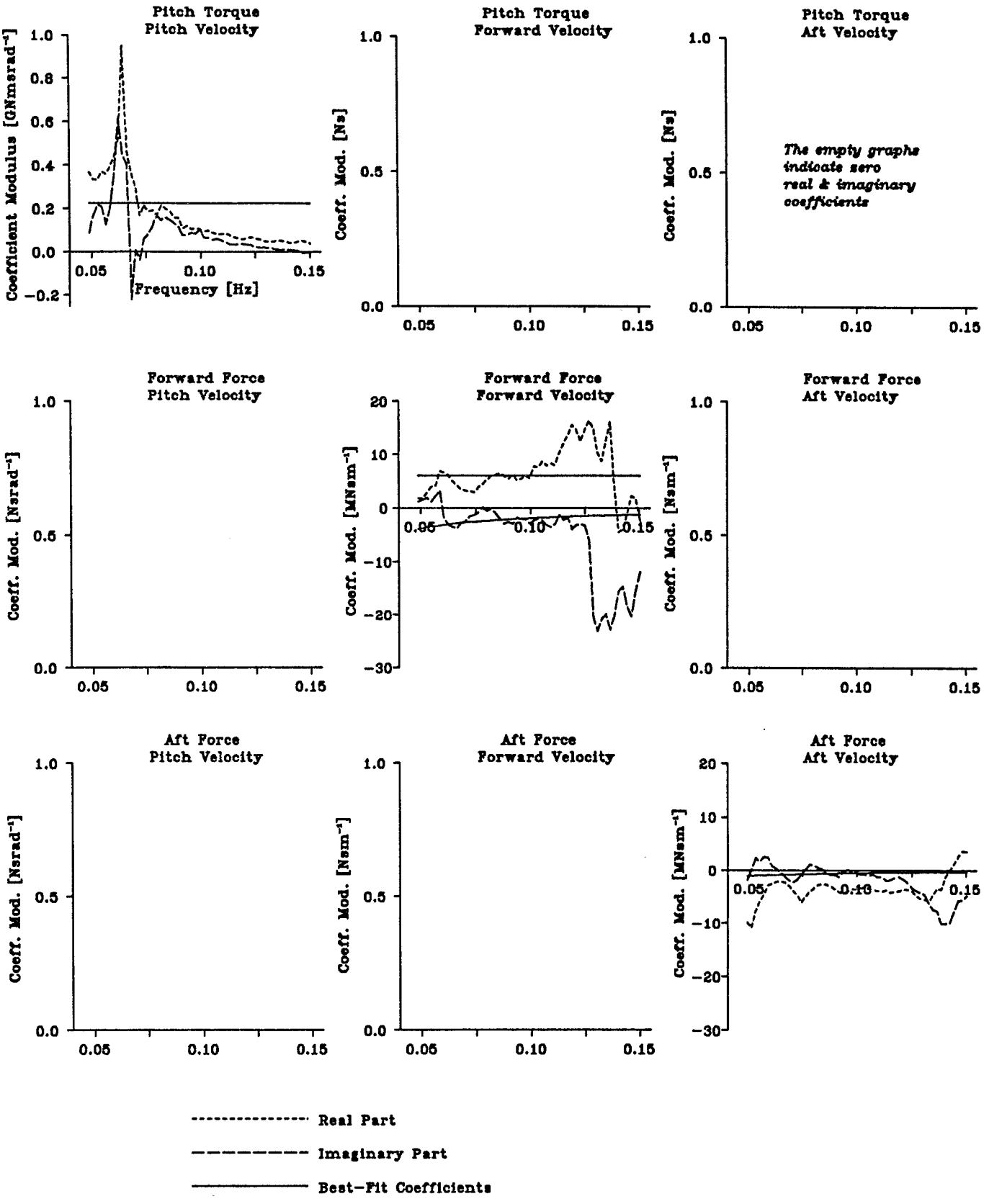

FIGURE 27: Standard complex-conjugate equivalent control matrix with best-fit passive coefficients

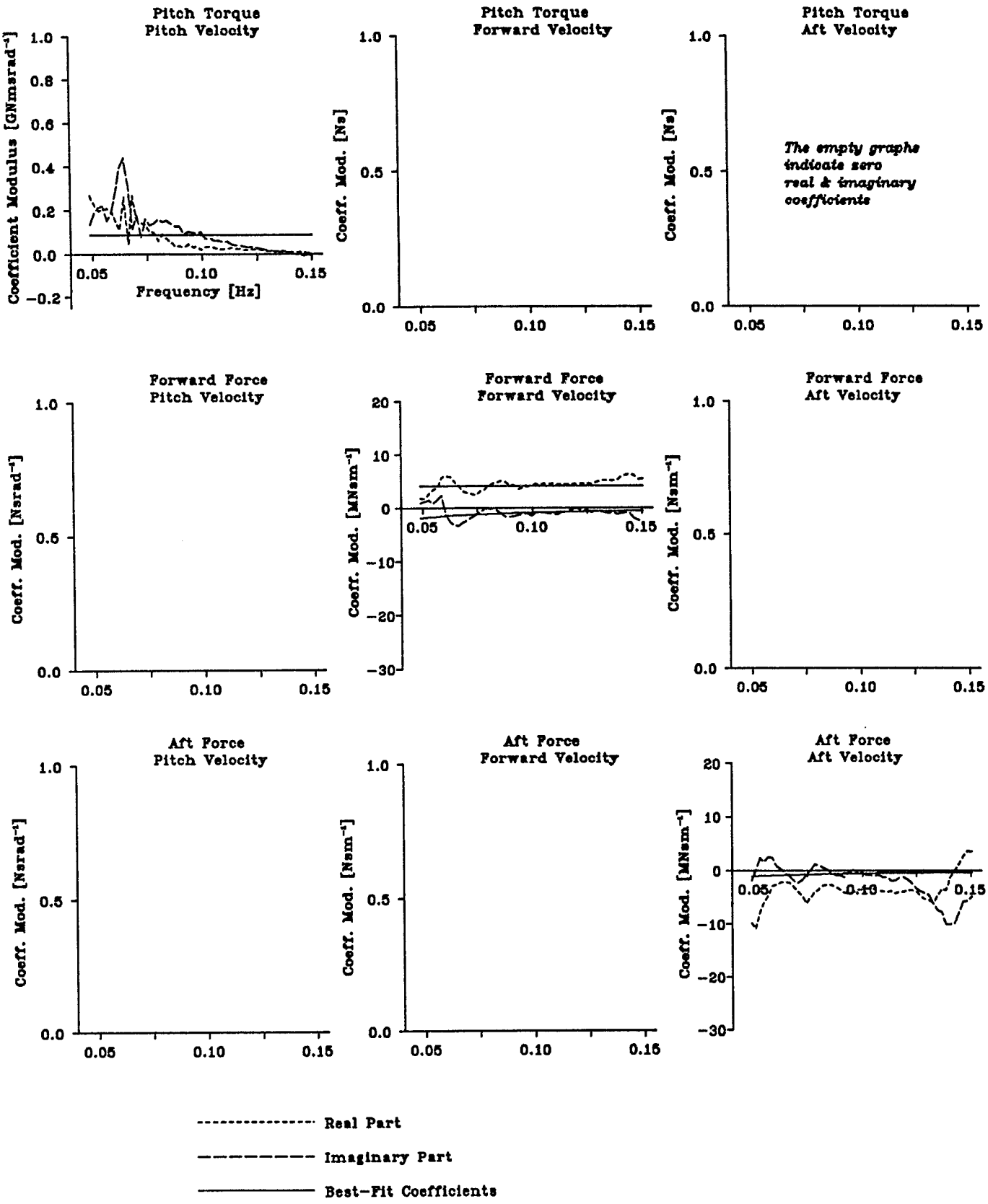

FIGURE 28: Translated–Axis complex–conjugate equivalent control matrix with best–fit passive coefficients

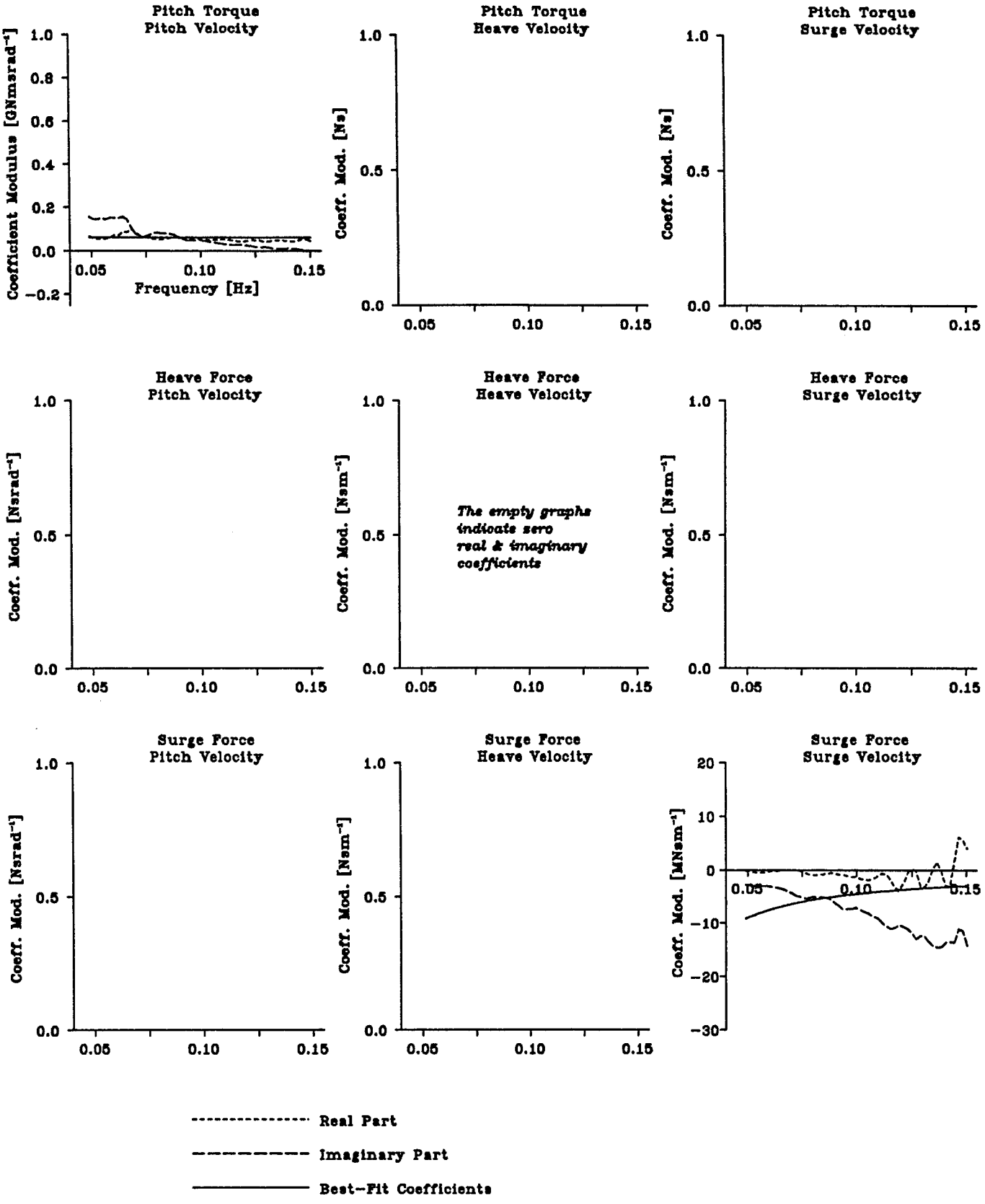

FIGURE 29: Fixed–Heave complex–conjugate equivalent control matrix with best–fit passive coefficients

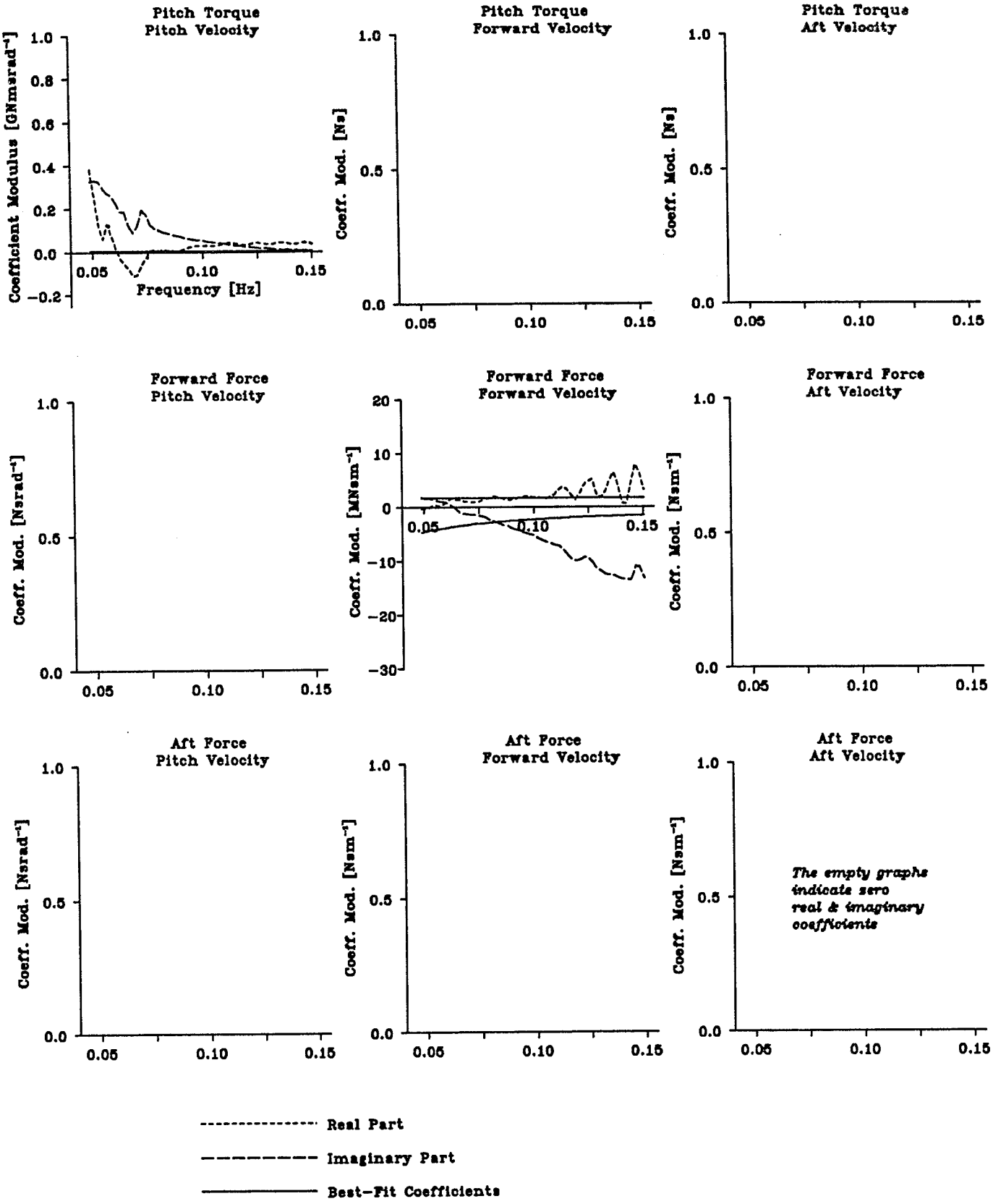

FIGURE 30: Fixed–Aft complex–conjugate equivalent control matrix with best–fit passive coefficients

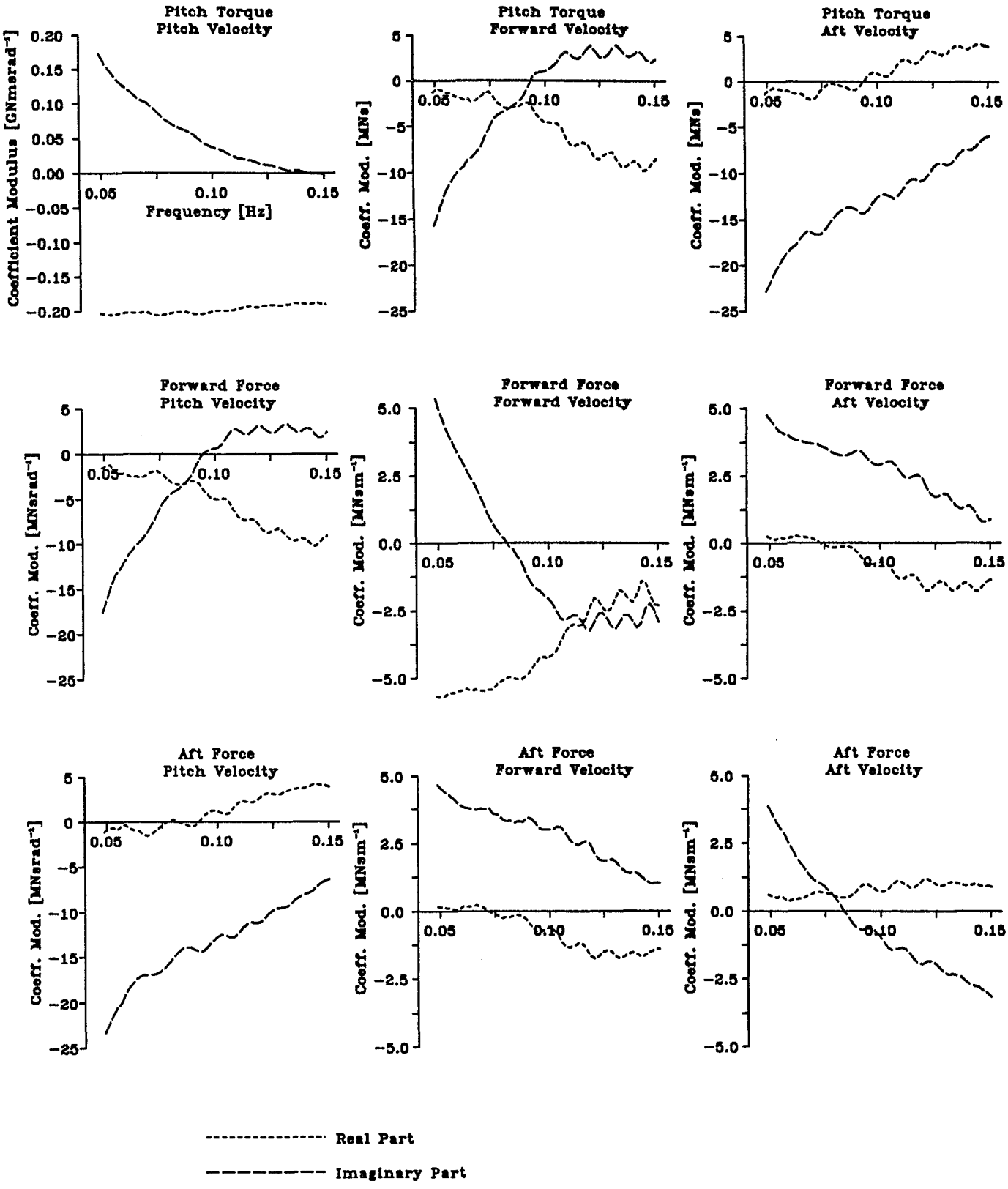

FIGURE 31: Standard active control matrix

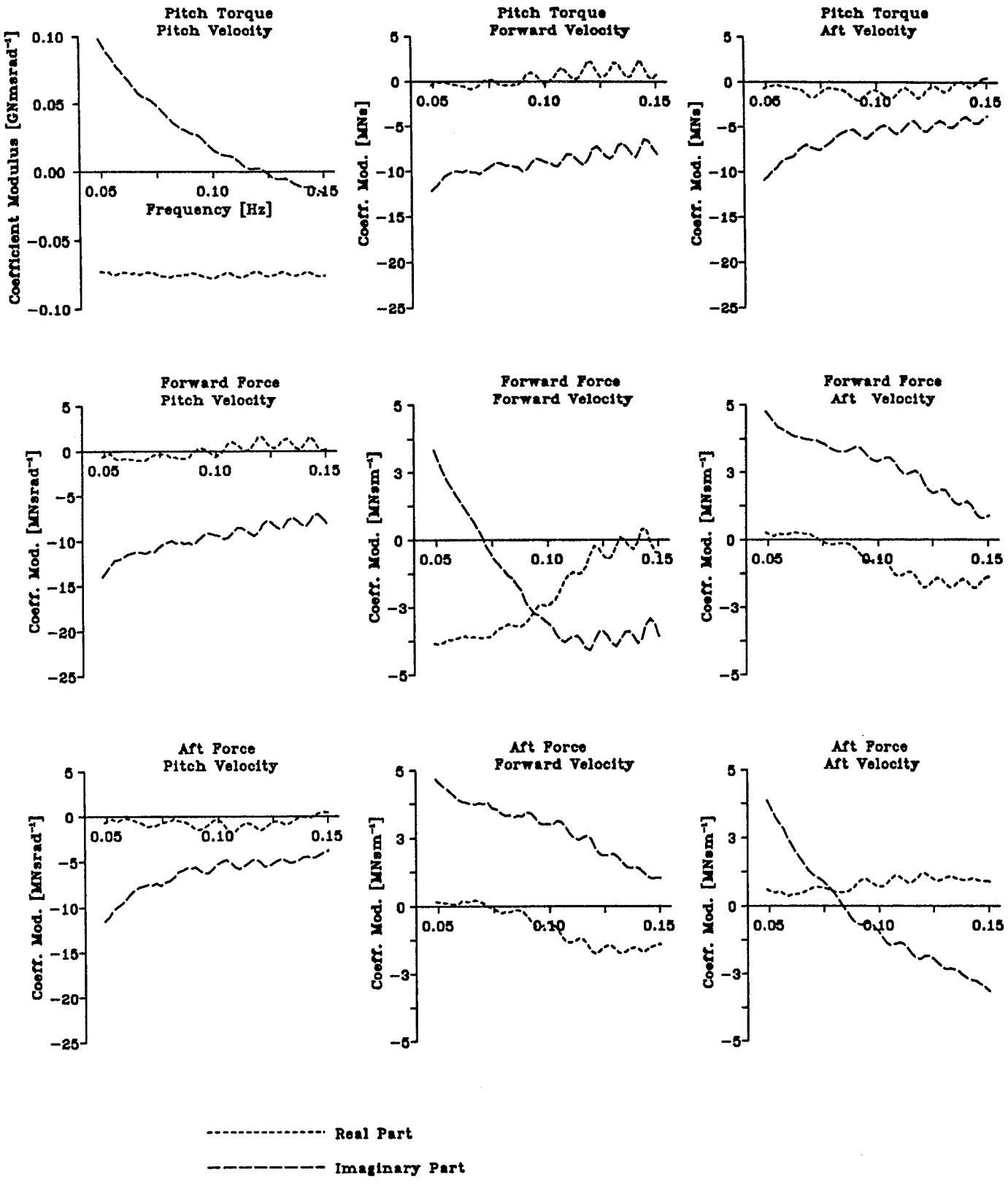

FIGURE 32: Translated–Axis active control matrix

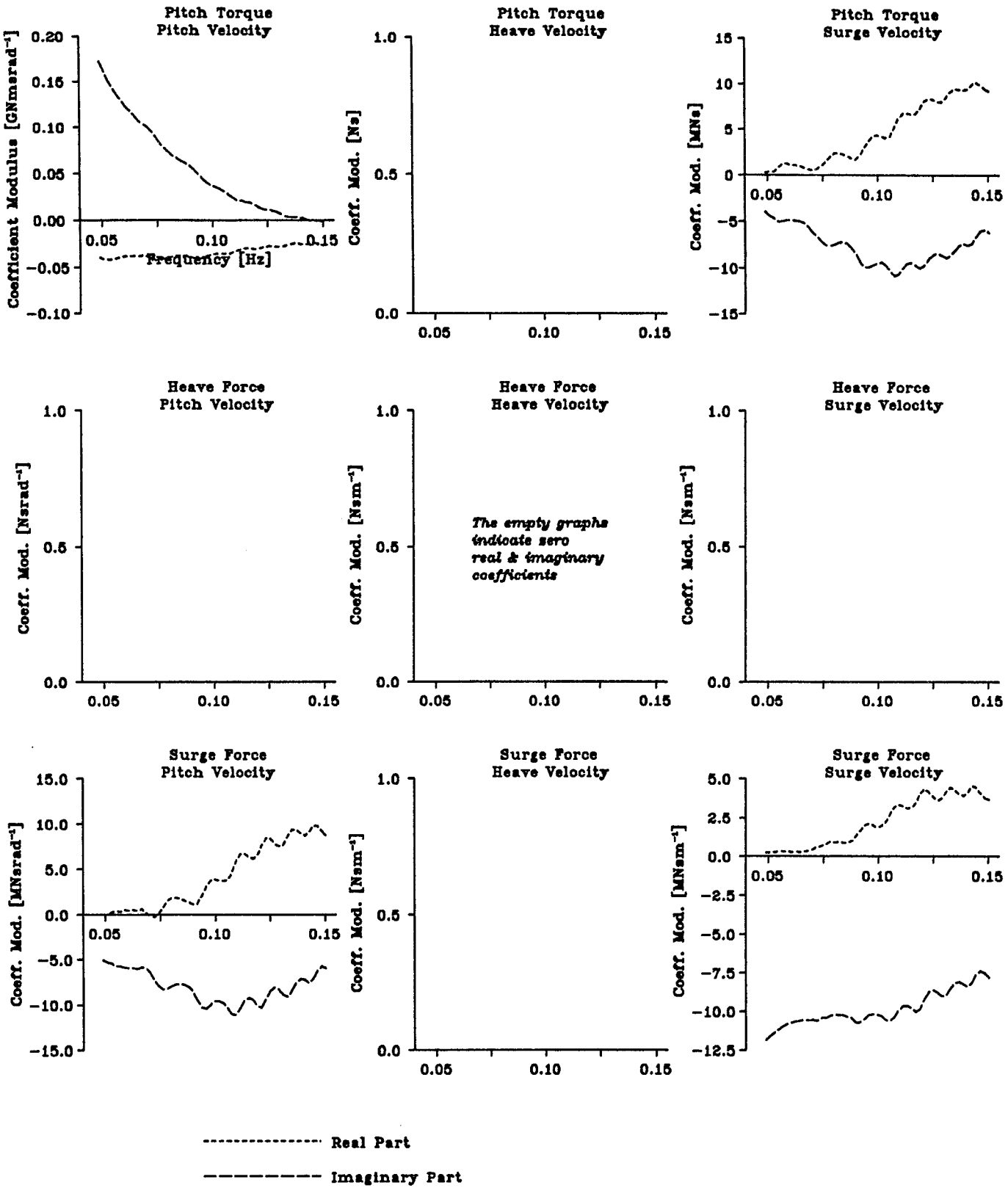

FIGURE 33: Fixed–Heave active control matrix

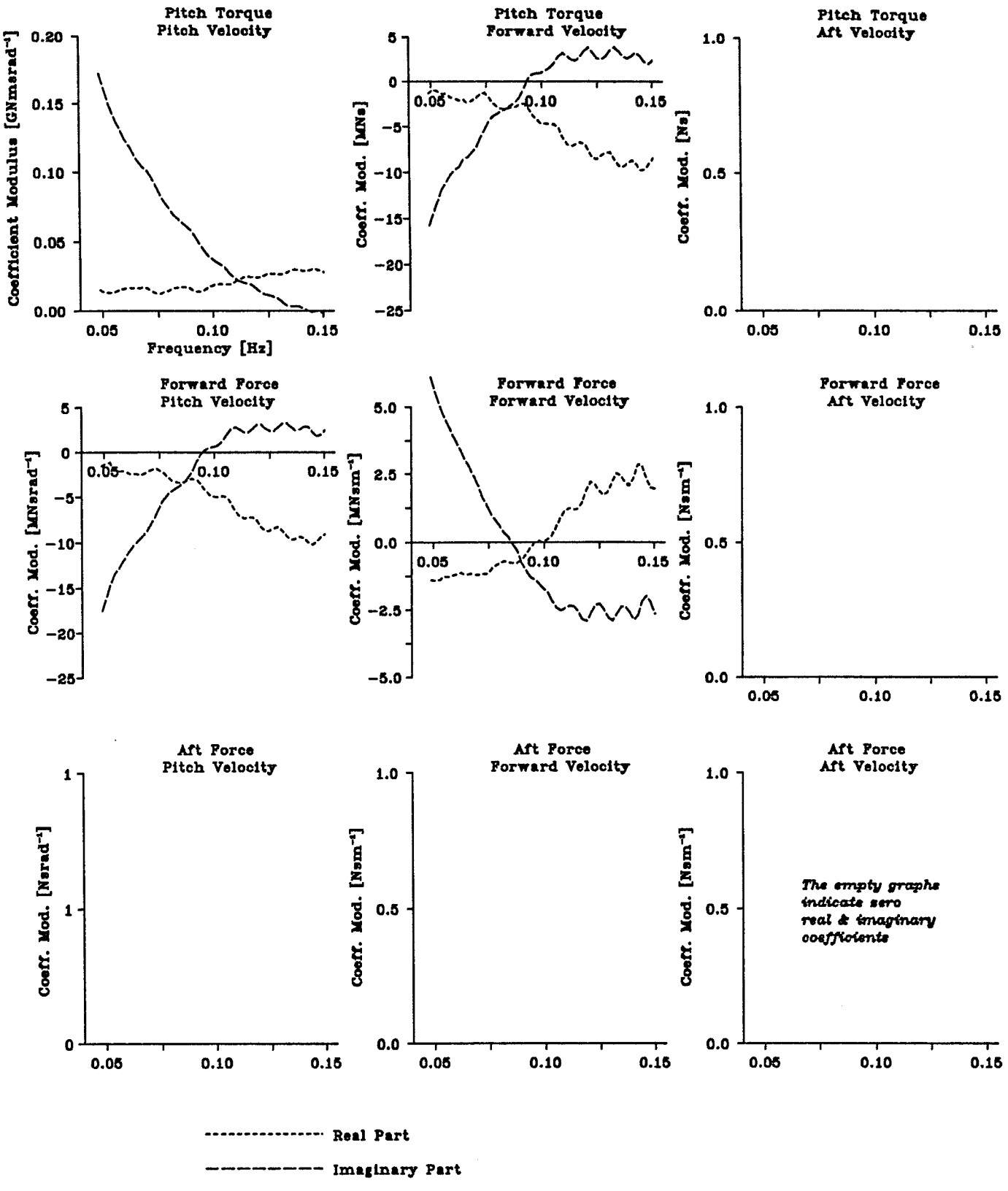

FIGURE 34: Fixed–Aft active control matrix

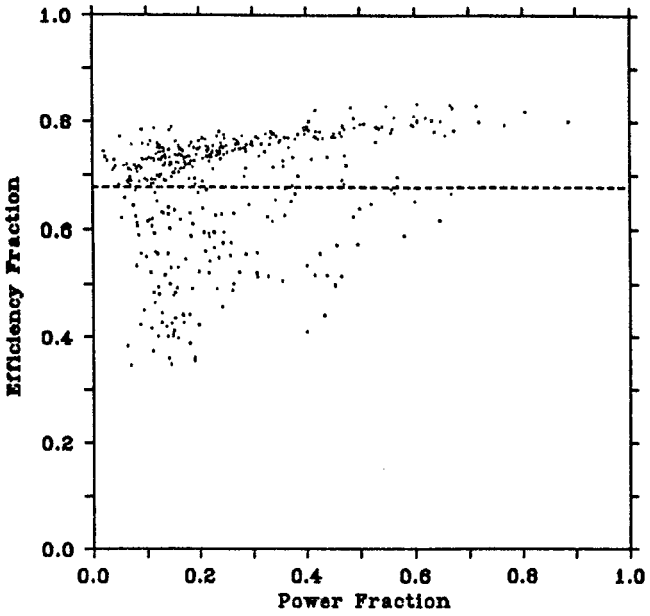

FIGURE 35: Maximum efficiency for Standard Individual–Weighting control in P–M seas

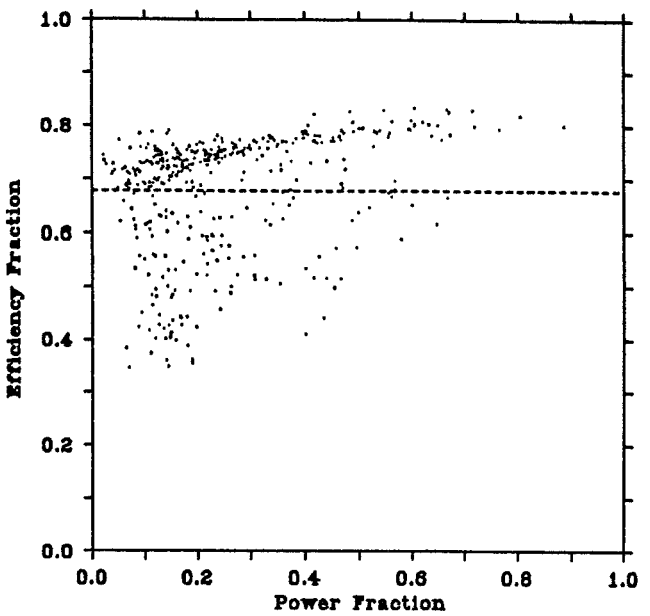

FIGURE 36: Maximum efficiency for Translated–Axis Individual–Weighting control in P–M seas

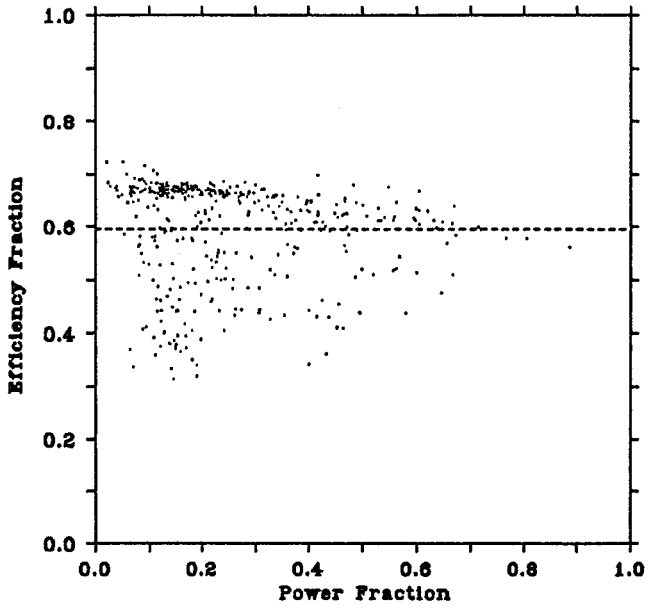

FIGURE 37: Maximum efficiency for Fixed–Heave Individual–Weighting control in P–M seas

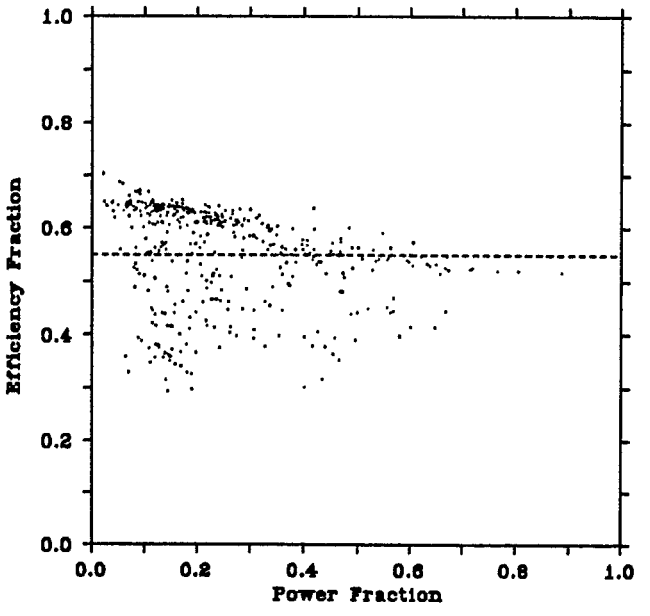

FIGURE 38: Maximum efficiency for Fixed–Aft Individual–Weighting control in P–M seas

---------- Mean Annual Efficiency

Note: All values are for a 10m dia. device in deep water

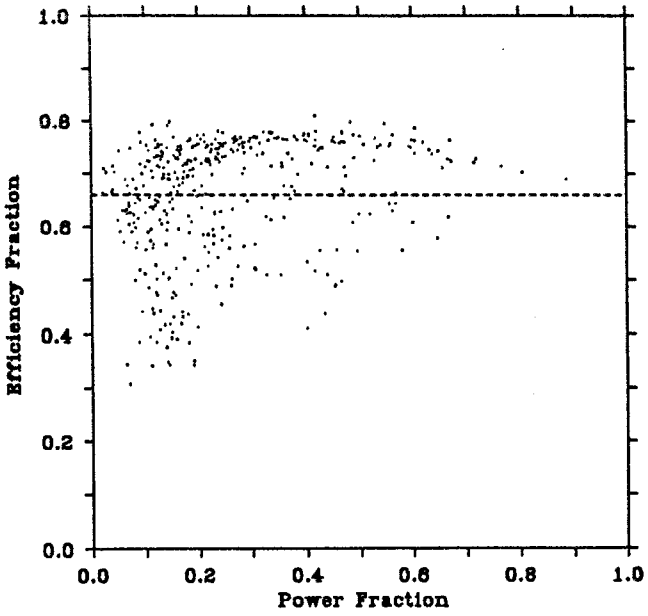

FIGURE 39: Maximum efficiency for Standard Annual–Weighting control in P–M seas

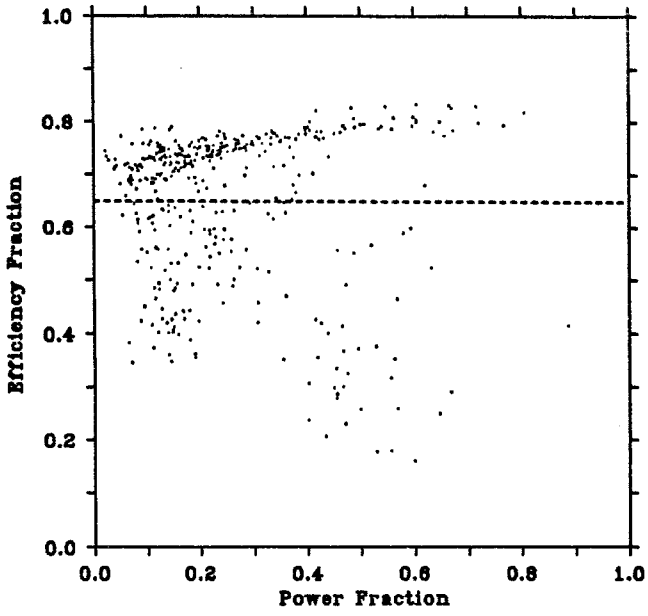

---------- Mean Annual Efficiency

Note: All values are for a 10m dia. device in deep water

FIGURE 40: Maximum efficiency for Non–Fixed Individual–Weighting control with 100KWm^{-1} power limit in P–M seas

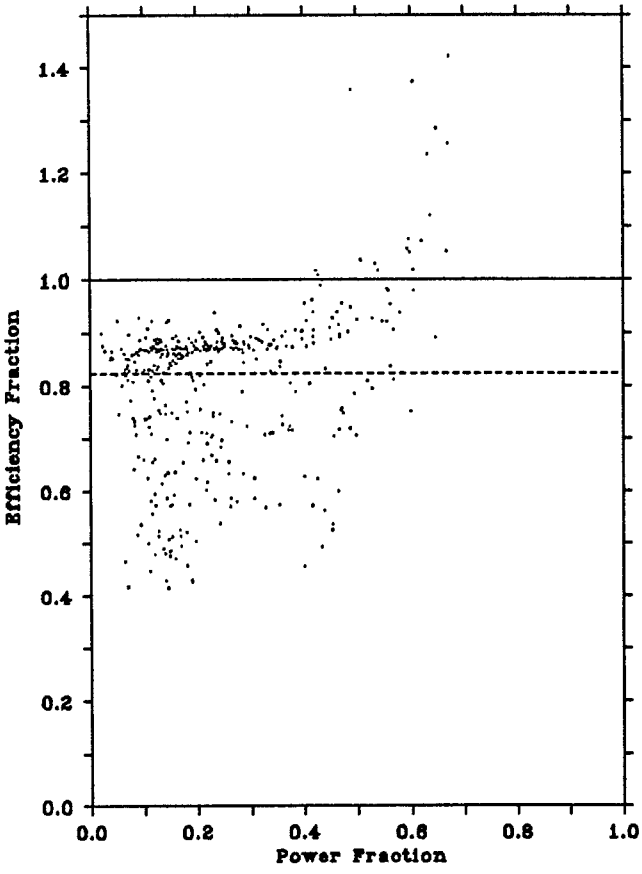

FIGURE 41: Maximum efficiency for Fixed–Aft Individual–Weighting control in P–M seas. Device losses have been approximated and accounted for.

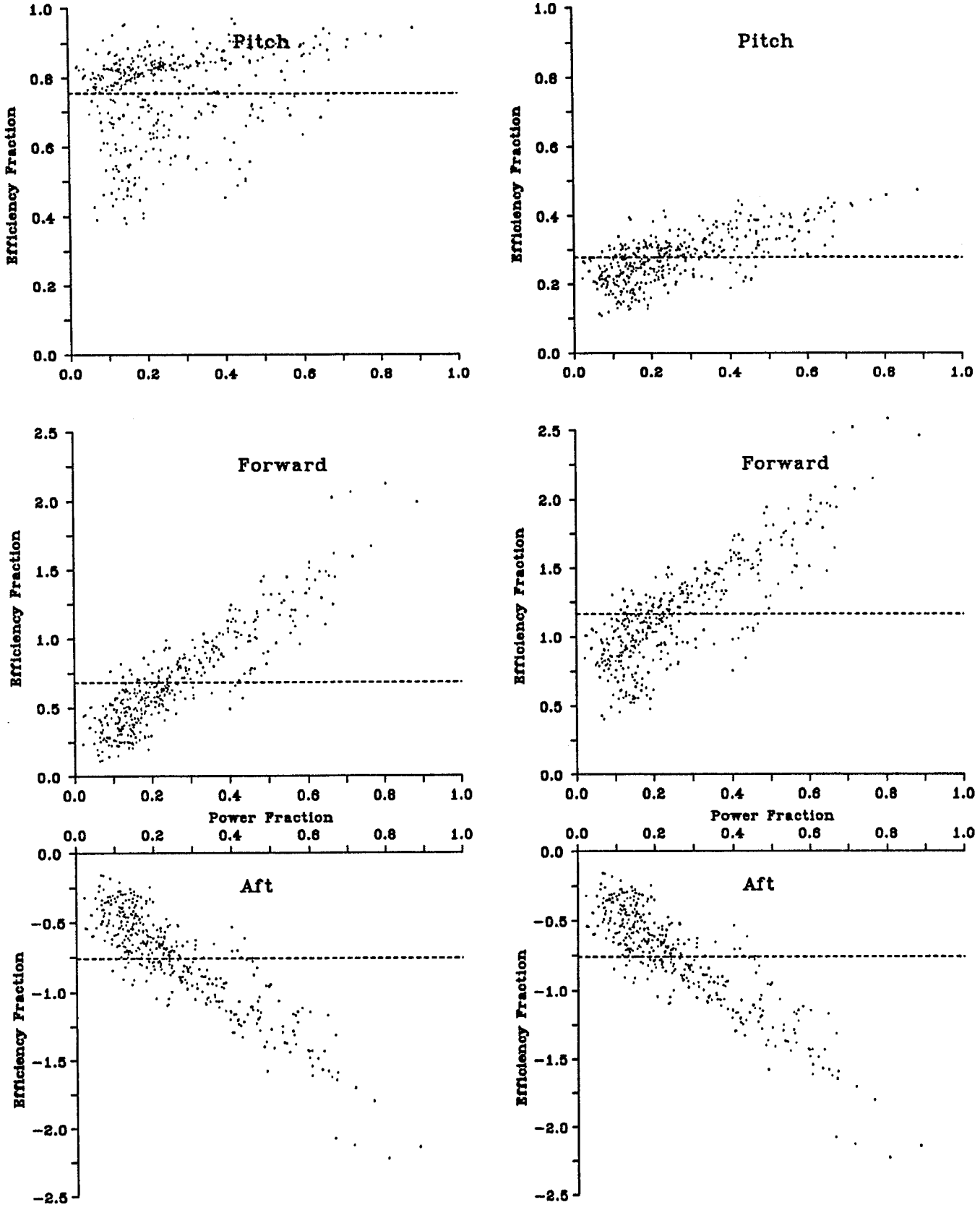

---------- Mean Annual Efficiency

Note: All values are for a 10m dia. device in deep water

FIGURE 42: Maximum efficiency for Standard Individual-Weighting control in P-M seas

FIGURE 43: Maximum efficiency for Translated-Axis Individual-Weighting control in P-M seas

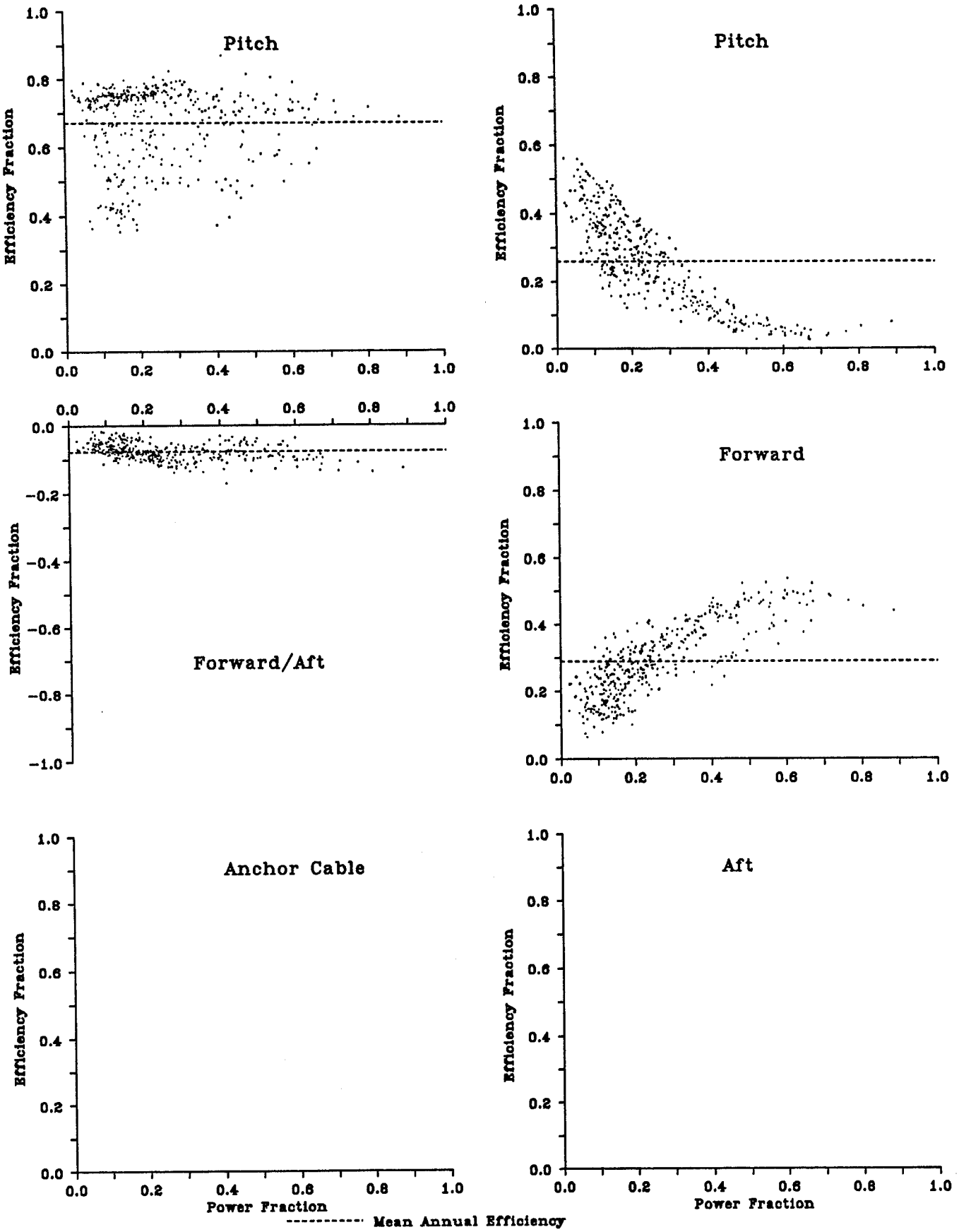

Note: All values are for a 10m dia. device in deep water

FIGURE 44: Maximum efficiency for Fixed–Heave Individual–Weighting control in P–M seas

FIGURE 45: Maximum efficiency for Fixed–Aft Individual–Weighting control in P–M seas

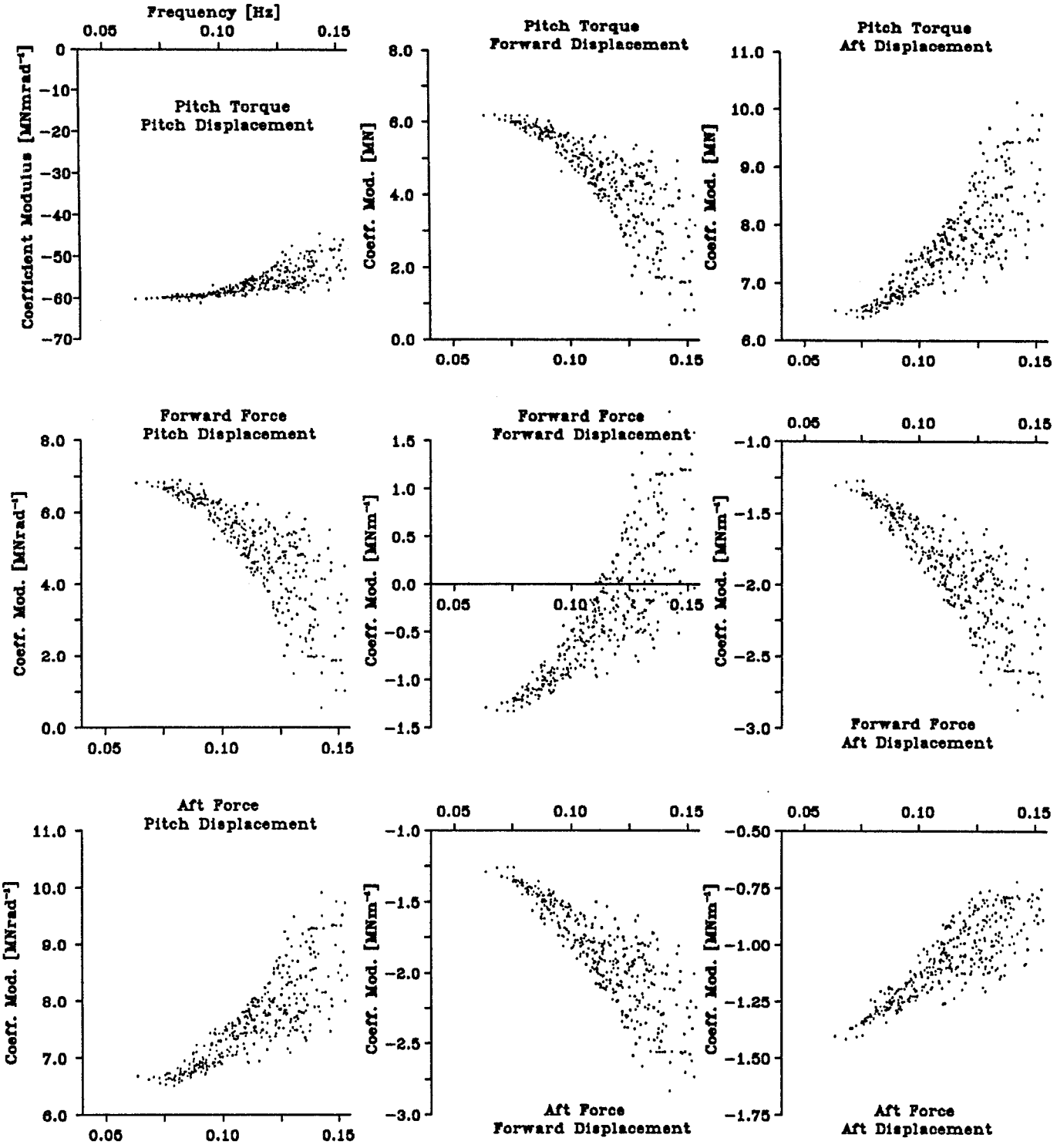

FIGURE 46: Spring coefficients for Standard Individual–Weighting control

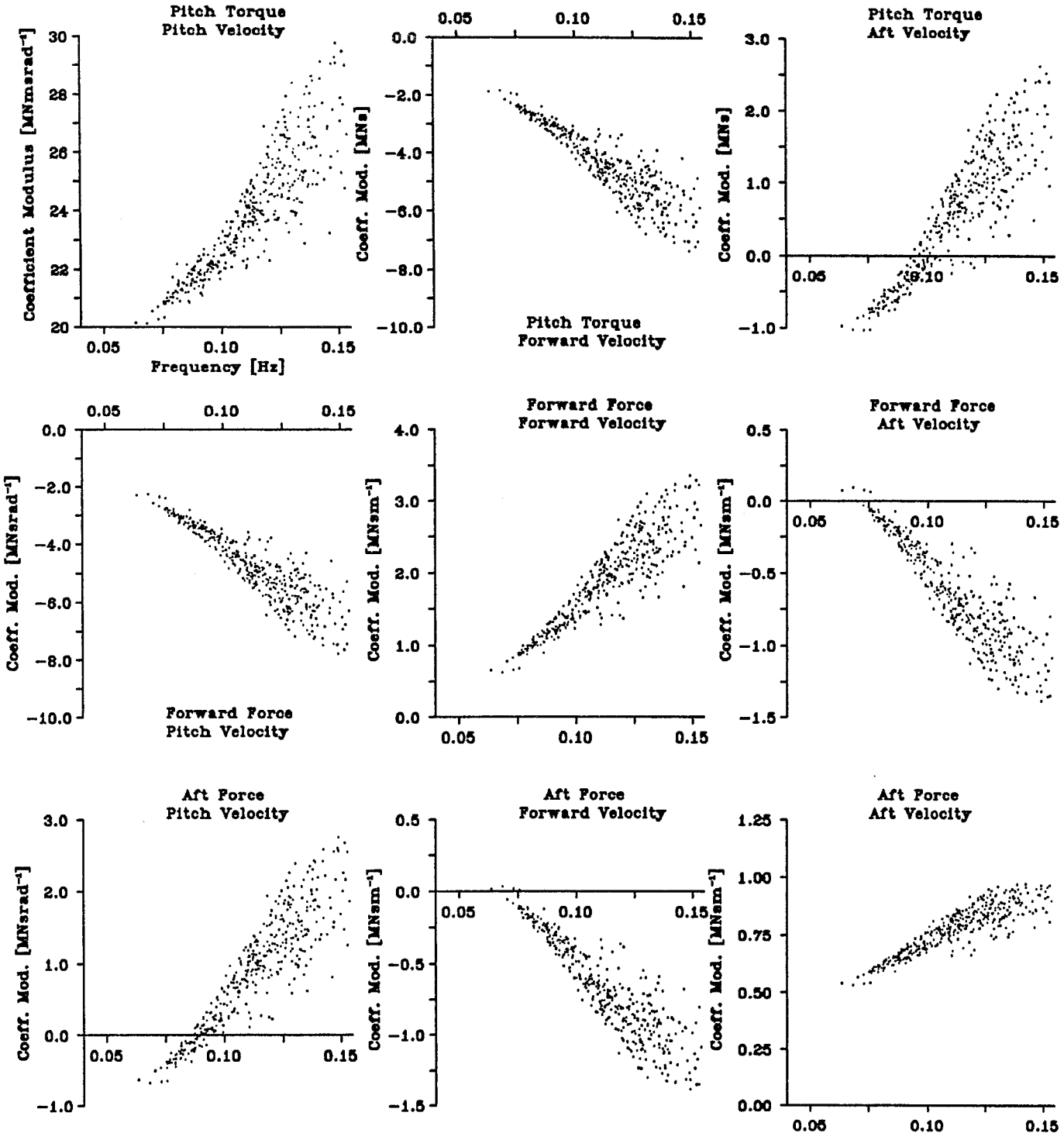

FIGURE 47: Damping coefficients for Standard Individual–Weighting control

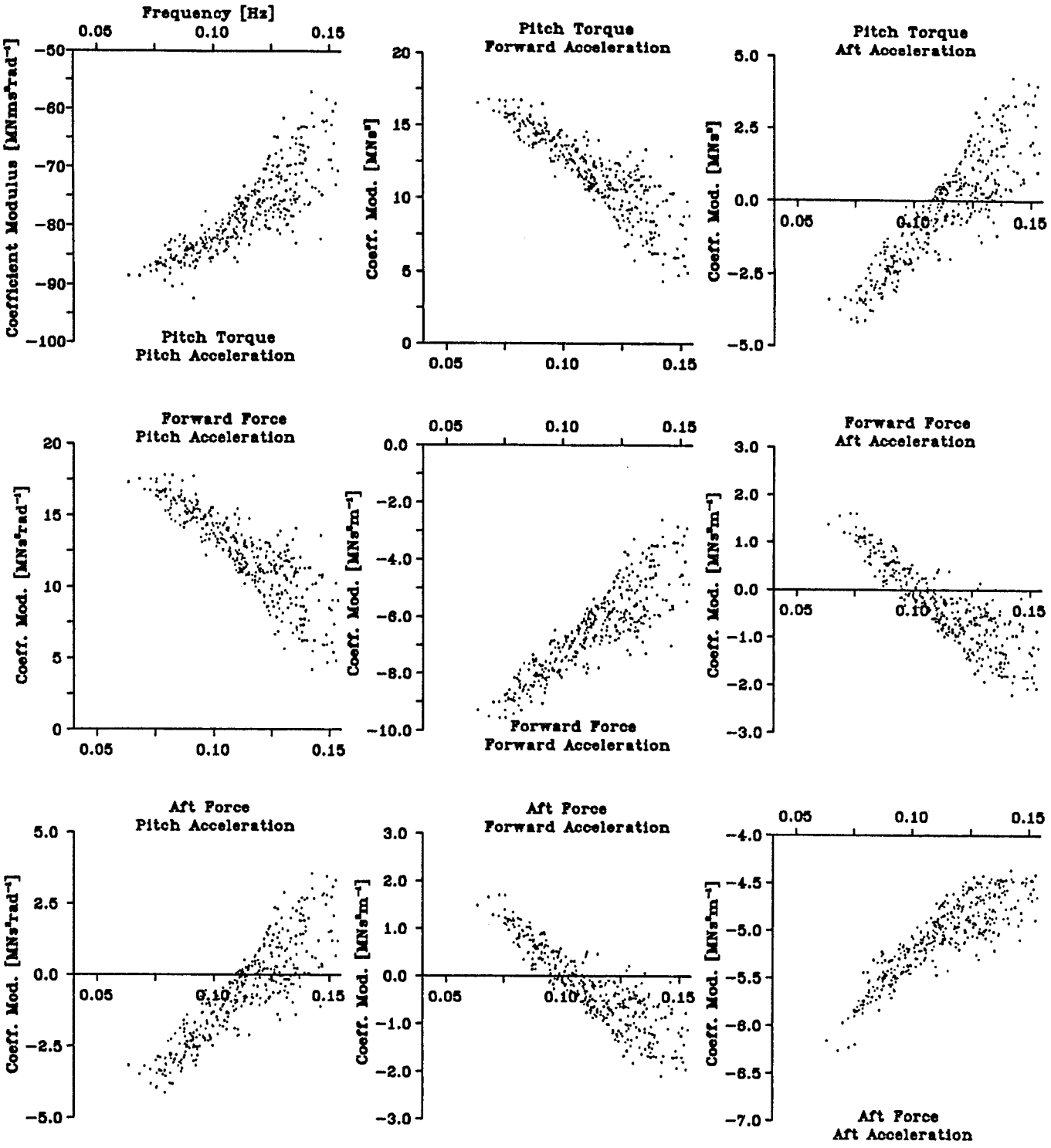

FIGURE 48: Inertia coefficients for Standard Individual−Weighting control

A Power fraction

In 1976 the Institute of Oceanographic Sciences began collecting wave data at a point 8 nautical miles to the west of South Uist in the Outer Hebrides. A Datawell Waverider buoy, sitting in about 42m of water, measured the surface elevation every 3 hours for a period of about 15 minutes.

By comparison with long term annual wind statistics Crabb [7] selected 399 wave records which represented a typical year, and converted them to frequency distributions. Each spectrum was then described as the sum of three Pierson-Moscowitz components, one for the local wind conditions, one for the conditions just prior to sampling and one for the effects of distant storms. The component seas each have a spectral compression factor[1] (C_f), an amplitude multiplier (ψ) and angular spreading distribution. These corrections to the standard P-M shape were required so that it could be fitted to the recorded data.

The power fraction expresses the percentage of total power available in the 399 spectra as a function of period. It is the integral with period of the sum of the power spectra of the 399 set.

The P-M spectrum is defined in appendix C. We require a definition of C_f such that a compressed wave contains the same energy and power as an uncompressed wave. C_f performs a linear mapping of period T onto T′ which preserves H_{rms} and T_e (note that a linear mapping in time does not produce a linear mapping in frequency).

A.1 Conservation of energy

The spectra S(T) and E(ω) are defined such that

$$H_{rms}^2 = \int_0^\infty S(T)dT = \int_0^\infty E(\omega)d\omega \tag{11}$$

Energy E per unit width of wave-front is directly proportional to the root mean square wave amplitude H_{rms}^2.

E(ω) is given in equation 50. We can derive S(T) given E(ω) by a change of variable;

$$\int_0^\infty S(T)dT = \int_0^\infty \frac{2\pi}{T^2} E(\frac{2\pi}{T})dT \tag{12}$$

$$\Rightarrow S(T) = \frac{2\pi}{T^2} E\left(\frac{2\pi}{T}\right) \tag{13}$$

The compression factor C_f is defined by the mapping

$$T' = C_f T + \theta \tag{14}$$

where θ is an offset such that T_e maps onto itself.

[1] C_f is really an expansion factor, but for historical reasons it is still referred to as a compression factor

If we make a change of variable from T to T′ in equation 11 we get

$$\int_0^\infty S(T)dT = \frac{1}{C_f}\int_\theta^\infty S\left(\frac{T'-\theta}{\phi}\right)dT' = \int_\theta^\infty S'(T')dT' \tag{15}$$

Thus

$$S'(T') = \frac{1}{C_f}S\left(\frac{T'-\theta}{C_f}\right) \tag{16}$$

A.2 Conservation of power

Power per unit width of wave-front is given by

$$P = \frac{\rho g^2 |a|^2 T}{8\pi} \tag{17}$$

for a monochromatic wave. Therefore for a spectrum

$$P \propto \int_0^\infty TS(T)dT \tag{18}$$

Substituting for T′ in 18 gives

$$\int_0^\infty TS(T)dT = \frac{1}{C_f}\int_\theta^\infty \left(\frac{T'-\theta}{C_f}\right) S\left(\frac{T'-\theta}{C_f}\right)dT' = \int_\theta^\infty T'S''(T')dT' \tag{19}$$

We can separate the integral in 19 such that

$$\int_0^\infty TS(T)dT = \frac{1}{C_f}\int_\theta^\infty \frac{T'}{C_f}S\left(\frac{T'-\theta}{C_f}\right)dT' - \frac{\theta}{C_f}\int_\theta^\infty \frac{1}{C_f}S\left(\frac{T'-\theta}{C_f}\right)dT' \tag{20}$$

Substituting for S′(T′) from equation 16 into 20 we get

$$\int_0^\infty TS(T)dT = \frac{1}{C_f}\int_\theta^\infty T'S(T')dT' - \frac{\theta}{C_f}\int_\theta^\infty S(T')dT' \tag{21}$$

which becomes

$$\underbrace{\int_0^\infty TS(T)dT}_{\kappa P} = \frac{1}{C_f}\underbrace{\int_\theta^\infty T'S(T')dT'}_{\kappa P} - \frac{\theta}{C_f}\underbrace{\int_\theta^\infty S(T')dT'}_{\kappa E} \tag{22}$$

from 15 and 19, where

$$\kappa = \frac{4\pi}{\rho g^2} \tag{23}$$

Therefore

$$\begin{aligned} P &= \frac{1}{C_f}P - \frac{\theta}{C_f}E \\ \theta &= (1 - C_f)\frac{P}{E} \\ \theta &= (1 - C_f)T_e \end{aligned} \tag{24}$$

Substituting for θ in equation 14 we get

$$T' = C_f T + (1 - C_f)T_e \tag{25}$$

We now have an expression for T′ in terms of T and the compression factor C_f. T_e maps onto itself as required. Note that the lower limit of integration for compressed seas is $T' = \theta$.

Since the figures in this report relate to experiments in which the incident wave is unidirectional, we can ignore the angular spreading distributions of the 399 component spectra.

The 399 data were measured in 42m of water. Mollison [8] points out that Crabb's synthesis [7] makes no account of this finite water depth. Refraction, which is negligable in 100m depth for all but the lowest frequencies, is significant in 42m depth for the wavelengths which carry most power. Consequently, a depth correction is included in the 399 set which modifies the raw spectral data to 100m depth.

We can now define the power fraction, $\mathcal{P}(T)$. The power fraction from period T_1 to period T_2, $\mathcal{P}(T)\Big|_{T_1}^{T_2}$, expresses the power available in waves between these periods as a percentage of the total power available in the 399 spectra. We can see from equation 19 that

$$T'S''(T') = \frac{1}{C_f}TS(T) \tag{26}$$

Rearranging equation 25 gives

$$T = T' - \frac{(1 - C_f)T_e}{C_f} \tag{27}$$

We can now define a new variable, $\nu(T')$, such that

$$T'S''(T') = \frac{1}{C_f}\left[T' - \frac{(1 - C_f)T_e}{C_f}\right]S(T) = \nu(T') \tag{28}$$

Therefore

$$\mathcal{P}(T)\Big|_{T_1}^{T_2} = \frac{\sum_{i=1}^{399}\left[(\psi^w)^2\int_{T_1}^{T_2}\nu_i^w(T')dT' + (\psi^o)^2\int_{T_1}^{T_2}\nu_i^o(T')dT' + (\psi^s)^2\int_{T_1}^{T_2}\nu_i^s(T')dT'\right]}{\sum_{i=1}^{399}\left[(\psi^w)^2\int_{\theta_i^w}^{\infty}\nu_i^w(T')dT' + (\psi^o)^2\int_{\theta_i^o}^{\infty}\nu_i^o(T')dT' + (\psi^s)^2\int_{\theta_i^s}^{\infty}\nu_i^s(T')dT'\right]} \tag{29}$$

The integral from θ to ∞ of the denominator of equation 26 is proportional to power. It is also equal to $\mathrm{H}_{rms}^2 \mathrm{T}_e$. We can therefore re-write equation 29 as

$$\mathcal{P}(T)\Big|_{\mathrm{T}_1}^{\mathrm{T}_2} = \frac{\sum_{i=1}^{399}\left[(\psi^w)^2 \int_{\mathrm{T}_1}^{\mathrm{T}_2} \nu_i^w(\mathrm{T}')\mathrm{d}\mathrm{T}' + (\psi^o)^2 \int_{\mathrm{T}_1}^{\mathrm{T}_2} \nu_i^o(\mathrm{T}')\mathrm{d}\mathrm{T}' + (\psi^s)^2 \int_{\mathrm{T}_1}^{\mathrm{T}_2} \nu_i^s(\mathrm{T}')\mathrm{d}\mathrm{T}'\right]}{(0.01361)^2 \sum_{i=1}^{399}\left[\left(\mathrm{H}_{rms_i}^w\right)^2 \mathrm{T}_{e_i}^w + \left(\mathrm{H}_{rms_i}^o\right)^2 \mathrm{T}_{e_i}^o + \left(\mathrm{H}_{rms_i}^s\right)^2 \mathrm{T}_{e_i}^s\right]} \tag{30}$$

where

$$\theta_i = \begin{cases} 0 & \text{if } \mathrm{C}_f > 1 \\ (1 - \mathrm{C}_{f_i})\,\mathrm{T}_{e_i} & \text{otherwise} \end{cases} \tag{31}$$

$$\mathrm{T}_1 = \begin{cases} \theta_i & \text{if } T_1 < \theta_i \\ \mathrm{T}_1 & \text{otherwise} \end{cases} \tag{32}$$

The superscripts w, o, s indicate the values of compression factor and H_{rms} multiplier for the wind sea, old wind sea and swell sea components respestively.

B Scale factors

If model figures are to be of any use in determining full-scale figures then some dynamic similarity must be established between the two systems. Gravity forces are important in any flow with a free surface [9]. Since the pressure at the surface is constant under steady state conditions only gravity can cause flow. Any disturbance of the free surface, such as wave motion, involves gravity forces since work must be done in raising the liquid against its weight. We therefore require factors which scale such that the ratio of inertial forces to gravity forces is the same for the model as for the full-sized device. This type of dynamic similarity is known as Froude scaling.

Table 1 contains the factors for specific parameters, described as an index of scale (Note: This list is reproduced from [10]).

C Depth correction

C.1 Monochromatic equivalent of a wave spectrum

Mei [11] states that

$$\omega^2 = gk \tanh kh \tag{33}$$

where

ω is the angular frequency.

g is the acceleration due to gravity.
h is the water depth ($h = 0.58m \times s$ for a scale factor s).
k is the wave number ($k = \frac{2\pi}{\lambda}$).
λ is the wavelength.

For deep water waves (kh $\gg$ 1) this becomes

$$\omega^2 = gk_d \tag{34}$$

where

k_d is the deep water wave number ($k_d = \frac{2\pi}{\lambda_d}$).
λ_d is the deep water wavelength.

This leads to the ratio of the wave length in water of any depth to the length in deep water as

$$\frac{\lambda}{\lambda_d} = \tanh kh \tag{35}$$

For a given frequency the energy in a wave remains constant regardless of depth (assuming no losses). The energy flux (or power) per unit width is given [11] by

$$\mathrm{P} = \frac{1}{2}\rho g \mathbf{a}^2 \left[\frac{1}{2}\frac{\omega}{k}\left(1 + \frac{2kh}{\sinh 2kh}\right)\right] \tag{36}$$

where

P is the power per unit width.
ρ is the density of water.
a is the wave amplitude.

Substituting for ω from equation 33 and rearranging, this becomes

$$\mathrm{P} = \frac{\rho g^2 \mathbf{a}^2 \mathrm{T}}{8\pi}\left[\tanh kh\left(1 + \frac{2kh}{\sinh 2kh}\right)\right] \tag{37}$$

where

T is the wave period.

Thus the ratio of power per unit width in water of any depth to power per unit width in deep water is

$$\frac{\mathrm{P}}{\mathrm{P}_d} = \tanh kh\left(1 + \frac{2kh}{\sinh 2kh}\right) \tag{38}$$

for a monochromatic wave.

Since P $\propto$ (a)^2, the ratio of wave amplitude in water of any depth to wave amplitude in deep water is given by

$$\frac{\mathbf{a}}{\mathbf{a}_d} = \left[\tanh kh \left(1 + \frac{2kh}{\sinh 2kh}\right)\right]^{\frac{1}{2}} \tag{39}$$

We can now express the deep water wave-steepness as a function of the shallow water wave-steepness;

$$\frac{\mathbf{a}_d}{\lambda_d} = \frac{\mathbf{a}_s}{\lambda_s} \cdot \frac{\mathbf{a}_d}{\mathbf{a}_s} \cdot \frac{\lambda_s}{\lambda_d} \tag{40}$$

Substituting from 35 and 39 we get

$$\frac{\mathbf{a}_d}{\lambda_d} = \frac{\mathbf{a}_s}{\lambda_s} \left[\frac{\tanh kh}{\left(1 + \frac{2kh}{\sinh 2kh}\right)}\right]^{\frac{1}{2}} \tag{41}$$

The Pierson-Moscowitz spectrum [12] best describes the sea-state in which a Duck will operate. The principal feature of this spectrum is that it is invariant under change of scale. In particular the wave-steepness is constant;

$$\frac{\mathrm{H}_{rms}}{\lambda_e} = \frac{1}{115} \tag{42}$$

where

H_{rms} is the root mean square wave amplitude of the spectrum (which is also the rms amplitude of a monochromatic wave containing the same energy and power as the spectrum - the monochromatic equivalent wave).

λ_e is the energy wavelength (i.e. the length of the monochromatic equivalent wave).

If equation 41 is equated to the P-M steepness we get

$$\frac{1}{115} = \frac{1}{\sqrt{2}} \left(\frac{\mathbf{a}_s}{\lambda_s}\right) \left[\frac{\tanh kh}{\left(1 + \frac{2kh}{\sinh 2kh}\right)}\right]^{\frac{1}{2}} \tag{43}$$

which when rearranged gives

$$\left(\frac{\mathbf{a}_s}{\lambda_s}\right) = \mathcal{W}_e = \frac{1}{115} \left[\frac{2\left(1 + \frac{2kh}{\sinh 2kh}\right)}{\tanh kh}\right]^{\frac{1}{2}} \tag{44}$$

$\mathcal{W}_e$ is the shallow water steepness of monochromatic P-M equivalent waves as a function of frequency and is shown in figure 7 (the factor of $\frac{1}{\sqrt{2}}$ is included because equation 41 relates to peak amplitude, not rms amplitude).

C.2 Spectral Wave-Steepness

The spectrum $\mathrm{E}(\omega)$ (see figure 6) is defined such that

$$\int_0^\infty \mathrm{E}(\omega)d\omega = \mathrm{H}_{rms}^2 \tag{45}$$

Since we are testing at discrete frequencies, this can be written as

$$\mathrm{H}_{rms}^2 = \sum_{i=1}^{n} (\mathrm{a}_{rms})_i^2 \tag{46}$$

where

$$(\mathrm{a}_{rms})_i^2 = \mathrm{E}(\omega_i)\delta\omega \tag{47}$$

Combining equations 33 and 41 gives an expression for rms wave amplitude as a function of shallow water wave-steepness (for a monochromatic wave);

$$\mathrm{a}_{rms_d} = \frac{\sqrt{2}g\pi}{\omega^2}\left(\frac{\mathrm{a}_s}{\lambda_s}\right)\left[\frac{\tanh kh}{\left(1+\frac{2kh}{\sinh 2kh}\right)}\right]^{\frac{1}{2}} \tag{48}$$

Equating 47 and 48, and rearranging, we can define the spectral wave steepness $\mathcal{W}_s$

$$\left(\frac{\mathrm{a}_s}{\lambda_s}\right) = (\delta\omega)^{+\frac{1}{2}}\mathcal{W}_s = \frac{\omega^2}{g\pi}\left[\frac{\mathrm{E}(\omega)\delta\omega\left(1+\frac{2kh}{\sinh 2kh}\right)}{2\tanh kh}\right]^{\frac{1}{2}} \tag{49}$$

The P-M spectrum is defined by

$$\mathrm{E}(\omega) = \sigma g^2\omega^{-5}exp\left(-\beta\left(\frac{\omega_0}{\omega}\right)^4\right) \tag{50}$$

where

$$\begin{aligned} \sigma &= 0.0081 \\ \beta &= 0.74 \\ \omega_0 &= \frac{g}{U_0} \end{aligned} \tag{51}$$

The P-M spectrum describes fully-developed wind-generated seas, and U_0 is the wind speed measured 19.5 metres above the still water surface.

We can make the spectrum a function of T_e (rather than U_0) using the following relation;

$$\begin{aligned} \mathrm{T}_e &= 0.626U_0 \\ \Rightarrow \omega_0 &= \left(\frac{6.14106}{\mathrm{T}_e}\right) \end{aligned} \tag{52}$$

Substituting for $E(\omega)$ in 49 we get

$$\mathcal{W}_s = \zeta \left[\frac{exp\left(-\beta\left(\frac{\xi}{\omega T_e}\right)^4\right)\left(1+\frac{2kh}{\sinh 2kh}\right)}{\omega \tanh kh} \right]^{\frac{1}{2}} \tag{53}$$

where

$$\begin{aligned} \zeta &= 0.020257 \\ \xi &= 6.14106 \end{aligned} \tag{54}$$

$\mathcal{W}_s$ is the shallow water wave-steepness spectrum, and is a function of $E(\omega)$. It is shown in figures 8 for several values of T_e.

To find the force spectrum , $F(\omega)$, for a particular value of T_e, we multiply the calculated values of force per unit wave-steepness (F_{ws}) by $\mathcal{W}_s$ to find the force of each spectral component. The rms force is given by

$$F_{rms} = \left(\int_0^\infty F(\omega)d\omega\right)^{\frac{1}{2}} = \left(\sum_{i=1}^{n}(F_{rms})_i^2\right)^{\frac{1}{2}} \tag{55}$$

where

$$(F_{rms})_i^2 = \left[\underbrace{F_i \cdot \left(\frac{\lambda_s}{a_s}\right)_i}_{(F_{ws})_i} \cdot (\mathcal{W}_s)_i \right]^2 \delta\omega \tag{56}$$

Combining 55 and 56 we get

$$F(\omega)_i = [(F_{ws})_i (\mathcal{W}_s)_i]^2 \tag{57}$$

Similarly, we can find displacement, velocity and acceleration spectra (see figure 9 for an example). When integrated these spectra give values of rms force, velocity, displacement and acceleration as a function of T_e (see figures 11 - 20).

D Least squares fit algorithm

The imaginary part, $\Im(\omega)$, of each element of the control matrix is to be approximated by the sum of two frequency independant terms - a spring and an inertia. This approximation is to be achieved using a least-squares-fit method. A weighting function $\varrho(\omega)$ is included.

$$\Im(\omega) = \omega M(\omega) - \frac{S(\omega)}{\omega} \tag{58}$$

where

$\Im(\omega)$ is the imaginary control coefficient.
$M(\omega)$ is the inertia coefficient, approximated by a constant M.
$S(\omega)$ is the spring coefficient, approximated by a constant S.

Let us define a function A which must be minimised

$$A = \frac{1}{n\varsigma}\sum_{i=1}^{n}\left(\varrho(\omega_i)\left\{M\omega_i - \frac{S}{\omega_i} - \Im(\omega_i)\right\}\right)^2 \tag{59}$$

where ς^{-1} is a factor such that $\sum_{i=1}^{n}\varrho(\omega) = 1$. Differentiating 59 gives

$$\frac{\partial A}{\partial M} = \frac{2}{n\varsigma}\sum_{i=1}^{n}\varrho(\omega_i)\left(M\omega_i^2 - S - \omega_i\Im(\omega_i)\right) \tag{60}$$

$$\frac{\partial A}{\partial S} = \frac{-2}{n\varsigma}\sum_{i=1}^{n}\varrho(\omega_i)\left(M - \frac{S}{\omega_i^2} - \frac{\Im(\omega_i)}{\omega_i}\right) \tag{61}$$

Maximising the above ($\frac{\partial A}{\partial M} = \frac{\partial A}{\partial S} = 0$) gives

$$\begin{bmatrix} \Sigma\,\omega^2\varrho(\omega) & -\Sigma\,\varrho(\omega) \\ \Sigma\,\varrho(\omega) & \Sigma\,\frac{\varrho(\omega)}{\omega^2} \end{bmatrix} \cdot \begin{bmatrix} M \\ S \end{bmatrix} = \begin{bmatrix} \Sigma\,\omega\Im(\omega) \\ \Sigma\,\frac{\Im(\omega)}{\omega} \end{bmatrix} \tag{62}$$

The real part, $\Re(\omega)$, of each element of the control matrix is to be approximated by a frequency independant damping term.

$$\Re(\omega) = D(\omega) \tag{63}$$

where

$\Re(\omega)$ is the real control coefficient.
$D(\omega)$ is the damping coefficient, approximated by a constant D.

The measure of error is given by

$$A = \frac{1}{n\varsigma}\sum_{i=1}^{n}\left(\varrho(\omega_i)\left\{D - \Re(\omega_i)\right\}\right)^2 \tag{64}$$

Differentiating A gives

$$\frac{\partial A}{\partial D} = \frac{2}{n\varsigma}\sum_{i=1}^{n}\left(\varrho(\omega_i)\left(D - \Re(\omega_i)\right)\right) \tag{65}$$

which when maximised ($\frac{\partial A}{\partial D} = 0$) becomes

$$D = \frac{\Sigma\,\varrho(\omega)\Re(\omega)}{\Sigma\,\varrho(\omega)} \tag{66}$$

Note that the factor $2(n\varsigma)^{-1}$ cancels when maximising.

E Notation

$\mathbf{a}$	Incident wave amplitude
$\underline{\underline{\mathbf{C}}}$	Control matrix
C_f	Spectral compresion factor
$D(\omega)$	Damping coefficient
$E(\omega)$	Wave spectrum (frequency)
$\underline{\mathbf{F}}$	Force vector
g	Gravity
H	Wave height (= wave amplitude)
h	Heave displacement, tank depth
$\Im$	Imaginary part
k	Wave number
$M(\omega)$	Inertia coefficient
P	Power
$\mathcal{P}(T)$	Power fraction
$\Re$	Real part
$\underline{\mathbf{r}}$	Translation vector
r	Modulus of translation vector
$\mathcal{S}$	Co-ordinate system
S(T)	Wave spectrum (time)
$S(\omega)$	Spring coefficient
s	Surge displacement
T	Period
T_e	Energy period
$\underline{\underline{\mathbf{T}}}$	Transformation matrix
$\underline{\mathbf{v}}$	Velovity vector
$\underline{\mathbf{W}}$	Wave-force coefficient vector
$\mathcal{W}$	Spectral wave-steepness
$\underline{\underline{\mathbf{Z}}}$	Impedance matrix

Subscripts

A	Active
d	Deep water
e	Equivalent (wave-steepness)
F	Force
fh	Fixed-heave
h	Heave
P	Passive
s	Surge
s	Shallow water, spectral (wave-steepness)
v	Velocity

Greek symbols

α	Argument of translation vector
β	Spectral constant
γ	Relative rotation of axes
ζ	Spectral constant
θ	Angular displacement, spectral offset
λ	Wavelength
ξ	Spectral constant
ρ	Density
$\varrho(\omega)$	Weighting function
σ	Spectral constant
τ	Torque
ψ	Amplitude multiplier
ω	Angular frequency

References

[1] Nebel P, *Maximising the efficiency of wave energy plant using complex-conjugate control*, Edinburgh Wave Power Project, 1991.

[2] Wiegel R.L., *Oceanographical Engineering*, Prentice-Hall, 1964.

[3] Skyner D.J., *Solo Duck linear analysis*, Edinburgh Wave Power Project, 1987.

[4] Ránky P.G. & Ho C.Y., *Robot Modelling*, Springer-Verlag, 1985.

[5] Snyder W.E., *Industrial Robots: Computer Interfacing and Control*, Prentice-Hall, 1985.

[6] Pizer D., *Numerical prediction of the performance of the solo Duck*, Edinburgh Wave Power Project, 1992.

[7] Crabb J.A., Synthesis of a directional wave climate in *Power from Sea Waves*, Count B., ed, Academic Press, London, 1980, 41-74.

[8] Mollison D, Wave energy losses in intermediate depths, *Applied Ocean Research*, 1983, **5**, (4), 234-236.

[9] Massey B.S., *Mechanics of Fluids*, 5^{th} ed., Van Nostrand Reinhold (UK), 1983.

[10] Young H.E. & Pollock J., *Variable coefficient control of a wave energy device*, Edinburgh Wave Power Project, 1985.

[11] Mei C.C., *The Applied Dynamics of Ocean Surface Waves*, World Scientific Publishing Co., 1989.

[12] Moscowitz L. & Pierson W., *J. Geophysical Res.*, 1964, **69**, (24), 5161-5190.

Maximising the efficiency of wave energy plant using complex-conjugate control

Paul Nebel

University of Edinburgh Department of Mechanical Engineering, Wave Power Project

The method for determining the hydrodynamic coefficients of a floating wave energy absorber is outlined, and the coefficients of a Salter's Duck are measured experimentally. A complex-conjugate synthesiser, derived from these coefficients, is used both theoretically and experimentally to predict and to measure the efficiency of a Duck in unidirectional monochromatic waves. The synthesis produces a higher efficiency over a greater bandwidth than has been achieved before. The reason for the improvement in efficiency is explained, and conclusions are drawn about the implications of complex-conjugate control for predicting practical engineering constraints on the design of a full-sized wave energy absorber.

Introduction

Diffraction theory provides a useful model for determining the hydrodynamic characteristics of a floating body [1] [2] [3] [4]. It has been shown that an optimum (complex-conjugate) control function for maximising power absorption by a wave energy device can be derived from knowledge of these characteristics [4] [5] [6]. Even though this relationship is widely quoted little attention has been given to implementing this control for a wave energy absorber.

Values of the frequency-domain coefficients must be known over a wide bandwidth to predict the response of the device to random seas or to formulate a time-domain simulation [7] [8]. Jefferys [9] has developed methods for characterising the hydrodynamics over a large range of frequencies using values of the coefficients found at a few frequency points.

Complex-conjugate control is strongly linked to the underwater shape of a device. For many economically viable shapes its implementation can require very large displacements to absorb power from seas with a small device size-to-wavelength ratio. The Salter's Duck is suited to complex-conjugate control in that, at low diameter-to-wavelength ratios, displacements are of a reasonable amplitude.

Complex-conjugate control is inherently unstable. A stable pseudo complex-conjugate controller must be designed which simulates optimum control over as wide a bandwidth as possible. The Edinburgh Wave Power Project has developed pseudo complex-conjugate control for flap-type wave-makers over a reasonable frequency bandwidth. It is therefore likely that the difficulties encountered in stabilising optimal control for a wave absorber can be overcome.

This paper describes a first attempt to synthesise complex-conjugate control for a Duck model. Synthesis is based on the transfer function relating signals operating the model to the forces and velocities experienced by the model. This transfer function is used to calculate the operating signals needed to achieve particular forces/velocities, as opposed to controlling the forces/velocities in real time. It is necessary because, for these tests, the model does not incorporate control. Synthesis is also useful because it is capable of simulating both stable and unstable controllers.

The paper begins by describing the Duck hydrodynamics and the experimental methods used to obtain the radiation impedance and wave force coefficients. Complex-conjugate synthesis is implemented for a Duck constrained to move in two and three degrees of freedom, subject to monochromatic incident waves. The results for both these cases agree well with predictions based on the model coefficients suggesting that the linear model can be used to predict the effect of changes in shape on the forces, displacements and velocities of an optimally controlled device.

The control matrix derived for complex-conjugate synthesis is compared with procedures used previously for optimisation of Duck performance. These procedures involved the application of ordinary reactive loading (i.e. spring, damping and inertia) terms on the leading diagonal of the control matrix. The off-diagonal coefficients were set to zero.

A complex-conjugate equivalent control matrix is derived, with coefficients on the leading diagonal only. Such a matrix will produce the same forces from a given velocity vector as will complex-conjugate control. Equivalent matrices can only be derived if the incident waves are unidirectional. These equivalents indicate that cross-terms are required in the matrix if the realisation of optimal control is not to become unstable.

The complex-conjugate method can be used in conjunction with numerical methods to evaluate the relative merits of different constraints and wave absorber shapes. It can derive information necessary for the economic optimisation of an absorber, and it can be implemented as a practical control strategy for an absorber.

Hydrodynamics

The following section defines the linear equation describing the interaction of the Duck with the water, and the expressions giving extracted power and efficiency for the particular control strategy implemented.

A rigid body moving in three dimensions has six degrees of freedom, comprising a rotation about and a translation in each dimension. In these two-dimensional tests Duck models are constrained to move in only three of their possible six degres of freedom, namely Pitch, Heave and Surge (see figure 1). The state of the duck is defined by six functions of time t, being three forces acting on the axis and three velocities measured at the axis. The incoming wave train is a function of position $\underline{r}$ as well as time.

The same symbols are used to represent a variable in the time and frequency domains. If the dependance of a variable is not explicitly stated, it may be assumed to be a function of frequency.

Equation of Motion

The linear equation of motion modelling the hydrodynamic system is best described by separating the external forces into two components [2] [3] [4]; those caused by the incident wave, and those caused by the radiated wave.

$$\underline{\mathbf{F}}(t) = \underline{\mathbf{F}}_r(t) + \underline{\mathbf{F}}_w(t) \qquad (1)$$

Where

$\underline{\mathbf{F}}_r(t)$ are the forces due to the motion of the Duck when driven in still water, and depend on Duck velocities $\underline{\mathbf{v}}$ only.

$\underline{\mathbf{F}}_w(t)$ are the forces due to the Duck being held stationary in the presence of an incident wave, and depend on incident wave amplitude **a** only.

The linear equation describing the motion of the duck is therefore given by

$$\underline{\mathbf{F}}(\omega,\alpha) = \underline{\underline{\mathbf{Z}}}(\omega)\cdot\underline{\mathbf{v}}(\omega,\alpha) + \underline{\mathbf{W}}(\omega,\alpha)\cdot\mathbf{a}(\omega,\alpha) \qquad (2)$$

Where

$\underline{\underline{\mathbf{Z}}}$ is the complex radiation impedance matrix.
$\underline{\mathbf{W}}$ is the complex wave force coefficient vector.

An explaination of these terms follows. The equation of motion relates Duck velocities to external forces and to wave forces. The matrix form of the equation indicates that the velocity in one degree of freedom depends on the forces acting in all the degrees of freedom - not just its own.

Here $\underline{\underline{\mathbf{Z}}}$ is a complex 3x3 frequency-dependant matrix relating modulus and phase of force in one degree-of-freedom to unit velocity in another degree-of-freedom. It is dimensionally inhomogenous due to the definitions of $\underline{\mathbf{F}}$ and $\underline{\mathbf{v}}$.

The imaginary part comprises an 'added mass' term (due to the inertia of the water that the Duck displaces when moving) plus a term representing hydrostatic spring and a term representing the Duck dry inertia. The latter must be removed from the imaginary part so that $\underline{\underline{\mathbf{Z}}}$ depends on the underwater shape of the duck only. The real part of $\underline{\underline{\mathbf{Z}}}$ is often referred to as the 'added damping' and is closely related to the power radiated from the duck when a component of velocity is in phase with force.

Using the equivalence $\frac{d}{dt} \equiv i\omega$ we can split $\underline{\underline{\mathbf{Z}}}$ into its component parts;

$$\underline{\underline{\mathbf{Z}}}(\omega) = \underline{\underline{\mathbf{D}}}_A(\omega) + i\omega\underline{\underline{\mathbf{M}}}_A(\omega) + i\omega\underline{\underline{\mu}} + \frac{1}{i\omega}\underline{\underline{\sigma}} \qquad (3)$$

Where

$\underline{\underline{\mathbf{D}}}_A$ is the frequency-dependant added damping matrix.

$\underline{\underline{\mathbf{M}}}_A$ is the frequency-dependant added mass matrix.
$\underline{\underline{\mu}}$ is the Duck inertia matrix.
$\underline{\underline{\sigma}}$ is the hydrostatic spring matrix.

Newman [3] has shown that the radiation impedance matrix is symmetrical about the leading diagonal.

The vector $\underline{\mathbf{W}}$ describes the forces required to hold the duck stationary when a wave of unit amplitude is incident. In this case the incident waves are unidirectional, so that $\alpha = 0$.

Control Equation

It is necessary to modify the motion of the duck if it is to extract power from an incident wave. The control function being implemented is;

$$\underline{\mathbf{F}} = -\underline{\underline{\mathbf{C}}}\cdot\underline{\mathbf{v}} \qquad (4)$$

$\underline{\underline{\mathbf{C}}}(\omega)$ is a 3x3 frequency-dependant matrix which expresses forces as linear functions of velocity.

The motion of the duck is now a function of $\underline{\underline{\mathbf{C}}}$. Combining equation 2 with 4 we get

$$-\underline{\underline{\mathbf{C}}}\cdot\underline{\mathbf{v}} = \underline{\underline{\mathbf{Z}}}\cdot\underline{\mathbf{v}} + \underline{\mathbf{W}}\cdot\mathbf{a} \;\Rightarrow\; \underline{\mathbf{v}} = -\left(\underline{\underline{\mathbf{C}}} + \underline{\underline{\mathbf{Z}}}\right)^{-1}\cdot\underline{\mathbf{W}}\cdot\mathbf{a} \qquad (5)$$

Substituting for $\underline{\mathbf{v}}$ in 4

$$\underline{\mathbf{F}} = \underline{\underline{\mathbf{C}}}\cdot\left(\underline{\underline{\mathbf{C}}} + \underline{\underline{\mathbf{Z}}}\right)^{-1}\cdot\underline{\mathbf{W}}\cdot\mathbf{a} \qquad (6)$$

Equation 4 describes how the hydrodynamic system is to be controlled (due to our definition of $\underline{\underline{\mathbf{Z}}}$ the hydrodynamic system is assumed, for the moment, to include Duck dry inertia).

The average power **P** passing through the Duck is given [4] by

$$\mathbf{P} = \frac{1}{2}\left[\Re\{\underline{\mathbf{F}}\}\cdot\Re\{\underline{\mathbf{v}}\} + \Im\{\underline{\mathbf{F}}\}\cdot\Im\{\underline{\mathbf{v}}\}\right] \qquad (7)$$

The definitions of $\underline{\mathbf{F}}$ and $\underline{\mathbf{v}}$ lead to **P** being negative when power is absorbed by the Duck.

A maximum for absorbed power [4] [5] [6] occurs when

$$\underline{\underline{C}} = \underline{\underline{Z}}^{*^T} \tag{8}$$

The relation expressed by equation 8 is referred to as 'complex-conjugate control'. Its application in this context is directly analagous to maximising the power output of a generator by connecting a load whose resistance is equal to its internal resistance.

The radiation impedance matrix $\underline{\underline{Z}}$ should be symmetrical [3] such that

$$\underline{\underline{Z}} = \underline{\underline{Z}}^T \tag{9}$$

and

$$\underline{\underline{C}} = \underline{\underline{Z}}^* \tag{10}$$

Hence for synthesis of complex-conjugate control the demand velocities and forces from equations 5 & 6 become

$$\underline{v} = -\frac{1}{2}\Re\left\{\underline{\underline{Z}}\right\}^{-1} \cdot \underline{\underline{W}} \cdot \mathbf{a} \tag{11}$$

$$\underline{F} = \underline{\underline{Z}}^* \cdot \frac{1}{2}\Re\left\{\underline{\underline{Z}}\right\}^{-1} \cdot \underline{\underline{W}} \cdot \mathbf{a} \tag{12}$$

Efficiency

For three-dimensional tests, Duck efficiency is defined to be

$$\eta = \frac{\text{Capture width}}{\text{Duck width}} \tag{13}$$

with Capture width being defined as

$$\mathrm{C} = \frac{\text{Power absorbed}}{\text{Power incident per metre}} \tag{14}$$

Budal and Falnes [10] showed that this leads to a theoretical upper limit on the capture width of a device with two degrees-of-freedom as width tends to zero of

$$\mathrm{C}_m = \frac{\lambda}{\pi} \tag{15}$$

which can lead to efficiencies of well above 100%. For two-dimensional tests in the Narrow Tank, however, Duck efficiency is defined to be

$$\eta = \frac{\text{Power absorbed}}{\text{Total power incident}} \tag{16}$$

The efficiency is therefore dependant on the tank width and not on the capture width. This means that, unlike the open sea, efficiencies in excess of 100% are not achievable by definition (i.e the Duck cannot extract more energy than is available in the system).

Total power absorbed by the Duck is the sum of the powers absorbed by each degree-of-freedom. Power is the scalar product of the force and velocity vectors in time. This was expressed as a function of frequency (equation 7).

Since the Narrow Tank is of intermediate depth all wave powers have been corrected to allow for depth dependant effects [11].

Efficiency is calculated two ways. The first is based on the wave amplitudes

$$\eta_1 = \frac{(\mathbf{P}_I \times \mathrm{w}_I) - (\mathbf{P}_R \times \mathrm{w}_R) - (\mathbf{P}_T \times \mathrm{w}_T)}{\mathbf{P}_I \times \mathrm{w}_I} \tag{17}$$

Where w is the tank width at the position of wave measurement. The second is based on the model forces and velocities

$$\eta_2 = \frac{\mathbf{P}_p + \mathbf{P}_h + \mathbf{P}_s}{\mathbf{P}_I \times \mathrm{w}_I} \tag{18}$$

These values should be the same, but in practice $\eta_1 > \eta_2$. This is because there are losses in the system. The unaccounted power represented by $(\eta_1 - \eta_2)$ contains energy lost through

1. Friction.
2. Tank attenuation.
3. Non-linearity of Duck motion.
4. Body losses (Viscous damping, vortex shedding etc.)

Experimental Set Up and Method

The tests described here were undertaken in the 6m long flume at the University of Edinburgh Wave Power Project. The tank is 300mm wide and has electrically operated flap-type wavemakers at both ends. The still water depth was 580mm. The Duck was mounted midway between the wavemakers. Two surface elevation wavegauges were placed in front of the model to measure incident and reflected waves, and one placed astern to measure transmitted waves. Beaching situated astern of the model absorbs the transmitted waves. Only about 3% of the wave power incident to the wavemakers is re-reflected, as they are of the absorbing type developed at Edinburgh. The ripples seen on the experimentally determined graphs may be due these reflections.

Experiments were controlled by a computer, connected to a synthesiser (a multi-frequency, multi-channel signal generator). The computer generated the test frequencies and sampled the data. The test frequencies were integer multiples of the reciprocal of the sampling time ($\frac{1}{51.2}$Hz) in the range 0.5Hz to 1.5Hz. This range was chosen because it covers the values of $\left(\frac{wavelength}{duck\ diameter}\right)$ which have proven most difficult to optimise. Depth corrected wavelength is given as a function of frequency in figure 2(a), and the ratio of depth corrected wavelength to model diameter is given in figure 2(b).

The incident wave amplitude was restricted to a maximum of 1.5mm to limit non-linearity, particularly at the low frequencies where the Pitch, Heave and Surge rig itself becomes significantly non-linear. Heave and surge velocities were restricted to a maximum of $0.01ms^{-1}$ for the same reason.

The rig was used to control a 100mm diameter Duck model, and constrains motion to the three degrees of freedom shown in figure 1. The rig incorporates no control for these experiments. Consequently, control was

achieved by 'synthesis'. To achieve synthesis a transfer function was evaluated relating the power amplifier signals operating the rig to the forces and velocities experienced by the model.

Demand forces/velocities were produced by working out the signals required to achieve them, and by supplying these signals to the power amplifiers during each test. This is as opposed to digitally controlling the forces/velocities in real time. Synthesis is capable of simulating both stable and unstable controllers.

The equation of motion (equation 2) can be split into two parts; forces due to motion of the Duck in still water (described by $\underline{\underline{Z}}$) which are dependant on $\underline{v}$ only

$$\underline{F} = \underline{\underline{Z}} \cdot \underline{v} \tag{19}$$

and forces due to the Duck being held stationary in the presence of an incident wave (described by $\underline{W}$) which are dependant on $\mathbf{a}$ only

$$\underline{F} = \underline{W} \cdot \mathbf{a} \tag{20}$$

In order to determine what proportion of the measured force is due to Duck motion in each degree-of-freedom and what proportion is due to the incident wave, four experiments were carried out. Three of these experiments involved driving one of the degrees of freedom of the Duck in still water while fixing the other two. In the fourth experiment all three axes are fixed in the presence of an incident wave.

Matrix $\underline{\underline{Z}}$ is a function of Duck forces and velocities which have been measured. Vector $\underline{W}$ is also a function of Duck forces and of incident wave amplitude, which has been measured. Any four experiments can be used to derive the coefficients. All that is required is that the experiments be as orthogonal as possible. This is best achieved by heavily damping the 'fixed' axes.

In order to account for possible energy losses in experimental determination of the impedance, the radiated wave was measured while the duck was being driven. The amplitude of the radiated wave at any point $\underline{r}$ can be related to the velocity vector $\underline{v}$ of the Duck by the radiation pattern vector $\underline{R}$, where

$$\mathbf{a}(\underline{r}) = \underline{R}(\underline{r}) \cdot \underline{v} \tag{21}$$

By equating power put into the water by the Duck with the power flux in the far field radiated wave we can relate the real part of the radiation impedance to the radiation pattern vector [4] by

$$\Re\{\mathbf{Z}_{jk}\} = \frac{\rho g^2}{2\omega} \sum_{n=0}^{N-1} \mathbf{R}_j^*(\alpha_n)\, \mathbf{R}_k(\alpha_n)\, \delta\alpha \tag{22}$$

Two complex-conjugate synthesis runs were undertaken. In the first, the model was allowed to move in all three of its possible degrees-of-freedom. In the second, the model was constrained to move in two degrees-of-freedom only (pitch and surge), being the motions easiest to engineer for full scale control of the Duck.

Discussion of Results

Figure 3 shows the coefficients of a complex-conjugate control matrix. Also included in this figure are the damping coefficients calculated from the energy flux in the radiated waves using equation 22. The imaginary parts of the predicted damping coefficients are included in figure 3. They are drawn to the same scale as their respective real parts. Their small size indicates that the values for $\underline{R}$ are good.

It can be seen that the calculated damping coefficients are somewhat smaller than the measured coefficients, particularly on the leading diagonal. This effect was also noted by Skyner [12] in tests with similarly sized and shaped Duck models, and points strongly to body losses in the model. Experiments are being undertaken at present to confirm and/or account for these apparent losses.

Figures 4 & 5 show respectively the coefficients of equivalent 3 & 2 d.o.f control matrices with no cross coupling terms. A complex-conjugate equivalent matrix will calculate the same forces from a given velocity vector as a complex conjugate matrix . These equivalent matrices can only be derived if the incident waves are unidirectional.

For 2 & 3 degree-of-freedom synthesis, the Duck is radiating energy in surge while it absorbs energy in pitch (and heave for 3 d.o.f). The leading diagonal equivalents shown in figures 4 & 5 require the damping applied in surge to be negative with respect to surge velocity over most of their range.

Previous Duck control strategies have been implemented using leading diagonal terms only. This is perhaps one reason why complex-conjugate synthesis achieves close to 100% efficiency over a wider bandwidth than previous strategies. Leading diagonal control prevents stable optimisation.

Complex-conjugate control is inherently unstable. The aim of these experiments is to produce pseudo complex-conjugate control which is stable over all frequencies, and maximally efficient over as wide a bandwidth as possible.

Theory suggests that a wave energy absorber with at least two orthogonal degrees of freedom which is capable of producing symmetric/anti-symmetric waves forward and astern should be capable of absorbing 100% of the incident power available in the tests described above [6]. Figures 6 & 7 show the predicted and measured efficiencies for the two synthesis runs.

The results for the three degree-of-freedom run are slightly better than those for the two degree-of-freedom run at low frequencies. This is partly due to the three degree-of-freedom case containing a redundant degree-of-freedom. Neither of the measured values of η_1 quite achieves the theoretical limit of 100% absorption. However, the measured results agree well with the predicted results in figures 6 & 7 (a) suggesting that this shortfall is due to non-linearity rather than failure of the theory.

Predictions of the reflected/transmitted wave ampli-

tudes do not compare as well with experimental results at low frequencies as do forces/velocities. The dip in the predicted η_1 at approximately 0.6Hz corresponds to the fundamental standing wave mode of the tank. The Narrow Tank is not quite long enough for us to be certain that transient wave modes [13] of the wavemakers and/or model are not corrupting wave measurements. Re-reflection of the transmitted/reflected waves may produce the 'ripple' seen on many of the following figures. A technique for eliminating re-reflection is being evaluated.

Ideally the radiation impedance matrix should be symmetrical (see equations 9 & 12). The impedance matrix used for synthesis in these experiments was calculated from one set of impedance tests only (due to time restrictions). It may not, therefore, be exactly symmetrical. This is one source of error. It would be better if impedance were averaged from multiple sets of impedance tests, as will be the case in future experiments.

The value of η_2 shown in figures 6 & 7 (a) falls some 20% short of η_1 for both the measured and the predicted values. This is consistent with the predicted impedances being lower than the measured impedances as a result of model losses. The real part of the complex-conjugate control matrix was replaced by the real part predicted from the radiation pattern vector. This new matrix was used to predict forces from the velocities measured in the synthesis runs. The power calculated from the product of the measured velocities and the predicted forces is plotted in figures 6 & 7 (b), and compares well with the measured η_1. This result also supports the presence of skin and corner losses in the model.

Figures 8, 9, 10 & 11 show force and displacement per unit wave steepness as a function of frequency for the 3 & 2 degree-of-freedom cases respectively. Wave steepness is here defined as $\left(\frac{Wave\ amplitude}{Wavelength}\right)$. Also shown in figures 8 & 9 are the ratios for the forces predicted from the radiation pattern vector.

These curves can be used (within the limits of linearity) to predict force/displacement for a particular incident wave amplitude. They indicate that at low frequencies and/or small device diameter-to-wavelength ratios the limit of linearity is reached rapidly for very small increases in incident wave size. For each amplitude there will be a cut-off frequency below which the device cannot operate as to do so would imply displacements such that it jumps out of the water.

From the point of view of material, construction and capital costs a full-scale Duck should have as small a diameter as possible. Reducing the diameter also reduces the extreme wave loading on the device. A smaller diameter must be weighed against the engineering and control practicality of such a device absorbing large amounts of power from seas with a wavelength very much greater than this diameter. By maximising the efficiency of the device at low frequency, complex-conjugate control allows the projected full-scale diameter of the Duck to be reduced without significant degredation of its performance.

A linear complex-conjugate controller applied to a small non-linear Duck may not be able to achieve maximum efficiency, but it will be able to achieve higher efficiencies than a leading diagonal controller for the same Duck diameter.

Work is being undertaken by the Wave Power Project to develop the high pressure oil hardware which will be able to control the Duck forces.

Conclusions and Future Work

The results obtained in this set of experiments strongly support theoretical predictions that a wave energy absorber which is constrained to move in at least two orthogonal degrees of freedom, and which has a shape capable of producing waves in both phase and antiphase forward and astern can absorb 100% of the incident power available in its own width in linear monochromatic waves. The bandwidth over which such absorption is achievable may be limited by the shape of the device.

Experimental values compare well with predicted results, suggesting that the linear model is good. Since complex-conjugate control is dependant upon impedance and wave force matrices which can be derived numerically, it can be incorporated in a numerical model to predict the effects of changes of shape and constraint on the practical aspects of a wave energy absorber. Such information can be used as a first comparison of different shapes/constraints which can guide model testing, and can help derive an economically viable size for an absorber.

Optimal control is only possible if the device is capable of radiating power in some degrees of freedom while power is being absorbed in others. This can be achieved by the inclusion of cross-coupling terms in the control matrix.

It is hoped that the complex-conjugate method will allow the full-scale diameter of a Duck to be reduced without significant loss of performance. For the Atlantic, this could mean a reduction from the projected figure of 14m to about 8m. The savings in material, construction and capital costs, lower body forces and greater economic efficiency could be achieved at the acceptable price of larger displacements and a highly sophisticated, possibly non-linear, controller.

The high-pressure oil hardware required for control of the Duck is being developed at the Wave Power Project. The next step in the realisation of complex-conjugate control is to improve the rig and refine the techniques for measuring absorber coefficients. Stable control will then be investigated in the three-dimensional Wide Tank at Edinburgh.

Acknowledgements

I should like to thank the Edinburgh University Wave Power Project. In particular, my thanks to Stephen

Salter for making this work possible, and to Peter Woodhead for providing its guidance and supervision.

Notation

$\mathbf{a}$	Incident wave amplitude
C	Capture width
$\underline{\underline{\mathbf{C}}}$	Control matrix
$\underline{\underline{\mathbf{D}}}_A$	Frequency-dependant added damping matrix
$\underline{\mathbf{F}}$	Force vector
g	Gravity
$\Im$	Imaginary part of complex number
$\underline{\underline{\mathbf{M}}}_A$	Frequency-dependant added mass matrix
$\mathbf{P}$	Power
$\underline{\mathbf{R}}$	Radiation pattern vector
$\underline{\mathbf{r}}$	Position of wave in tank
$\Re$	Real part of complex number
t	time
$\mathbf{T}$	Sampling period
$\underline{\mathbf{v}}$	Duck velocity vector
w	Tank width
$\underline{\mathbf{W}}$	Wave force coefficient vector
$\underline{\underline{\mathbf{Z}}}$	Complex radiation impedance matrix

Greek Symbols

α	Wave angle
η	Efficiency
λ	Wavelength
$\underline{\underline{\mu}}$	Duck inertia matrix
ρ	Density of water
$\underline{\underline{\sigma}}$	Hydroststic spring matrix
ω	Angular frequency

Superscripts

T	Transpose of matrix
$*$	Complex-conjugate

Subscripts

I	Incident wave
r	Radiation condition
R	Reflected wave
T	Transmitted wave
w	Diffraction condition

References

[1] Mei C.C., *The Applied Dynamics of Ocean Surface Waves*, World Scientific Publishing Co., 1989.

[2] Evans D.V., Some Theoretical Aspects of Three-Dimensional Wave-Energy Absorbers, *Symp. Ocean Wave Energy Utilization, Gothenburg*, 1979.

[3] Newman J.N., The Interraction of Stationary Vessels with Regular Waves, *Proc. 11th Symp. Naval Hydrodynamics, London*, 1976, 491-501.

[4] Skyner D.J., *Solo Duck Linear Analysis*, Edinburgh Wave Power Project, 1987.

[5] Evans D.V., A Theory for Wave-Power Absorption by Oscillating Bodies, *J. Fluid Mech.*, 1976, **77**, (1), 1-25.

[6] Mei C.C., Power Extraction from Water Waves, *J. Ship Res.*, 1976, **20**, 63-66.

[7] Jefferys E.R., *Modelling and Optimisation of a Wave Energy Converter*, PhD Thesis, University of Cambridge, 1979.

[8] Count B., *On the Physics of Absorbing Energy From Ocean Waves*, PhD Thesis, Marchwood Engineering Laboratories, 1982.

[9] Jefferys E. R., Interpolation and Extrapolation of Hydrodynamic Coefficients, *Applied Ocean Research*, 1983, **5**, (3), 145-149.

[10] Budal K. & Falnes J., Marine Science Communications, 1977, **3**, (2), 133-150.

[11] Edinburgh Wave Power Project, Fourth Year Report, 1978.

[12] Skyner D. J., The Hydrodynamics of Solo Ducks, *Proc. Conf. Wave Energy Devices*, 1989, 52-60.

[13] Hyun J. M., Theory for Hinged Wavemakers of Finite Draft in Water of Constant Depth, *J. Hydronautics*, 1976, **10**, (1), 2-7.

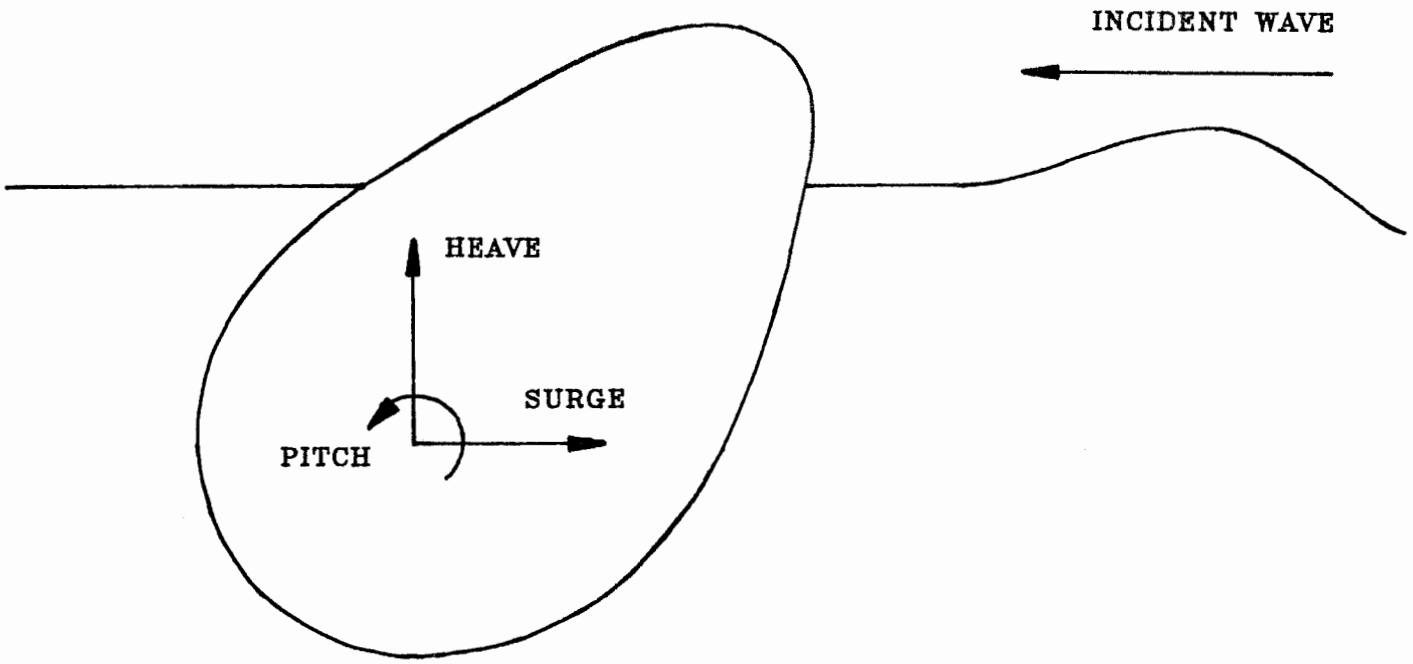

FIGURE.1. DEFINITION OF DUCK DEGREES-OF-FREEDOM

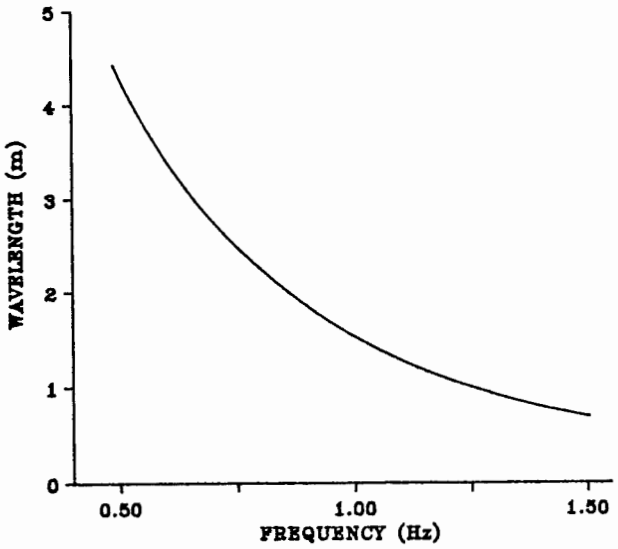

FIGURE.2(A). DEPTH CORRECTED WAVELENGTH

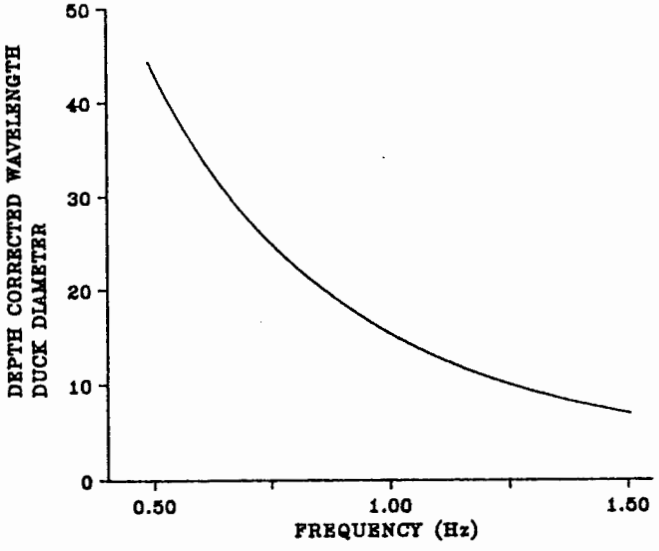

FIGURE.2(B). RATIO OF DEPTH CORRECTED WAVELENGTH TO DUCK MODEL DIAMETER

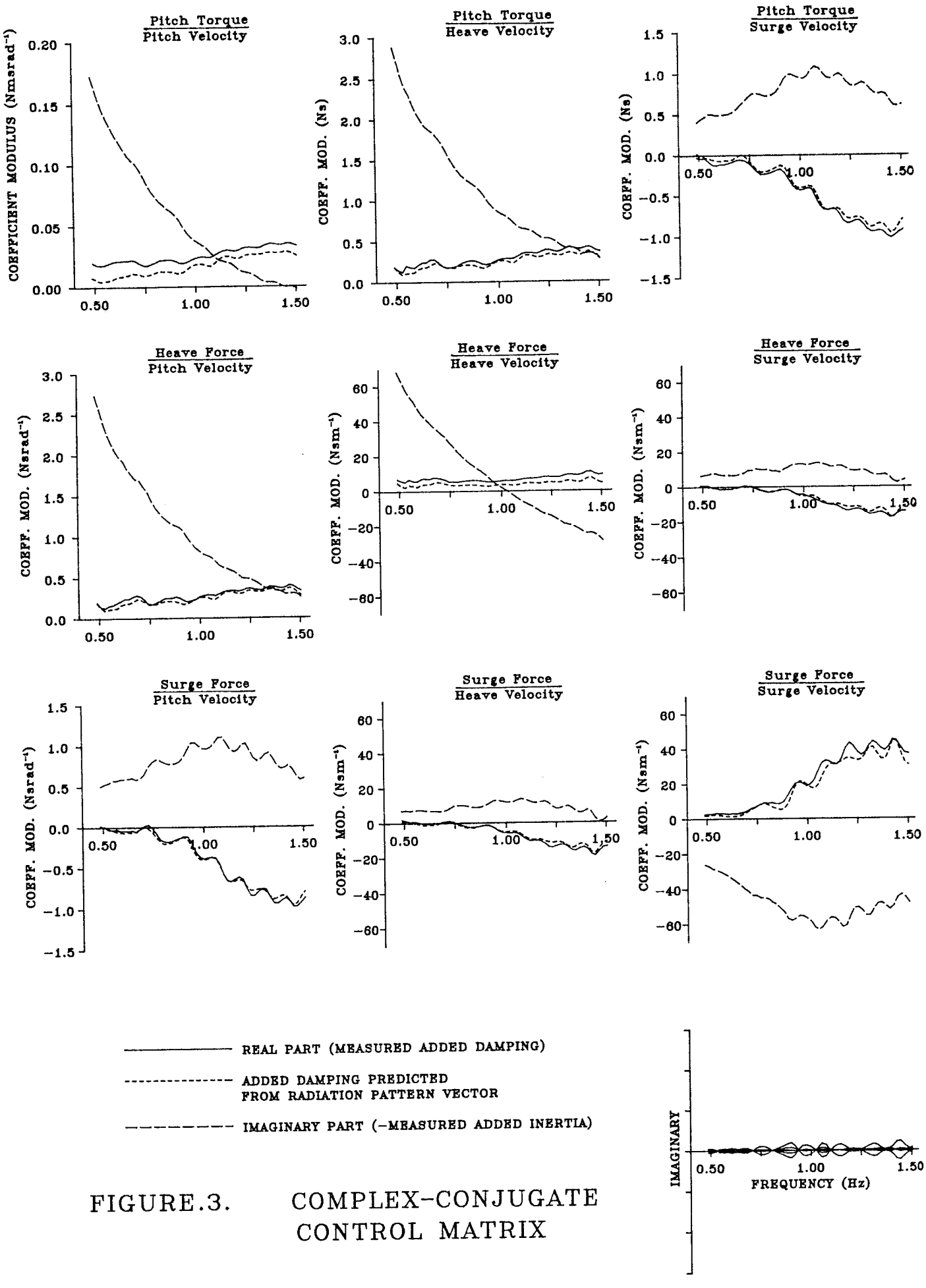

FIGURE.3. COMPLEX-CONJUGATE CONTROL MATRIX

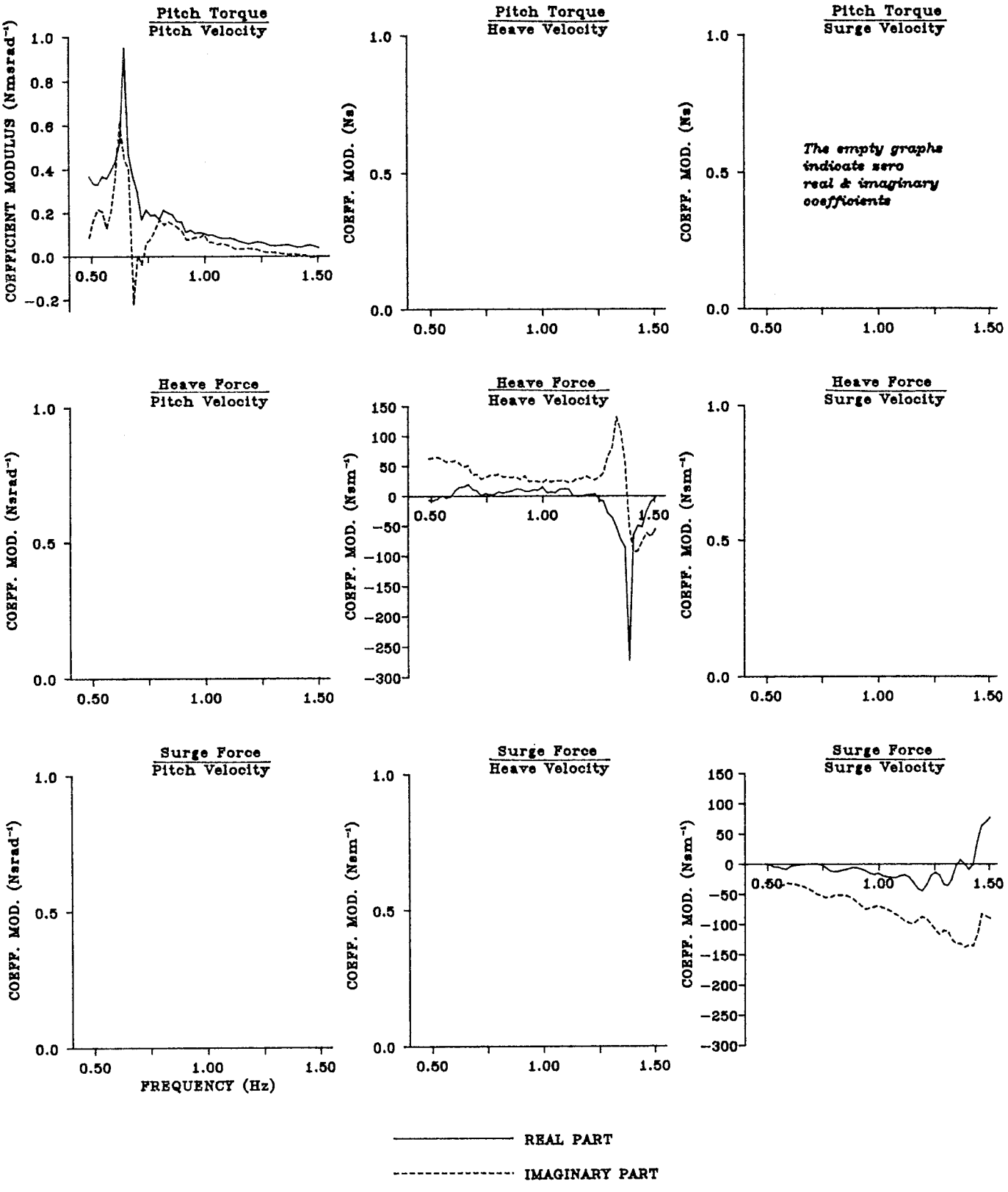

FIGURE.4. LEADING DIAGONAL COMPLEX-CONJUGATE EQUIVALENT CONTROL MATRIX FOR 3 DEGREE-OF-FREEDOM SYNTHESIS

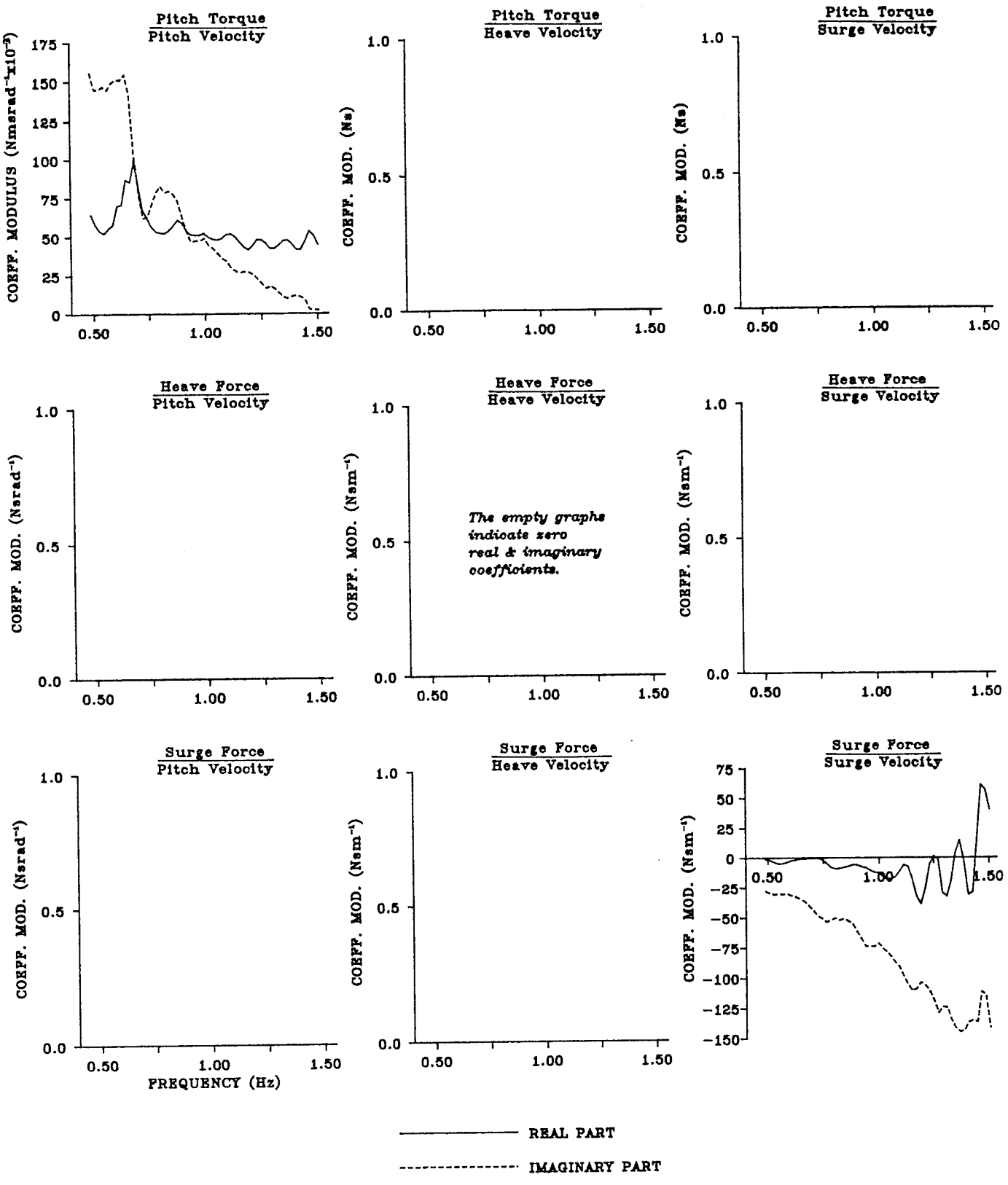

FIGURE.5. LEADING DIAGONAL COMPLEX-CONJUGATE EQUIVALENT CONTROL MATRIX FOR 2 DEGREE-OF-FREEDOM SYNTHESIS

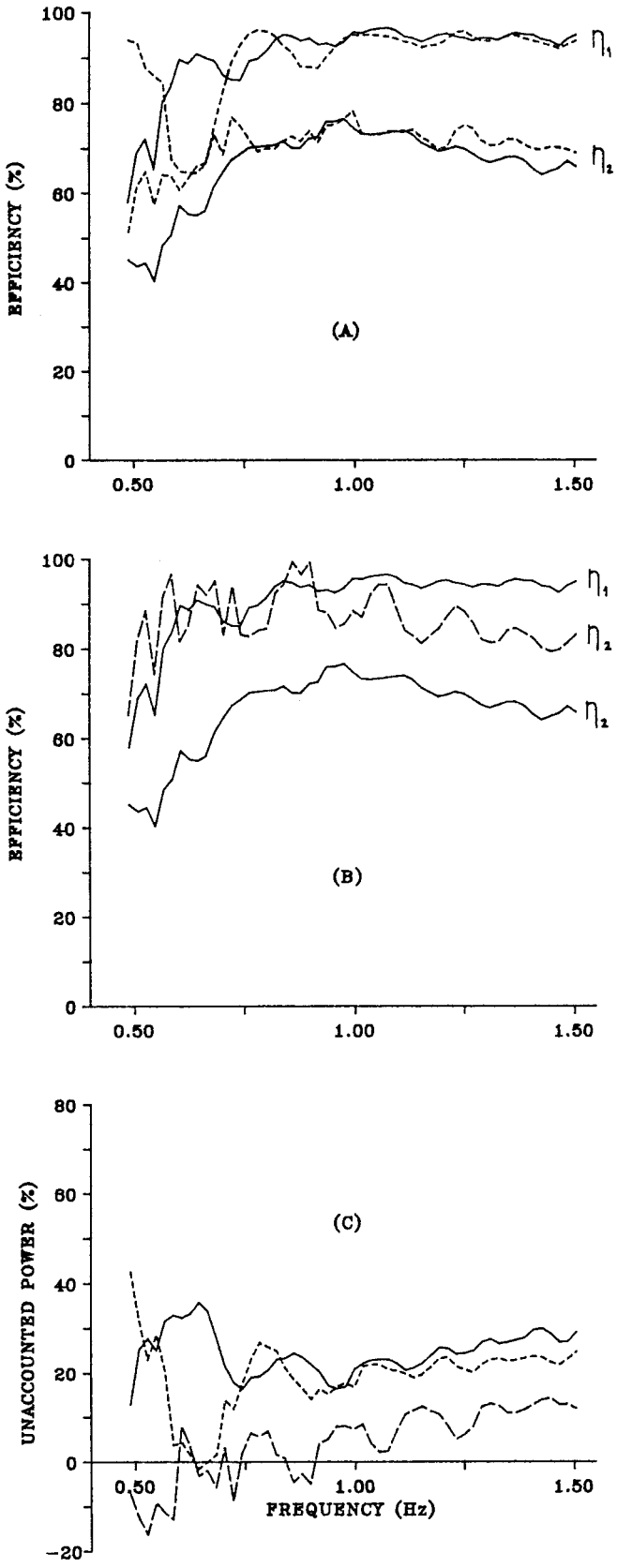

FIGURE.6. EFFICIENCY & POWER BALANCE FOR 3 DEGREE-OF-FREEDOM COMPLEX-CONJUGATE SYNTHESIS

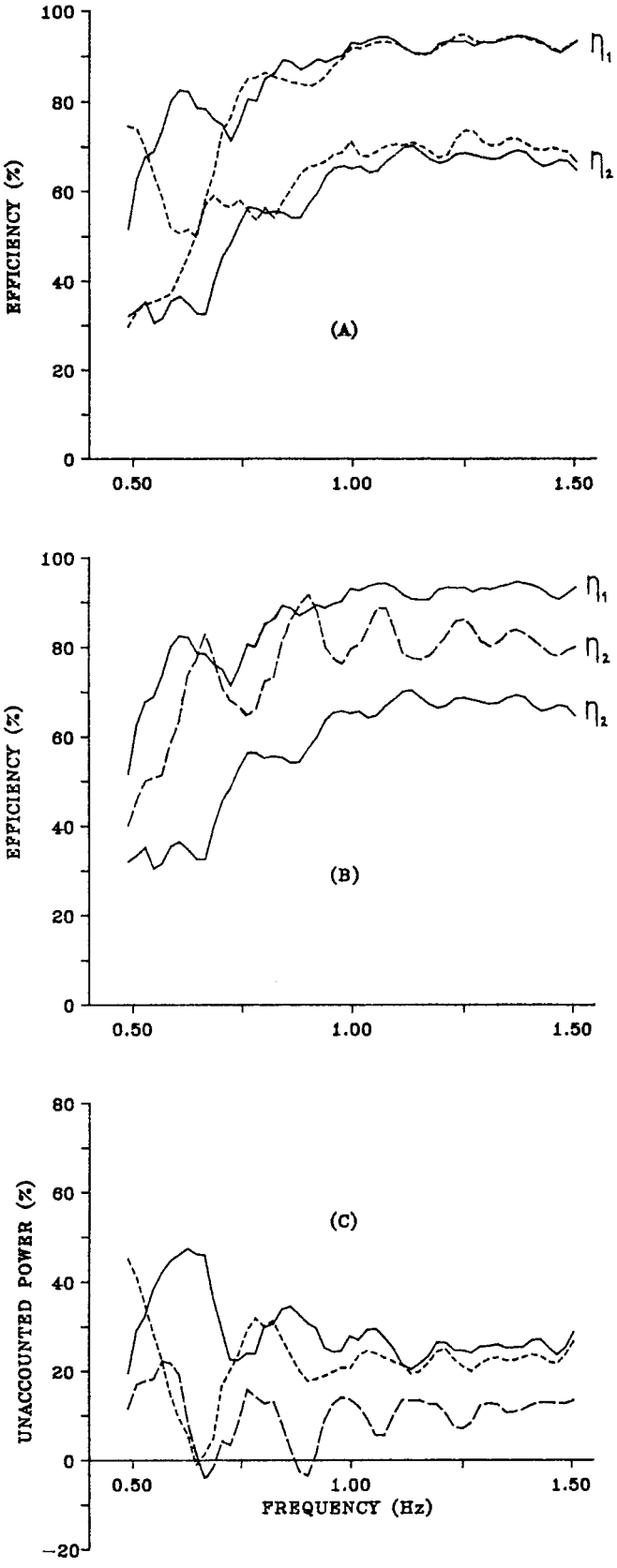

FIGURE.7. EFFICIENCY & POWER BALANCE FOR 2 DEGREE-OF-FREEDOM COMPLEX-CONJUGATE SYNTHESIS

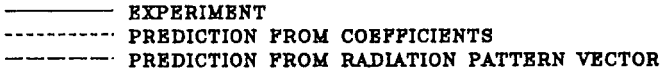

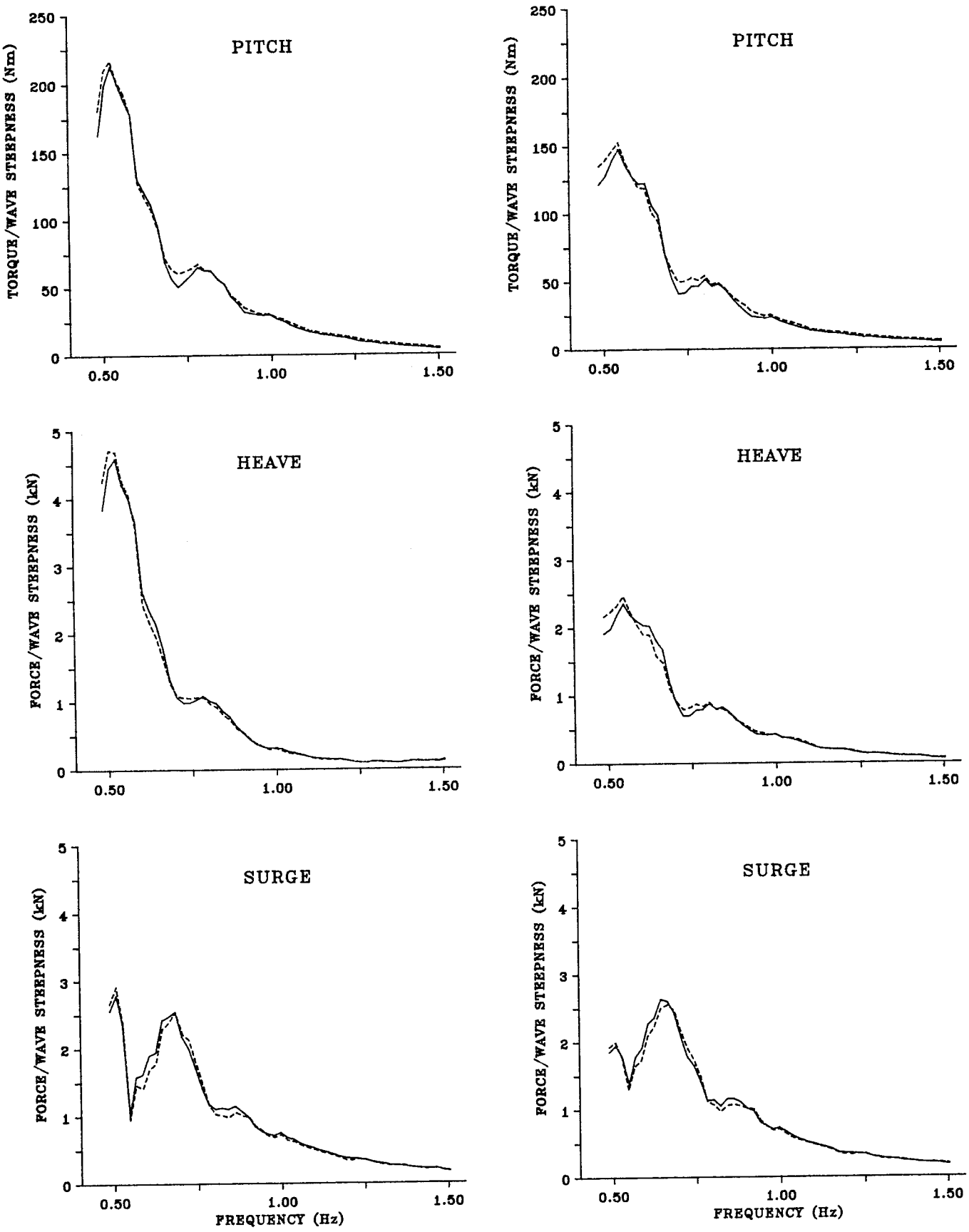

FIGURE.8. FORCE PER UNIT WAVE STEEPNESS FOR 3 DEGREE-OF-FREEDOM COMPLEX-CONJUGATE SYNTHESIS

FIGURE.9. FORCE PER UNIT WAVE STEEPNESS FOR 2 DEGREE-OF-FREEDOM COMPLEX-CONJUGATE SYNTHESIS

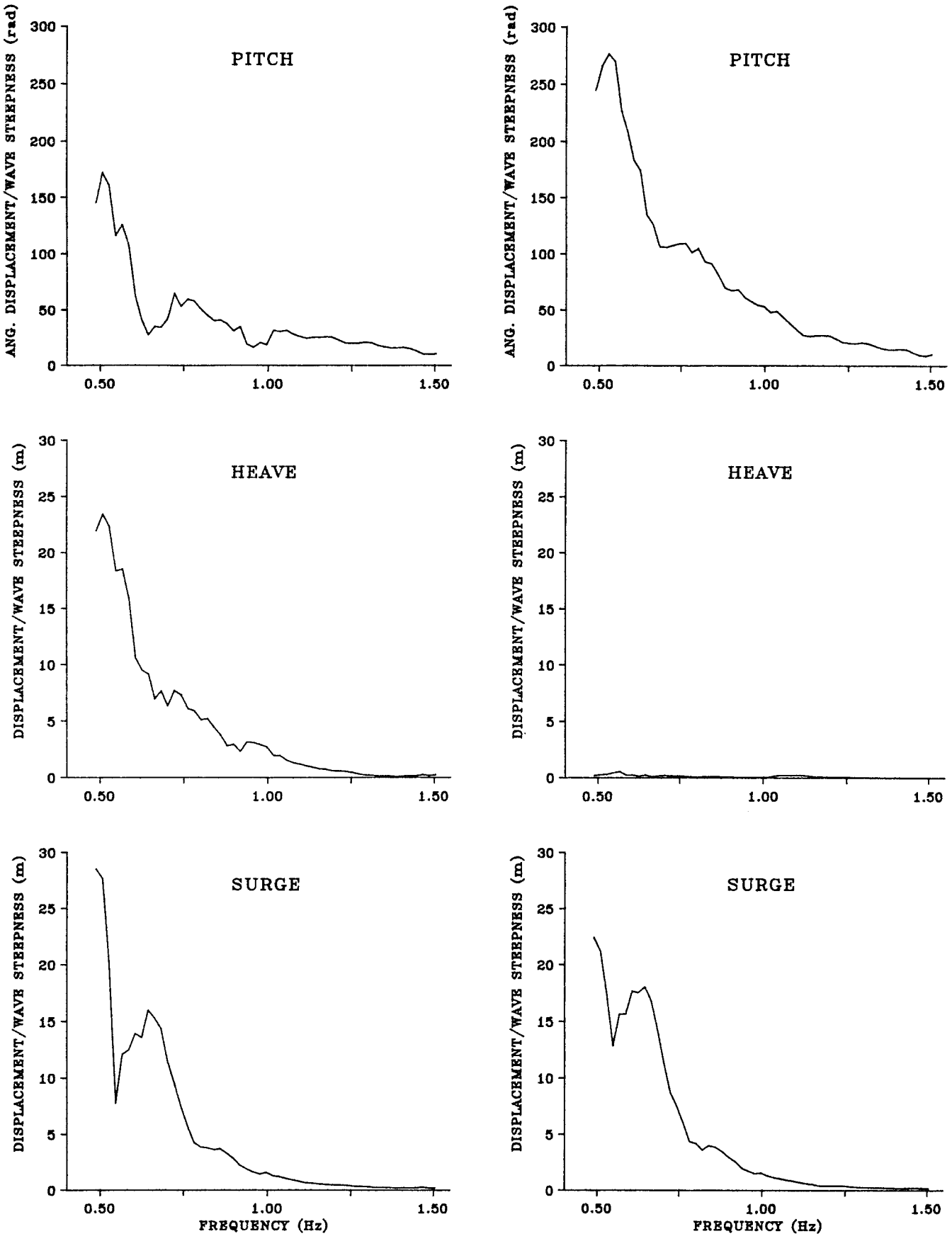

FIGURE.10. DISPLACEMENT PER UNIT WAVE STEEPNESS FOR 3 DEGREE-OF-FREEDOM COMPLEX-CONJUGATE SYNTHESIS

FIGURE.11. DISPLACEMENT PER UNIT WAVE STEEPNESS FOR 2 DEGREE-OF-FREEDOM COMPLEX-CONJUGATE SYNTHESIS